Acknowledgements

TABLE OF CONTENTS

LIST OF FIGURES 7

CHAPTER ONE: INTRODUCTION 11

CHAPTER TWO: OVERVIEW OF THE THERMAL STRUCTURE AND THE CIRCULATION FEATURES IN THE EQUATORIAL AND SOUTHEAST ATLANTIC 14

2.1 Geographic Setting 14

2.2 Atmospheric Variability 15

2.2.1 Intertropical convergence zone (ITCZ) 15

2.2.2 Remote vs. local forcing 15

2.2.3 Wind stress, windstress curl and Ekman pumping 16

2.3 Equatorial Currents 18

2.3.1 Equatorial undercurrent (EUC) 19

2.3.2 South Equatorial undercurrent (SEUC) 21

2.3.3 South Equatorial countercurrent (SECC) 22

2.4 Thermocline Structure 23

2.4.1 Ridge-trough-ridge structure 23

2.4.2 Seasonal fluctuation 24

2.5 Poleward Coastal Currents 24

2.5.1 Gabon-Congo undercurrent (GCUC) 24

2.5.2 Angola Current 25

2.6 Angola Benguela Frontal Zone (ABFZ) 25

2.6.1 Frontal characteristics 25

2.6.2 Maintenance of frontal position 27

2.7 Cyclonic features in eastern equatorial basins 27

2.7.1 The Angola Gyre 27

2.7.2 The Angola Dome 29

2.7.3 The Guinea Dome 32

2.7.4 Costa Rica Dome 34

CHAPTER THREE: DATA **36**

3.1 OPA/ Ocean General Circulation Model (OGCM) **36**
3.1.1 The primitive equations 37
3.1.2 The time- stepping scheme 38
3.1.3 Boundary conditions 38
3.1.4 The TOTEM configuration 38
3.1.5 The CLIPPER ATL6 configuration 39

3.2 European Remote Sensing Satellites (ERS 1 & 2) **40**
3.2.1 The Active Microwave Sensor (scatterometer) 41
3.2.2 Calibration 41
3.2.3 Gridded Swath Data 43

CHAPTER FOUR: METHODS **44**

4.1 OPA- model data (velocity field and hydrothermal parameters) **44**
4.1.1 Divergence 44

4.2 ERS- satellite data (surface wind speed) **45**
4.2.1 Wind stress, windstress curl and Ekman pumping 45

CHAPTER FIVE: RESULTS AND DISCUSSION **48**

5.1 Thermohaline Characteristics **48**
5.1.1 Monthly mean composites at 45m 49
Temperature 49
Salinity 55
5.1.2 Vertical configuration 58
Thermocline structure 59
Meridional and zonal temperature sections 63
Monthly mean salinity sections 67
5.1.3 Synopsis 70

5.2 Circulation Features **72**
5.2.1 Monthly mean composites of zonal and meridional velocity 72
The northern and southern limbs (zonal velocity sections) 72
The eastern and western limbs (meridional velocity sections) 78
5.2.2 Vertical velocity field 87

5.2.3 Synopsis 90

5.3 The Atmospheric Connection 92

5.3.1 Wind stress variability in the south Atlantic. 93

5.3.2 Local vs. remote forcing 96

5.3.3 Windstress curl and Ekman pumping 99

5.3.4 Synopsis 103

5.4 Finer-scale structures resolved by the CLIPPER-ATL6 model 104

5.4.1 The Angola Gyre 104

5.4.2 The region of the Angola Dome 105

5.4.3 Synopsis 108

CHAPTER SIX: CONCLUSIONS 110

LIST OF FIGURES

Figure 2.1: Topography and coastal configuration of the SE Atlantic Ocean.

Figure 2.2: Plot of the averaged windstress curl fields for the full Seasat-A satellite scatterometer mission (7 July – 10 October 1978) for the tropical Atlantic (Chelton *et al.*, 1990).

Figure 2.3: Idealized representation of austral winter currents at 0, 100 and 200m depth in the near equatorial region of the central Atlantic. Abbreviated terms are: North Equatorial Countercurrent (NECC), South Equatorial Current (SEC), South Equatorial Countercurrent (SECC), North Equatorial Undercurrent (NEUC) and the South Equatorial Undercurrent (SEUC). (Peterson and Stramma, 1991)

Figure 2.4: Schematic representation of the undercurrents in the equatorial Atlantic and their relation to the Guinea and Angola Domes (Voituriez and Herbland, 1982).

Figure 2.5: Schematic map showing the horizontal distribution in the upper 100m for austral autumn (top) and spring (bottom). Abbreviations: North Equatorial Current (NEC), North Equatorial Countercurrent (NECC), South Equatorial Current (SEC), with northern, central and southern branches (nSEC, cSEC and sSEC respectively), the South Equatorial Countercurrent (SECC), the Angola and Guinea Domes (AD and GD), the Gabon-Congo Undercurrent (GCUC), the Angola Current (AC), the North Brazil Undercurrent (NBUC) and the Angola Benguela Front (ABF). (from Peterson and Stramma, 1991)

Figure 5.1(a-f): Monthly mean OPA/TOTEM temperatures (°C) at a depth of 45m (January to June). The contour interval is 0.5°C.

Figure 5.2(a-f): Monthly mean OPA/TOTEM temperatures (°C) at a depth of 45m (July to December). The contour interval is 0.5°C.

Figure 5.3(a-f): Monthly mean OPA/TOTEM salinities (psu) at a depth of 45m (January to June). The contour interval is 0.05psu.

Figure 5.4(a-f): Monthly mean OPA/TOTEM salinities (psu) at a depth of 45m (July to December). The contour interval is 0.05psu.

Figure 5.5(a-f): Monthly mean thermocline structure in the Angola Basin derived from OPA/TOTEM temperatures (January to June).

Figure 5.6(a-f): Monthly mean thermocline structure in the Angola Basin derived from OPA/TOTEM temperatures (July to December).

Figure 5.7(a-f): Monthly mean OPA/TOTEM temperature sections along 5°E (January to June).

Figure 5.8(a-f): Monthly mean OPA/TOTEM temperature sections along 5°E (July to December).

Figure 5.9(a-f): Monthly mean OPA/TOTEM salinity sections along 5°E (January to June).

Figure 5.10(a-f): Monthly mean OPA/TOTEM salinity sections along 5°E (July to December).

Figure 5.11(a-f): Monthly mean zonal velocity sections at 5°E (January to June). Positive and negative velocities correspond to eastward and westward flow respectively. Contour Interval is 0.02m.s^{-1}.

Figure 5.12(a-f): Monthly mean zonal velocity sections at 5°E (July to December). Positive and negative velocities correspond to eastward and westward flow respectively. Contour Interval is 0.02m.s^{-1}.

Figure 5.13 Monthly mean meridional velocity sections at 5°S (January to June). Positive and negative velocities correspond to northward and southward flow respectively. Contour Interval is 0.01m.s^{-1}.

Figure 5.14 Monthly mean meridional velocity sections at 5°S (July to December). Positive and negative velocities correspond to northward and southward flow respectively. Contour Interval is 0.01m.s^{-1}.

Figure 5.15: Monthly mean resultant horizontal flow pattern and magnitude at 45m (January to June). Overlaid is an outline of the cool feature at 45m for January, February and June, as defined by the bounding isotherms.

Figure 5.16: Monthly mean resultant horizontal flow pattern and magnitude at 45m (July to December). Overlaid is an outline of the cool feature at 45m for July – November, as defined by the bounding isotherms.

Figure 5.17: Monthly mean horizontal current divergence and temperatures at 45m for months during which the cool features is most distinct (January, February, September, October and November).

Figure 5.18: OPA/TOTEM vertical velocities of a section at 5°E (January to June). Positive and negative velocities correspond to upward and downward velocities respectively.

Figure 5.19: OPA/TOTEM vertical velocities of a section at 5°E (July to December). Positive and negative velocities correspond to upward and downward velocities respectively.

Figure 5.20: Sketch of the southward movement of the thermocline- ridge that results in the pattern of downward and upward motion within its cool, circular expression at 45m (approximately the position of the blue line). The dashed and solid lines represent the position of the thermocline in September and October respectively.

Figure 5.21: Plot of wind stress magnitude (unit: $N.m^{-2}$, contour interval: 0.01 $N.m^{-2}$) and direction of the South Atlantic Ocean for January (top) and July (bottom).

Figure 5.22: Standard deviation of wind stress magnitude in the south-east Atlantic Ocean. Superimposed are boxes A (20°W-30°W, equator - 10°S) and B (Greenwich meridian - 10°E, equator - 10°S).

Figure 5.23: Monthly mean zonal wind stress component in the eastern equatorial Atlantic (box B, top) and the western equatorial Atlantic (box A, bottom).

Figure 5.24: Monthly mean zonal velocity component in the eastern equatorial Atlantic (box B).

Figure 5.25: Monthly mean thermocline depth in the eastern equatorial Atlantic (box B).

Figure 5.26(a & b): Windstress curl for January and July. Contour Interval is 0.2 $N.m^{-3}$.

Figure 5.26(c): Monthly mean windstress curl in the eastern equatorial Atlantic (box B).

Figure 5.27(a & b): Ekman pumping velocities for January and July. Contour Interval is 0.1 $m.d^{-1}$.

Figure 5.27(c): Monthly mean Ekman pumping velocity in the eastern equatorial Atlantic (box B).

Figure 5.28: A comparison between the OPA/TOTEM (right) and CLIPPER (left) temperature output at 45m for the month of October.

Figure 5.29: Seasonal mean resultant horizontal flow pattern and magnitude at 45m as resolved by the CLIPPER model.

Appendix 1: Plots of temperature change between consecutive months at 45m: a positive (negative) value indicates an increase (decrease) in temperatures between successive months.

Appendix 2: Monthly mean thermocline depth, calculated as the position of the most intense vertical temperature gradient.

Appendix 3: Hoffmöller plot of the monthly mean thermocline depth along 5°E.

Appendix 4: Plot of wind speeds (unit: $m.s^{-1}$, contour interval: 0.5 $m.s^{-1}$) and direction of the South Atlantic Ocean for January (top) and July (bottom).

Appendix 5: Monthly mean CLIPPER temperatures at 42m.

Appendix 6: Seasonal mean resultant horizontal flow pattern and magnitude at 45m as resolved by the CLIPPER model.

CHAPTER ONE:
INTRODUCTION

The eastern equatorial and tropical margins of both the Pacific and Atlantic Oceans are associated with vigorous upwelling regimes, which produce the highly-productive systems that exist there. Included within these economically important systems are thermal domes that are characterized by an upward-doming of the thermocline, bringing cold and deep water closer to the surface. The Costa Rica and Guinea Domes have been located at approximately 10°N in the eastern tropical Pacific and Atlantic basins respectively. The Angola Dome is less well defined than its counterparts in the northern hemisphere. Despite this, it has been noted as a perennial feature situated at about 10°S (Hay and Brock, 1992), within the Angola Basin. Unique to the Angola Dome is the fact that it has been identified as a mesoscale gyre (100-300km in diameter) situated within a larger-scale (1000-2000km) cyclonic feature; the Angola Gyre (Mohrholz *et al.*, 2001). On the other hand, certain investigations (detailed in the following section) of cyclonic circulation within the Angola Basin have not provided clear evidence of a distinction between the two cyclonic features.

The exact forcing mechanism of the Angola Dome is a lingering debate, but it is generally attributed to the termination of the eastward equatorial undercurrents, local wind stress resulting in Ekman upwelling in the region of the dome and, to some extent, the fluctuations of the thermocline as a response to remote wind stress variability. It is probable that the actual dynamics of the Angola Dome are a consequence of interplay between some or all of these mechanisms. The generation of the Angola Gyre is commonly considered to be solely related to the large-scale current field.

The relationship of the Angola Gyre to the large-scale current field allows for the relatively distinct definition of its boundaries. The northern limb of the gyre is associated with the South Equatorial Undercurrent (SEUC) and the South

Equatorial Countercurrent (SECC) (Waconge and Piton, 1992), the Angola Current is its eastern limb and the offshore deflection and northwestward movement of the Benguela Current at the Angola Benguela Front (ABF) forms its southern and western limbs respectively. As a consequence of the less explicit driving force of the Angola Dome, its boundaries are not as apparent. However, its northern limb has been associated with the South Equatorial Undercurrent (SEUC) by Voituriez (1981) and its seasonal variability has been related to the seasonal uplift of the thermocline which, in turn, is a result of fluctuations of the SECC (Waconge and Piton, 1992). The equatorial currents are therefore an integral component of the cyclonic circulation features in the Angola Basin.

When investigating the characteristic circulation patterns in the eastern tropical Atlantic basin it is important not to overlook the interaction between the ocean and atmosphere. This is partly because the equatorial currents result (directly or indirectly) from the zonal wind stress that acts upon the surface of the ocean. Therefore, seasonal variations of the large-scale wind field will be reflected in some way by the system of equatorial currents. In turn, a seasonal signal of the eastward equatorial undercurrents will have an effect on the circulation of the Angola Gyre and Dome. On interannual timescales, atmospheric anomalies in the western portion of the basin can affect the eastern equatorial and tropical Atlantic. Equatorial currents respond quickly and coherently to changes in the wind, so that a sudden change in wind-stress off the coast of Brazil is associated with upwelling off the coast of Guinea (Cury and Roy, 1985).

This dissertation aims to improve the understanding of the pattern of cyclonic circulation within the Angola Basin. It addresses the following questions:

- What are the key cyclonic circulation features in the Angola Basin?
- What is the nature of their horizontal and vertical structure and what is their characteristic seasonal signal?
- Is the Angola Dome a prominent feature of the Angola Basin?

- If so, what is its relationship to possible larger-scale cyclonic circulation patterns in the Angola Basin?
- How significant is the system of equatorial currents and coastal currents in the formation and/ or seasonal signal of cyclonic circulation features within the Angola Basin?
- How does wind field, local and/ or remote, influence the circulation patterns of the southeast equatorial Atlantic?

With these objectives in mind, the structure of this dissertation is as follows:

Chapter two is a review of research that has focused on circulation in the Angola Basin thus far. It is designed such that the supposed forcing mechanisms (i.e. atmospheric forcing, equatorial current system, thermocline structure) of the Angola Dome and/ or Gyre are discussed separately, but the fundamental linkages between them are emphasized. Included are brief descriptions of the Costa Rica and Guinea Domes, allowing for comparisons to be made with the Angola Dome.

Chapter three outlines the data sources (OPA/TOTEM and CLIPPER model temperature, salinity and velocity as well as ERS satellite-derived winds).

Chapter four is a synopsis of the methods employed for data processing and analysis.

Chapter five is a description of the results as well as a general discussion.

Chapter six concludes this work, summarizing the results and focusing on salient points of the discussion.

CHAPTER TWO:

OVERVIEW OF THE THERMAL STRUCTURE AND CIRCULATION FEATURES IN THE EQUATORIAL AND SOUTHEAST ATLANTIC

2.1 Geographic Setting

The topographical setting of this study is characterized by the Angola Basin, which extends into the abyssal plain of the South Atlantic, reaching depths of 5000m (see Figure 2.1). The Angola Basin is separated from the Cape Basin to the south by the Walvis Ridge, which extends in a southeasterly direction from the coast at approximately 20°S and, at shallowest, is at depths of between 1000km and 2000km. North of the Walvis Ridge the shelf-edge narrows fairly abruptly until 10°S, at which point it begins to broaden progressively until it reaches the equator. The northern boundary of the Angola Basin is characterized by a broad and slight rise in the topography, also oriented from the coast toward the south- east, from about 4°S to the equator.

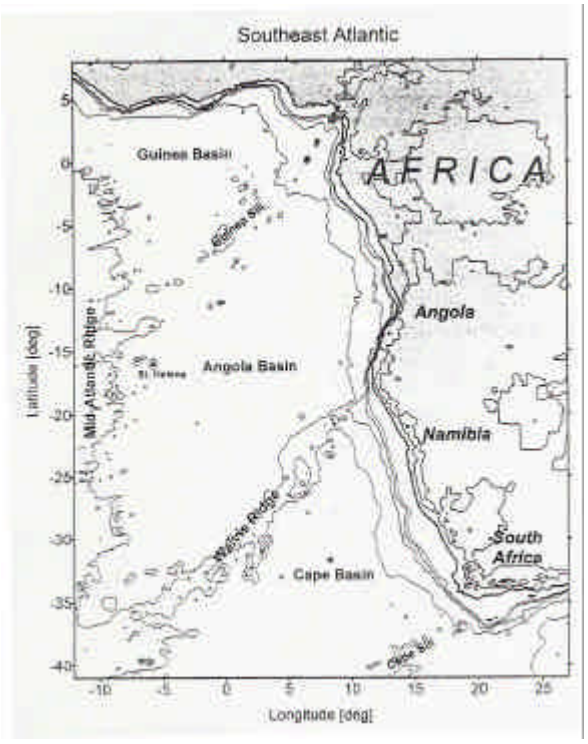

Figure 2.1: Topography and coastal configuration of the SE Atlantic Ocean.

2.2 Atmospheric Variability

2.2.1 Intertropical convergence zone (ITCZ)

The mean windstress field in the Tropical Atlantic Ocean is dominated by northeast and southeast trade winds that converge north of the equator to form the ITCZ. These winds are connected to the Azores and St. Helena anticyclones. When the southeast trades are strongest in August and September, the ITCZ lies furthest north. The ITCZ is closest to the equator during March when the southeast trades are weak. The north-south migration of the ITCZ leads to a similar varying wind field, which is, in turn, reflected by the annual cycle of the surface currents (Stramma and Schott, 1999). The direct forcing of the ITCZ on equatorial currents (and their respective sea surface height signals) occurs most prominently in the northeastern currents (particularly the North Equatorial Counter Current), while its effect on the variability of the southern equatorial currents has been postulated to be a remote response that is associated with local thermodynamic effects (Merle and Arnault, 1985). McCreary *et al*'s (1984) model study of forcing mechanisms in the eastern tropical Atlantic Ocean, confirms the remotely forced suggestion of Merle and Arnault (1985). McCreary *et al.* (1984) found that when the tradewinds in the western Atlantic strengthen the thermocline rises in the eastern tropical Atlantic.

2.2.2 Remote vs. local forcing

In the eastern equatorial and tropical Atlantic Ocean, the tradewinds weaken in July and August but intensify in November (Philander and Pacanowski, 1986), thus developing the prominent semi-annual signal of the eastern Atlantic. In contrast to this, the western Atlantic is characterized by an annual signal. From their study, based on a general circulation model, Philander and Pacanowski (1986) found that the response of the tropical Atlantic Ocean was in phase and corresponded reasonably well with local winds. They noted that east of the Greenwich meridian, correlations to local wind forcing are weakest, yet a strong semi-annual signal of the zonal current component implies that the winds that

dominate its forcing are local. The remote forcing by winds off Brazil therefore was thought to be of secondary importance.

The response of the ocean to variable winds depends on the timescale of changes in the wind field. If changes in the wind are sudden then waves (i.e. Kelvin waves) are evident in the oceanic adjustment, whereas if the winds vary on a much longer timescale then the waves are not present and the response of the ocean is practically in phase with the winds (Philander and Pacanowski, 1986). Philander and Pacanowski's model showed that an abrupt change in the winds east of 30°W in May and June excites a wave that remains evident even when the winds have ceased to change. It should therefore be kept in mind that oceanic variability is not necessarily in phase with its wind forcing mechanism and may persist after the wind perturbation has come to an end. This is particularly evident in the eastern portion of the basin, while the oceanic response near Brazil seems to be in equilibrium with the fluctuating winds. Cane and Moore (1981) showed that low frequency waves (Kelvin waves and their reflected Rossby waves) in the eastern Atlantic that are excited by wind variations in the western portion of the basin affect only the thermocline depth, which may be strongly tied to the structure and variability of the Angola Dome. Philander and Pacanowski showed that the downward slope of the thermocline toward the African continent is a result of the eastward component of the local wind.

2.2.3 Wind stress, windstress curl and Ekman pumping

Windstress is the force exerted by surface winds on the sea surface, indirectly causing currents in the direction of wind. Horizontal shear of the windstress (i.e. windstress curl) contributes positive or negative vorticity to the surface layer of the ocean. A negative (cyclonic) windstress curl in the southern hemisphere gives rise to an upward forcing of the thermocline. In turn, windstress curl drives Ekman pumping, which is the vertical motion of upper layers of the ocean due to

the surface wind. Surface divergence and upwelling is associated with a negative curl and convergence and downwelling occurs under the influence of a positive curl. Although the vertical motion due to Ekman pumping is small compared to the horizontal motion, the length scale is also small, being of the order of the mixed layer depth (McClain and Firestone, 1993). Therefore, its effect on the Angola Dome, which is within the thermocline, may be significant.

The climatology of windstress curl produced by Han and Lee (1981) (cited in Peterson and Stramma, 1991) as well as that of Hellerman and Rosenstein (1983), Chelton (1990) (Figure 2.2), Risien (2002) and Chelton *et al.* (2004) all show a line of zero curl extending from the tip of Africa to the promontory of Brazil. Negative curl exists to the north of this line and is consistent with the presence of a cyclonic gyre in the Angola Basin.

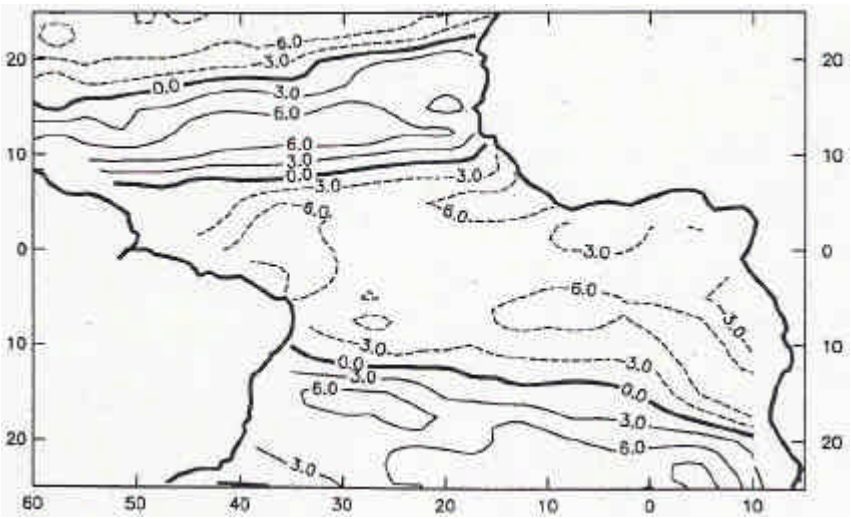

Figure 2.2: Plot of the averaged windstress curl fields for the full Seasat-A satellite scatterometer mission (7 July – 10 October 1978) for the tropical Atlantic (Chelton *et al.*, 1990) Units are dyne.cm^{-3}.

In an investigation of Ekman upwelling in the north Atlantic, McClain and Firestone (1993) found that areas of maximum upwelling coincided with the region of the Guinea Dome. Their study analyzed timeseries' of monthly, seasonal and annual mean Ekman pumping velocities computed from winds provided by the Fleet Numerical Oceanography Center (FNOC) and the European Centre for Medium-Range Weather Forecasts (ECMWF). They showed that at low latitudes there is a strong coupling between surface divergence fields (generated by surface winds) and subsurface hydrography.

2.3 Equatorial Currents

The equatorial current system, in both the Pacific and Atlantic oceans, has been recognized as an integral component of the dynamics in the eastern tropical portions of each of these basins. Part of the importance of equatorial currents on circulation in eastern tropical ocean basins lies in their ability to respond quickly and coherently to changes in the wind patterns (Picaut, 1985). For example, Cury and Roy (1985, cited in Picaut, 1985) have shown that the zonal wind stress off Brazil is associated with upwelling in the Gulf of Guinea, with a lag time of one month (the time it takes for a Kelvin wave to cross the Atlantic basin). A more direct relationship between the equatorial currents and circulation features in the eastern Atlantic basin (both north and south of the equator) is the effect of the termination of the eastward equatorial currents at the African coast. Among others, Mercier *et al.* (2003), Stramma and England (1999), Stramma and Schott (1999), Waconge and Piton (1992), Picaut (1985), Voituriez (1981) have studied this phenomenon and have reached a common conclusion that certain eastward equatorial currents form the northern limb of a cyclonic gyre in the south-east Atlantic.

The specific eastward equatorial currents on and south of the equator are illustrated in Figure 2.3 and are discussed below.

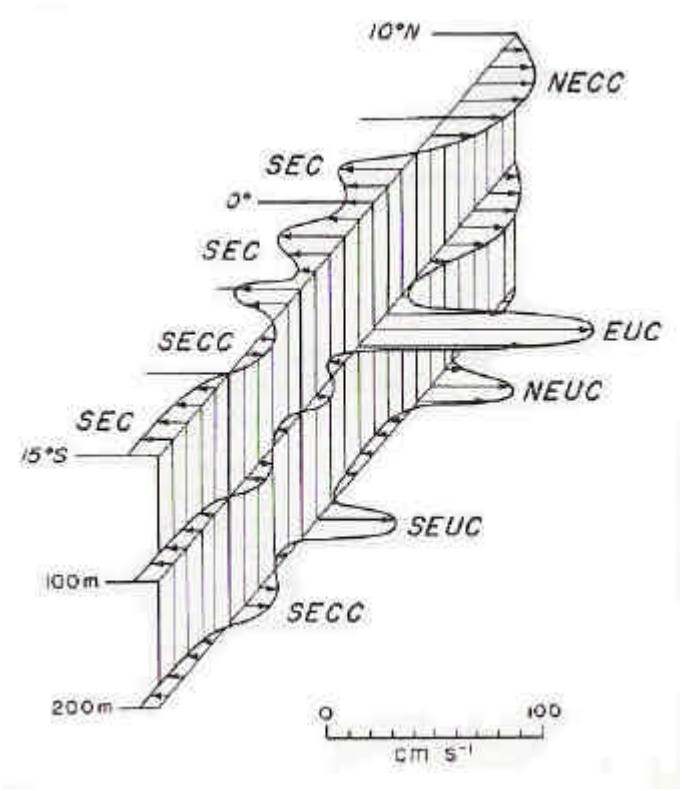

Figure 2.3: Idealized representation of austral winter currents at 0, 100 and 200m depth in the near equatorial region of the central Atlantic. Abbreviated terms are: North Equatorial Countercurrent (NECC), South Equatorial Current (SEC), South Equatorial Countercurrent (SECC), North Equatorial Undercurrent (NEUC) and the South Equatorial Undercurrent (SEUC). (Peterson and Stramma, 1991)

2.3.1 Equatorial undercurrent (EUC)

According to Peterson and Stramma (1991), the EUC is a narrow jet less than 100m below the surface with a width of 3° latitude and that flows eastwards with velocities reaching over 100cm.s^{-1}. From *in situ* measurements of the salinity maximum associated with the EUC, Schott *et al.* (1998) showed that the depth of the EUC corresponds to the depth of the thermocline.

The forcing mechanism of the EUC has been directly related to the zonal wind stress acting on the surface layers: the westward wind stress is balanced by an eastward pressure gradient, which occurs as a downward tilting of the sea surface toward the east. The eastward flow of the EUC is therefore driven by the pressure gradient force that exists in the subsurface layer as a result of the 'piling-up' of waters in the western equatorial Atlantic (Picaut, 1985; Peterson and Stramma, 1991; Blanke and Delecluse, 1993).

Tracing the high salinity core associated with the EUC, Henin *et al.* (1986) (cited in Waconge and Piton, 1992) were able to show that the EUC terminates at the African coast by branching into poleward undercurrents to the north and to the south. From model results, Rothstein (1984) confirmed this, showing a continuity of flow from the EUC into northward and southward coastal undercurrents that extended to at least 10°N and 10°S respectively. Waconge and Piton (1992) used direct measurements to describe a highly variable poleward undercurrent between 1°S and 6°S and referred to it as the Gabon-Congo Undercurrent (GCUC) and recognized it as the southern branch of the bifurcating EUC at the equator. However, Mercier *et al.* (2003) used ADCP measurements to show that the transports of the eastward flowing EUC and Guinea current balance that of the westward flow of the Northern South Equatorial Current (NSEC) and the Equatorial South Equatorial Current (ESEC). The implication being that the contribution of the EUC to a poleward eastern boundary current (i.e. the Gabon-Congo Undercurrent) is small. The results of Mercier *et al.* (2003) are consistent with the model results of Cane (1979) as well as Philander and Pacanowski (1980): both simulated a recirculation of the EUC in both the northern and southern hemispheres, whereby the poleward flow separated from the coast within 3-4° of the equator. The poleward limbs of the cyclonic recirculation cells in the northern and southern hemispheres may correspond to the NSEC and ESEC respectively.

From equatorial current meter moorings at 28°W and 4°W (Weisberg and Colin, 1986, cited in Waconge and Piton, 1992), Waconge and Piton (1992) revealed that rather than a seasonal fluctuation of the transport or velocity of the EUC, the seasonal cycle consists of a deepening of maximum eastward flow. Evidence of this also exists in a primitive equation simulation by Philander and Pacanowski (1986). It was noted by Waconge and Piton (1992) that the bifurcation of the EUC occurs at the African coast during austral winter when the deep EUC is most intense while, at other times, it branches off before 1°E. When the EUC bifurcates further west, the south-eastward flow that results is between 2°S and 8°S and, on reaching the coast may contribute to the southern GCUC or to the Angola Current.

2.3.2 South Equatorial undercurrent (SEUC)

The SEUC is observed between 3°S and 8°S and takes its energy from the EUC in the western and mid-Atlantic basin (McPhaden, 1984, cited in Picaut, 1985). Once near the eastern boundary is completely detached from the EUC and, similarly is deflected poleward upon reaching the coast. Tsuchiya (1986) showed that the SEUC is related to the equatorial thermostad and that it is present almost completely across the basin, from 5°S in the west and shifting progressively poleward toward the east. The SEUC has been observed to have a width of approximately 100km and is situated beneath the thermocline at depths of between 100- 500m (Molinari *et al.*, 1981, cited in Peterson and Stramma, 1991).

Waconge and Piton (1992) speculate that a seasonal surface eastward flow between 2°S and 8°S is an outcropping of the SEUC east of 12°W. The basis of their theory is that path of the SEUC and eastward surface flow are compatible and that the thermostad is shallower in the east than in the west, therefore a surface seasonal signal of the SEUC is more probable in that region. Furthermore, the disappearance of the eastward surface flow between 2°S and 8°S corresponds to a suggested time for a seasonal minimum of the SEUC

(Reverdin *et al.,* 1991, cited in Waconge and Piton, 1992). Reverdin *et al.* (1991) observed that the eastern SEUC was weakest during July and September while its western counterpart was strongest during this period. Since this flow is weakest in austral winter when the cyclonic windstress curl is weakest, Waconge and Piton (1992) precluded the curl from being its forcing mechanism.

Voituriez (1981) speculates that the termination of the equatorial thermostad at the African coast produces a tight cyclonic circulation of the SEUC near 9°E, 9°S, thus relating the so-called 'Angola Dome' to the SEUC and to the thermocline structure.

2.3.3 South Equatorial countercurrent (SECC)

According to Waconge and Piton (1992) the SECC is a surface eastward geostrophic flow in the region of 10°S that is possibly related to the windstress curl. They base their hypothesis on the fact that the year-round persistence of the SECC is consistent with the permanent cyclonic windstress curl. According to Peterson and Stramma (1991) the SECC has maximum velocities below the surface (e.g. 10cm.s^{-1} at 275m), but is typically accompanied by an eastward flowing surface component.

Tracing its definitive oxygen maximum, Mercier *et al.* (2003) also found the SECC to be situated at 10°S, not only at the surface, but to a depth of 200m. Along with the EUC and SEUC, they noted that the SECC re-circulated into various branches of the South Equatorial Current (SEC) and contributed to the Angola Gyre. Though observations have shown that both the SEUC and the SECC impinge on the coast and feed the Angola Current, their specific contributions remain unresolved.

It is conjectured by Peterson and Stramma (1991) that anomalously warm events in the tropical Atlantic result in an intensification of the eastward flow of the SECC.

2.4 Thermocline Structure

2.4.1 Ridge-trough-ridge structure

Hastenrath and Merle (1986) provided evidence from *in situ* data that the thermocline, across the equatorial and subequatorial Atlantic basin, exhibits a ridge-trough-ridge structure, whereby it is deepest at the equator and shallowest at 4°N and 4°S. The doming of the thermocline at 4°S is present through much of the year, whereas its equivalent at 4°N moves to as far as 10°N near the end of boreal winter. A model study conducted by McPhaden (1984) corresponded to the observations by Hastenrath and Merle; his schematic account of this structure related it to patterns of convergence and divergence between the equator and 4°S (from the surface to 200m) that result from surface easterlies (producing Ekman divergence at the equator), the EUC and a reversal of the pressure gradient force with depth. Ultimately then, the ridge-trough-ridge structure of the tropical Atlantic thermocline appears to be directly related to the zonal wind component along the equator that gives rise to Ekman divergence and to the east-west slope of the sea surface that gives rise to the eastward EUC. The fact that the ridge in the northern hemisphere does not persist in boreal summer at 4°N may be related to the distinct asymmetry of the surface wind field and associated windstress curl.

From their numerical model of the tropical Atlantic Busalacchi and Picaut (1983) simulated the shoaling of the thermocline towards the east and the zonal ridge-trough-ridge structure. They noted that the termination of the ridge in each hemisphere is characterized by a dome-like feature (i.e. the Guinea Dome in the northern hemisphere and the Angola Dome in the southern hemisphere).

2.4.2 Seasonal fluctuation

The thermal structure of the subsurface tropical Atlantic is dominated by the annual cycle of the surface wind field, with maximums in April and August. In response, the thermocline along the equator deepens from April through to August, with greatest variability in the western portion of the basin where the thermocline is deep (Hastenrath and Merle, 1986). According to Busalacchi and Picaut (1983), the minimum thermocline depth in the east is during July and the maximum is during September-October.

Although the seasonal variability of the Angola Dome has been associated with thermocline fluctuations by Voituriez (1981), he suggests that it is probably a permanent feature in subthermoclinal layers and is related to the cyclonic circulation of the SEUC at this level.

2.5 Poleward Coastal Currents

2.5.1 Gabon-Congo undercurrent (GCUC)

Waconge and Piton (1992) used current profilers off Gabon and Congo to resolve the highly variable poleward undercurrent along the continental break. They named this current the Gabon-Congo Undercurrent and interpret it as a branch of the terminating EUC. According to them, the EUC is most intense during boreal summer and upon reaching the African continent replenishes a salt reservoir thus creating a poleward pressure gradient force and ultimately resulting in a deep, salty southeastward flow (the GCUC) that eventually reaches and forms part of the Angola Current. At other times, the EUC bifurcates prior to reaching the eastern boundary and feeds either the GCUC at 4-6°S or the Angola Current further south. Waconge and Piton indicated that there may be a possibility of the GCUC in boreal summer separates from the coast and re-circulates westward before 5°S.

2.5.2 Angola Current

From observations made by Moroshkin *et al.* (1970), it could be seen that the flow field made up of both the SEUC and the SECC partly re-circulates offshore and partly impinges on the coast and feeds the Angola Current. Again from direct *in situ* measurements Mohrholz *et al.*, (2001) located a southeastward flow, that they surmised to be the SECC, between about 6-8°S. When it reached the coast it continued poleward with a maximum speed of about 40cm.s^{-1}, extending to a depth of 150m at which point a northward flow of 15-20cm.s^{-1} was observed. A review by Shannon and Agenbag (1987) (cited in Shannon *et al.*, 1987), defined the Angola Current as a poleward flowing current in the upper 200m of the continental slope off Angola and persists throughout the year, but is weakest in late winter and spring. Shannon *et al.*, (1987) also noted that the subsurface poleward flow indicative of the Angola Current existed within about 200km of the coast.

A westward bend in the surface component of the Angola Current at approximately 15-19°S was noted by Shannon *et al.* (1987). Somewhat abrupt, this westward movement coincides with the position of the Angola- Benguela frontal zone (ABFZ), which has been recognized as the confluence between the Angola and Benguela Currents. The offshore movement of the Angola Current was also described by Mohrholz *et al.* (2001), who detected it merging with the westward Ekman drift at the ABFZ.

2.6 Angola Benguela Frontal Zone (ABFZ)

2.6.1 Frontal characteristics

The ABFZ has been investigated by *in situ* measurements (e.g. Shannon *et al.*, 1987) and by satellite SST observations (e.g. Meeuwis and Lutjeharms, 1990 and Kostianoy and Lutjeharms, 1999), which have shown that the frontal zone lies between 15-17°S. These studies have also shown that the frontal zone is characterized by sharp horizontal temperature and salinity gradients, particularly

in the upper 50m, but vestiges of the front do exist down to a depth of about 200m (Shannon *et al.,* 1987). It has an average width of about 200km, but it can be much smaller, with steeper temperature gradients (the typical temperature gradient near the coast is 4°C per 1° of latitude). Alternatively, it can be present as a series of sharp multiple fronts, particularly in austral summer when the Angola Current is strongest (Shannon *et al.,* 1987). The frontal zone is a region of great temporal and spatial variability that exists in the form of mesoscale features such as eddies, meanders and filaments. The front is most intense within 250km of the coast, but traces of it have been noted as far west as the Greenwich meridian (Shannon and Nelson, 1996).

By means of hydrographic and current measurements, Lass *et al.* (1999) confirmed prior findings, namely that the front exists at approximately 16°30'S and that it separates a 40m-thick warm and saline tongue of southward-flowing Angola Current water from the cold and less saline water that is definitive of the northward-flowing Benguela Current to the south.

Despite the permanent nature of the ABFZ, temporal and spatial variability of the frontal zone has been investigated by several authors including Shannon *et al.* (1987), Meeuwis and Lutjeharms (1990) Kostianoy and Lutjeharms (1999), Mohrholz *et al*. (2001) and Veitch *et al.* (2003). Meeuwis and Lutjeharms (1990) found that the front is most distinct, widest and furthest south in summer months and Shannon *et al.* (1987) noted that the seasonal shift of the ABFZ spans approximately 2° of latitude. Boyd *et al.* (1987) found the seasonal cycle of the ABFZ to be related to the fluctuation of the northward wind stress and its influence on upwelling in the northern Benguela. Despite the clear seasonal signal of the frontal zone, its seasonal variability is of the same order of magnitude as fluctuations that occur on the order of days (Shillington, 1998). Kostianoy and Lutjeharms (1999) found that large short term displacements of the frontal zone are best correlated to the atmospheric pressure gradient of the South Atlantic

Anticyclone. Mohrholz *et al.* (2001) also noted that short-term changes in the ABFZ are related to the local wind field.

2.6.2 Maintenance of frontal position

A remarkable feature of the ABFZ is that it is generally confined to an exceptionally narrow range of latitudes. For this reason, Shannon and Nelson (1996) suggest that it seems unlikely that its forcing mechanism is solely a result of the confluence of the Angola and Benguela Currents as was postulated by Meeuwis and Lutjeharms (1990). Shannon *et al.* (1987) postulated that coastline orientation, bathymetry, stratification and windstress could be determining factors of the relative stability of the position of the frontal zone. They hypothesize that the maintenance of the frontal position is due to a combination of the above aspects and that its seasonal migration is a result of changes in the intensity of the SEUC or the SECC. Shannon and Nelson (1996) however, viewed the windstress as the most important mechanism for the maintenance of the frontal within a relatively narrow range of latitudes.

2.7 Cyclonic features in eastern equatorial basins

2.7.1 The Angola Gyre

The Angola Gyre is situated in a region of predominantly negative windstress curl, which, according to Sverdrup (1947) drives cyclonic circulation. Along with the negative windstress curl, another driving force of the cyclonic motion of the Angola Gyre has been identified as the termination of the eastern equatorial currents at the African coast.

The aim of a detailed hydrographic survey conducted in 1967 was to verify the cyclonic nature of water circulation in eastern tropical ocean basins. From this survey, Moroshkin *et al.* (1970), resolved a cyclonic gyre, centered on about 14°S 4°E, approximately 1000km in diameter and evident at depths of between 10-300m. The wind-driven surface layer was found to mask the cyclonic

circulation in this area. They noted that the northern boundary of the gyre is associated with the SECC, which they located between 5-9°S. The Angola Current was considered to be a southward branch of the SECC and formed the eastern limb of the gyre. The southern and western limbs of the gyre were attributed to the offshore movement of the Benguela Current at approximately 18°S (the position of the ABFZ) and its broad meandering characteristic toward the northwest.

A more in-depth study that focused on the gyre was carried out by Gordon and Bosley (1991) and used *in situ* data collected from an extensive hydrographic station array between 1983 and 1984. Generally their results agreed well with those of Moroshkin *et al.* and they too found unequivocal evidence of a weak and climatically stationary cyclonic gyre in the eastern tropical Atlantic. They also made note of the fact that the cyclonic circulation is not evident in the surface layers due to offshore Ekman transport induced by the surface winds. Their gyre was centered at about 13°S 5°E, shifting southward with depth (i.e. at 500m it is situated at about 18°S) and had a diameter of the order of 2000km. Like Moroshkin *et al.* (1970), they define the northern and eastern boundaries of the gyre as the SECC and Angola Current respectively. They regard the ABFZ as the boundary between the Angola Gyre and the subtropical gyre (effectively the southern limb of the Angola Gyre).

Waconge and Piton (1992) looked more closely at what constitutes the northern limb of the gyre. Their motivation being that the SECC had been thought of as the main contributor to the northern limb despite the lack of observational evidence for its steadiness, meridional extent and precise path, as well as the fact that two other currents also terminate in that area (namely, the EUC and the SEUC). Both of these currents have a strong signature of zonal velocity on meridional sections, which extend into relatively shallow water and both ‘bend’ in a southeasterly direction when reaching the coast. The implication being that contribution to the northern limb of the gyre may come from any of these

currents. This agrees with the findings of Mercier *et al.* (2001) who observed that both the SEUC and the SECC contribute to the northern limb of the Angola Gyre.

The water within the cyclonic gyre is characterized by a salinity maximum and an oxygen minimum (Gordon and Bosley, 1991), which is somewhat surprising if one considers that the suspected source water (the subtropical anticyclone) does not share these characteristic water properties. Gordon and Bosley (1991) surmised that the salinity maximum arises from a regional excess in evaporation that requires a 4-10 year residence time (including fresh- water input from all of the rivers that drain into the Angola Basin) to account for the salinity difference. The oxygen minimum is also a consequence of the high residence time of water within the gyre and the enhanced productivity in the eastern tropical South Atlantic (Voituriez and Herbland, 1982).

2.7.2 The Angola Dome

The Angola Dome has been described as a dome-like feature at the terminating edge of the west-to-east shoaling thermocline ridge (Busalacchi and Picaut, 1983). The dome has been studied intermittently from about 1967 and its position appears to vary from year to year within about 2° of latitude.

Using bathythermograph and hydrocast measurements in the region of the dome, collected between 1902 and 1963, Mazeika (1967) located the Angola Dome and was able to ascertain a seasonal signal. He detected the dome to be centered on approximately 9°S 9°E at 20m and saw that it persists to a depth of about 150m. According to him, the Angola dome is only present between January and April. However, he noted that another dome structure exists during austral winter, along 1.5°S and extends zonally from 8°W to 3°E. This region corresponds to a zone of intense upwelling associated with wind-induced surface divergence that occurs as a result of the dominating easterly component of the southeasterly

trade winds. The thermocline structure of the Angola Dome is probably related to a different forcing mechanism.

The seasonal signal of the dome has been well-established (present during austral summer), though Voituriez and Herbland (1982) verify that the seasonal cycle is limited to the thermocline layer and suggest that the Angola Dome is a permanent feature at subthermoclinal levels. Because they noted that the Angola Dome extends beneath the thermocline, they suggested that the current involved in its formation is more likely to be the deeper, SEUC rather than the SECC (see Figure 2.4).

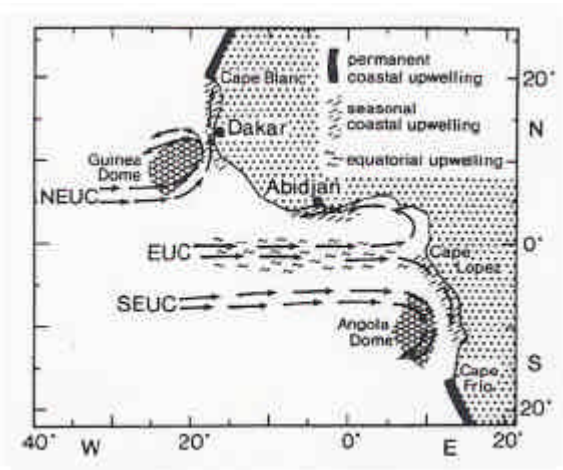

Figure 2.4: Schematic representation of the undercurrents in the equatorial Atlantic and their relation to the Guinea and Angola Domes (Voituriez and Herbland, 1982).

There have been some conflicting ideas as to whether the Angola Gyre and Dome are one and the same or not. Mohrholz *et al.* (2001) provide compelling evidence that they are in fact separate features and Stramma and Schott (1999) outline the distinctly different forcing mechanisms of each.

During a survey aboard the R.V. Poseidon in April 1999, several mesoscale cyclonic gyres (100-300km) were found to be embedded within the larger Angola Gyre, which was observed by Mohrholz *et al.* (2001) as a large area of low

dynamic height. The most developed of these mesoscale features at 9°S 8.5°E was subthermoclinal and was interpreted by Mohrholz *et al*. (2001) as the Angola Dome. Like Mazeika (1967) they observed the dome at 20m, extending to a depth of 150m and with its centre shifting southwards with increasing depth.

Their study revealed another dome-like feature beneath the ABFZ at 50m depth and centered at about 16°S 9.5°E.

According to Waconge and Piton (1992), the seasonal uplift of the thermocline, definitive of the Angola Dome is connected to the seasonal cycle of the SECC which is related to the seasonal wind fluctuation.

From a numerical simulation, Yamagata and Izuka (1995) show that the wind-field of the South Atlantic shows little seasonal variability and the horizontal divergence of the SECC or SEUC always tends to cool the region of the Angola Dome. They put forward a more complex forcing mechanism: along with patterns of divergence of flow near the thermocline, the negative surface heat flux from March through to August drives the Angola Dome diabatically.

In a review paper, Peterson and Stramma (1991) emphasize that results from previous studies show that the northern limit of the Angola Dome coincides with the SEUC, while the northern limb of the Angola Gyre is often considered to be the SECC, which along with the SEUC and the EUC (via the Gabon-Congo Undercurrent) feed the Angola Current. Refer to Figure 2.5 for a schematic representation of their conclusions. In a similar, though more recent, review paper, Stramma and Schott (1999) recapitulate the different mechanisms involved in the formation of the Angola Dome and the Angola Gyre. The Angola Dome is connected to the seasonal uplift of the thermocline as a result of lowered atmospheric pressure that causes a windstress curl that is conducive to upwelling. The Angola Gyre, on the other hand, is thought to be purely a result of the large-scale current field.

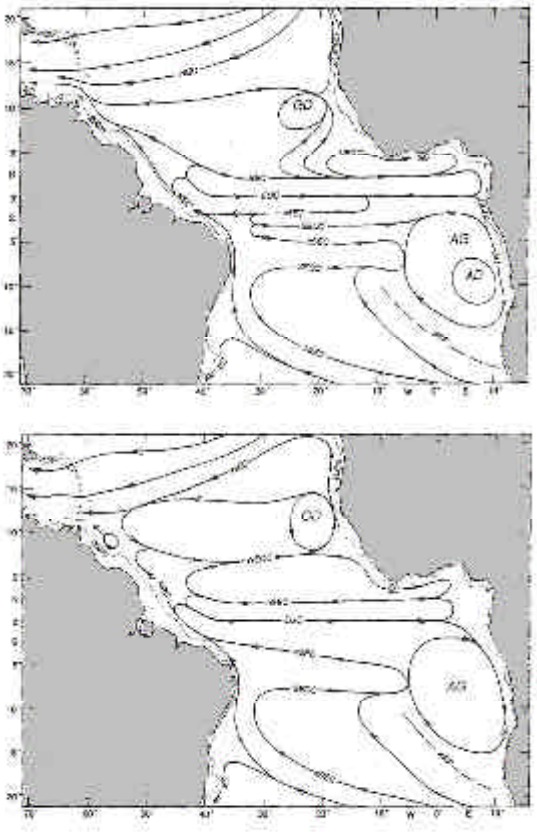

Figure 2.5: Schematic map showing the horizontal distribution in the upper 100m for austral autumn (top) and spring (bottom). Abbreviations: North Equatorial Current (NEC), North Equatorial Countercurrent (NECC), South Equatorial Current (SEC), with northern, central and southern branches (nSEC, cSEC and sSEC respectively), the South Equatorial Countercurrent (SECC), the Angola and Guinea Domes (AD and GD), the Gabon-Congo Undercurrent (GCUC), the Angola Current (AC), the North Brazil Undercurrent (NBUC) and the Angola Benguela Front (ABF). (from Peterson and Stramma, 1991)

2.7.3 The Guinea Dome

The Guinea Dome is the northern tropical counterpart to the Angola Dome. Like the Angola Dome, Busalacchi and Picaut (1983) found that the Guinea Dome corresponds to a doming of the terminating edge of a thermocline ridge. It is bounded to the south by the North Equatorial Undercurrent (NEUC), which re-circulates northwards into the North Equatorial Current (NEC). During Busalacchi

and Picaut's (1983) investigation the dome had a width of approximately 600km and was about 1500km long, the center being situated at approximately 12°N, 25°W.

More recent studies (Philander and Pacanowski, 1986; Siedler *et al.*, 1992; Yamagata and Iizuka, 1995 and Hagen, 2001) are in general agreement regarding the location and size of the Guinea Dome, i.e. ±12°N 25°W and a size of the order of 1000km in diameter. All agree that the dome is most intense during boreal summer (June to September) and Siedler *et al.* (1992) make note of the fact that it is a permanent feature present in the thermoclinal and subthermoclinal layers, moving toward the northeast in boreal winter, i.e. from 9°N 25°W in summer to 10.5°N 22°W in winter. Siedler *et al.* (1992) found considerable seasonal variations of the dome, for instance, the upward doming varied between 30-80m and the horizontal scale fluctuated between 700-1000km. Major seasonal variations occurred in the northern part of the dome, which is related to the seasonal signal of the North Equatorial Countercurrent (NECC). They also showed that the dome is elongated in a NE-SW orientation during summer, but has a more circular shape during winter.

Maps of wind stress curl such as those produced by Hellerman and Rosenstein (1983) show that the thermocline ridge corresponds with a zonal region of annual positive curl. Siedler *et al.* (1992) suggested that the upward motion of the thermocline is therefore a result of Ekman pumping due to the surface winds. The maps of Isemer and Hasse (1987) (cited in Siedler *et al.,* 1992) reveal a local maximum of upward motion in the vicinity of the Guinea Dome as well as a maximum in the seasonal variability of Ekman pumping. Similarly, McClain and Firestone (1993) calculated a maximum of Ekman pumping in the region of the Guinea Dome and related it to the generation of the dome. However, a comparison of the local Ekman vertical velocity fields and geostrophic flow and geopotential anomaly in the region of the dome are not well correlated. The implication of this is that the Guinea Dome is probably not forced by local winds,

but rather by the large-scale wind field. This is in accord with Busalacchi and Picaut's (1983) hypothesis that the dome is a relatively stationary feature due to the interplay of local Ekman pumping in the north and non-local equatorial waves from the south. This is also consistent with the outcome of Yamagata and Iizuka's (1995) study in which they concluded that the Guinea Dome develops due to a divergence of heat transport that is related to the local windstress curl. Furthermore, they showed that the coastal Guinea area is warmed twice a year by the northward propagation of downwelling Kelvin waves.

2.7.4 Costa Rica Dome

Like the Angola and Guinea Domes, the Costa Rica Dome, in the eastern tropical Pacific, is situated at the eastern terminating edge of the ridging, zonally oriented thermocline. From *in situ* data (Fiedler, 2002) and using a numerical model (Umatani and Yamagata, 1991) the dome has been located at about 8°N 91°W. Its size varies seasonally and according to Fiedler (2002), its east-west diameter is 300km in June and 1000km in November.

In austral summer/autumn a cyclonic flow exists that encompasses the Costa Rica Dome: the NECC flows eastwards and is deflected poleward at the coast, forming the northward Costa Rica Coastal Current (CRCC), which then flows into the westward NEC.

The model results of Umatani and Yamagata (1991) show that the dome develops in late boreal spring and matures in boreal summer and that this process is closely related to the seasonal migration of the ITCZ and its effects on the NECC.

Fiedler (2002) regarded the Costa Rica Dome as a permanent feature in the thermocline in the sense that the upward curve of the thermocline always exists in that area. A seasonal signal exists in terms of its size and location. Like

Umatani and Yamagata (1991), he identified the ITCZ and its associated windstress curl patterns to be closely related to the seasonal variability of the Costa Rica Dome. Although strikingly similar to the generation mechanism of the Guinea Dome, the Costa Rica Dome is influenced by a coastal wind jet during winter (Fiedler, 2002).

According to Picaut (1985), the effect of Rossby waves is dominant for seasonality of the Angola Dome, whereas it is only significant to the seasonal variability of the Costa Rica Dome. This is consistent with the fact that the seasonal signal is dominant in the eastern tropical Atlantic, whereas the eastern tropical Pacific has a prominent annual signal. The strong seasonal of the Atlantic compared to the Pacific is probably related to the fact that the zonal extent of the Atlantic is about three times smaller than that of the Pacific (Philander and Chao, 1991).

Based on the symmetry observed in the Angola and Guinea Domes, their relationship to equatorial currents and the partial parallel in the eastern Pacific (the Costa Rica Dome), Voituriez (1981) proposed the possible existence of a ‘Peru Dome’ that is likely to be situated near 8°S, 85°W. According to Voituriez (1981), the hypothetical Peru Dome is limited to the subthermoclinal layers because, unlike the other domes, the wind stress distribution in its vicinity is not conducive to upwelling in the surface layer. Evidence of the so-called ‘Peru Dome’ has yet to be found.

CHAPTER THREE:
DATA

The data for this dissertation is based primarily on the three-dimensional velocity field and the thermohaline variables simulated by the OPA/TOTEM (Océan Parallélisé/ Trois Océans Tropicaux) ocean general circulation model (OGCM). Output from a higher resolution model, CLIPPER, was made available near the end of this investigation and was therefore only briefly analyzed. The ocean-atmosphere connection is explored by analysis of the wind-field obtained from the European Remote Sensing (ERS 1 & 2) satellite. The following section presents a description of the parameters of both the model and satellite data sources.

3.1 OPA/ Ocean General Circulation Model (OGCM)

The OPA model was developed at the Laboratoire d'Océanographie Dynamique et de Climatologie (LODYC) by Delecluse *et al.* (1993), cited in Maes *et al.* (1998) and updated by Madec *et al.,* 1998. It is a primitive equation model that aims to resolve both global and regional ocean circulation patterns. Its prognostic variables are the u-, v-, and w- velocity components, temperature and salinity.

Monthly mean outputs of each of the prognostic variables from January 1979 to December 1999 are examined in this thesis. The region of interest extends from the equator to 20°S and from the Greenwich Meridian to the African coast. Although the data is explored to a depth of 300m, in-depth analyses concentrate on the upper 100m.

The model is forced by zonal and meridional wind stress, net surface solar radiation, net surface heat flux and net water flux (evaporation minus precipitation, including river run-offs).

3.1.1 The primitive equations

The model describes the ocean in terms of the primitive equations (i.e. the Navier-Stokes equations) with adequate boundary conditions (including a rigid lid boundary as the sea-surface). The following assumptions are made, based on their insignificant influence on the general circulation:

- The spherical Earth approximation (gravity is parallel to the Earths radius).
- The thin-shell approximation (the depth of the ocean is negligible compared to the radius of the Earth).
- The turbulent closure hypothesis (turbulent processes are expressed in terms of large-scale features).
- The Boussinesq hypothesis (i.e. density variations are ignored except in their contribution to the buoyancy force).
- The hydrostatic hypothesis (the vertical pressure gradient balances the buoyancy force).
- The incompressibility hypothesis (the three-dimensional divergence of the velocity field is zero).
- The sea surface is assumed to be a rigid boundary in order to filter the fast surface gravity waves.

The primitive equations that ensue from the aforementioned approximations and assumptions are discretized on a three- dimensional Arakawa-C-type grid, that has prescribed depth (Z-) levels (Madec *et al.*, 1998) and are written as follows (Blanke and Delecluse, 1993):

$$\partial_t U_h = -[k.(\nabla \times U_h) + f]k \times U_h - W\partial_z U_h - r_o^{-1}\nabla_h(P + 0.5\, r_o U_h^{\,2}) + F^u(U) \qquad (3.1)$$

$$\partial_t T + \nabla.(TU) = F^T(T) \qquad (3.2)$$

$$\partial_t S + \nabla.(SU) = F^S(S) \qquad (3.3)$$

$$\partial_z P = -rg \qquad (3.4)$$

$$\nabla.U = 0 \qquad (3.5)$$

Where, U is the velocity component (u, v, w), U_h its horizontal projection, T, S and P are the temperature, salinity and pressure respectively. k is the local vertical axis, f is the Coriolis parameter and g is the gravitational acceleration. $?_o$ is a reference value for density ($10^3 kg.m^{-3}$) and the actual density, ?, is computed from the Eckhart nonlinear (1958) equation of state. F^U, F^T and F^S define the sub-grid processes, which include eddy viscosity and diffusivity, as well as the effects of solar radiation. The equations definitive of these processes are in Blanke and Delecluse (1993).

3.1.2 The time-stepping scheme

The time stepping of the model is achieved with a basic leapfrog differencing structure associated with an Asselin (1972) time filter, while a forward scheme is used for the horizontal turbulent diffusion terms and a backward one for the turbulent vertical diffusion term (Maes *et al.,* 1998). Each time-step is set to 3600s to fulfill the requirements of the numerics.

3.1.3 Boundary conditions

No-slip boundary conditions and no flux conditions for heat and salt are applied to the bottom and coastal boundaries. Whereas the surface fluxes of momentum, salinity and heat are prescribed through the specifications of the wind-stress (provided by the European Centre for Medium-Range Weather Forecasts, ECMWF, prior to 1992 and then by ERS), the fresh water budget (i.e. river runoff) and the non- penetrative portion of the solar flux at the sea surface (Maes *et al.*, 1998).

3.1.4 The TOTEM configuration

The TOTEM (Trois Oceans Tropicaux) grid of the OPA model has been especially developed for studies of equatorial dynamics. The domain covers the

tropical oceans, between 45°N and 45°S. The resolution of the zonal mesh increases in places where coastline crosses the equator and decreases toward the centre of the basin. In the vicinity of the equator and near the margins of the basin, the zonal resolution is 0.33°, decreasing to 0.75° in the middle of the ocean basin. The meridional resolution is irregular; 0.33° at the equator, increasing gradually to 1.5° at the poleward limits of the grid. The vertical mesh has 30 layers, extending to a depth of 5000m. To a depth of approximately 150m, the vertical resolution is 10m and increases gradually to the bottom layer. The bottom topography is defined by the ETOPO5* data set, averaged over each grid box.

In the model there is no restoring in the oceanic interior in the temperature and salinity between 20°N and 20°S. Outside this free-restoring belt, a linear restoring term is applied toward the monthly mean temperature and seasonal salinity fields of Levitus (1982) (Masson and Delecluse).

3.1.5 The CLIPPER ATL6 configuration

The main objective of the CLIPPER project is to model the Atlantic Ocean circulation at a high resolution. The CLIPPER numerical experiments are jointly carried out by four French laboratories (LEGI in Grenoble, LEGOS in Toulouse, LODYC in Paris and LPO in Brest). The CLIPPER ATL6 model is configured using the same primitive equation code as OPA.

The model domain encompasses the Atlantic Ocean from 98.5°W to 30°E and from 76°S to 70°N and has a horizontal, isotropic (1/6°) Mercator grid. As a result the resolution decreases from about 5km at high latitudes to 18.5km at the equator. The vertical grid consists of 43 layers for temperature, salinity and velocity parameters, with analytical stretching for finer resolution at the surface.

* Marine Geology and Geophysics Division, National Geophysics Data Centre. Boulder, Colorado.

The resolution of the vertical grid is constant in the upper levels (approximately 10m) and decreases rapidly below 200m and at depth is once again constant (about 100-200m).

The bottom topography is based on a high resolution bathymetry field derived from altimetry and in situ measurements (Smith and Sandwell, 1997). However, the domain is limited to 72°N and 72°S and it is therefore necessary to use the global Terrainbase 5 dataset (NOAA) at the southern latitudes of the CLIPPER domain. The bathymetry is interpolated onto the model grid using a bilinear interpolation using the 4 nearest points.

3.2 European Remote Sensing Satellites (ERS 1 & 2)

The European Remote Sensing satellites, 1 and 2, were launched in July 1991 and April 1995 respectively and are operated by the European Space Agency (ESA). The ability of satellite-borne radars, to obtain high temporal and spatial coverage of sea surface data and their ability to do so in all-weather conditions has provided the means to a better understanding of oceanic circulation and to the Earths climate in general. Surface parameters are measured by three instruments on the ERS 1 and 2 satellites; an altimeter, a synthetic aperture radar (SAR) and an Active Microwave Sensor (AMI) or scatterometer, dedicated to measuring the sea surface wind field.

The zonal and meridional wind data used within this work was processed by the French ERS Processing and Archiving Facility (CERSAT, Centre ERS d'Archivage et de Traitement), a division of the French Research Institute for exploitation of the sea (IFREMER, Institut Français de Recherche pour l'Exploitation de la Mer). Gridded weekly- or monthly- mean data with a spatial resolution of 1° x 1° extending from 82°S to 82°N and from 180°W to 180°E is freely available from http://www.ifremer.fr/cersat. The gridded product used is the monthly mean January 1992 to December 1999 zonal and meridional wind speeds.

3.2.1 The Active Microwave Sensor (scatterometer)

The ERS scatterometer operates at a frequency of 5.3GHz (the C-band) in order to minimize the atmospheric effects of rain and water vapour. Three beams from the three antennae of the radar sample the sea surface at azimuth angles of 45°, 90° and 135° with respect to the path of the satellite. The swath illuminated by the radar is 500km in width and has an angle of incidence between 18° to 57°. The measurements are divided into 50km-wide overlapping cells so that the centers of each cell are 25km apart. The backscatter coefficient (s_0), measured by the three beams, is then calculated for each 25km x 25km grid cell (http://www.eumetsat.de/en/).

3.2.2 Calibration

The scatterometer measures radar backscattering from surface waves and from this wind speed and direction is derived (Sheng *et al.,* 2002). In the open ocean, wind speed and direction measurements are derived from the backscattering coefficients by means of the Bragg mechanism: the backscattering coefficient is directly related to the surface wave power density spectrum within the wavelength range of the scatterometer. Therefore, as the surface wind increases, the spectral power density decreases and so does the backscattering coefficient.

Calibration of the sensor data is one of the main tasks required in processing raw scatterometer data. It involves a two step procedure; the determination of an empirical model (an example is given in equation 3.6) and the development of an algorithm that is able to retrieve the surface wind data (equation 3.7). Another important task involved in calibration is the validation of the accuracy of the backscatter coefficients and the wind estimates derived from them by comparisons with other sources of data (Piolle *et al.,* 2002).

The most reliable method of inversions of scatterometer measurements data rely on empirically-derived algorithms (Bentamy *et al.*, 1996). The following model-

formula is typically used to reveal the empirical relationship between the backscatter coefficient and wind speed and direction (Piolle *et al.*, 2002):

$$s_0 = \sum_{j=0}^{k} A_j(l, P, q, U)\cos(jc) \qquad (3.6)$$

Where, s_0 is the backscatter coefficient and k refers to the number of harmonics (i.e. the degree to which s_0 uses cosines as orthogonal basis), *?* is the wavelength of the scatterometer, *P* is the polarization, *T* is the radar incidence angle, *U* is the wind speed and *?* is the angle between the wind direction and the radar azimuth. A_j *(?, P, T, U)* are the model coefficients to be determined through regression analysis.

The actual wind vector at a given height is obtained by minimization, in *U* and *?* space, of the Maximum Likelihood Estimator (MLE) function. This function is given by:

$$F = -\sum_{j=1}^{i=N} \frac{(s_i^0 - s_m^0)^2}{Var(s_m^0)} \qquad (3.7)$$

Here, s_0 and s_m are the measured (obtained from 3.6) and estimated backscatter coefficients respectively, $Var(s_m^0)$ is an estimation of the variance of s^0 and *N* is the number of measured backscatter coefficients used in the wind vector estimation.

This approach produces up to four estimates of wind speed and direction. It is therefore necessary to conduct an ambiguity removal procedure so that the most probable wind vector estimate is selected (Piolle *et al.,* 2002). The ambiguity removal procedure is documented in Quilfen *et al.* (1993). A limitation of the ERS scatterometer coverage is the fact that it is discrete in both time and space. Its asynoptic nature is due to its limited swath- width and its quasi-polar orbit.

3.2.3 Gridded Swath Data

Details of the gridding procedure of the polar orbit satellite data are given in Bentamy *et al.* (1996). In order to overcome the problem of asynopticity, an objective method of statistical interpolation was performed on the swath data in order to reconstruct the gaps of the discrete observations over each time- period.

CHAPTER FOUR:
METHODS

Climatologies of the monthly mean OPA/TOTEM, CLIPPER and ERS products were created for analyses of the seasonal signals. In the case of the OPA data, the climatology was calculated as the average of each month from 1979 to 1999. The climatology for the ERS data was created from the 8 years of data, spanning January 1992 to December 1999.

4.1 OPA- model data (velocity field and hydrothermal parameters)

Horizontal and vertical sections of the OPA- model parameters are investigated in this study. From a preliminary inspection of horizontal temperature plots at several different depths, it became clear that the upwelling of the thermocline, which is associated with a cyclonic circulation feature in the Angola Basin, is most distinct at 45m. All horizontal sections analyzed in this thesis, including temperature, salinity and all velocity components are therefore plotted at a depth of 45m. Zonal and meridional vertical sections were chosen at latitudes and longitudes that best approximated the center of the cool feature at its mean annual position. The subsequent analyses take into account that the zonal and meridional sections do not cross the dome/ gyre center precisely because the dome/ gyre varies in size, shape and position throughout the year. It was decided to extend the vertical sections to a depth of 100m, in order to obtain greater clarity in the region of interest, i.e. the thermocline and mixed layer. Although analyses were confined to the upper- 100m, deeper sections were briefly examined in order to resolve any subthermoclinal structure that might be present.

4.1.1 Divergence

Divergence or convergence of the horizontal velocity fields can lead to vertical motion in the form of downwelling or upwelling. The probability that the circular cool feature is associated with divergent flow of the zonal and meridional velocity

fields and the subsequent upward motion of deeper waters is investigated by calculating and plotting the regions of divergence to a depth of 100m.

Regions of convergence and divergence were calculated using equation 4.1, which is based on the principle of conservation of mass.

$$-\frac{\partial w}{\partial z} = \frac{\partial u}{\partial x} + \frac{\partial v}{\partial y} \qquad (4.1)$$

Again, the irregular grid of the OPA model was taken into account when calculating the fields of divergence and convergence.

4.2 ERS- satellite data (surface wind speed)

The wind data was obtained as monthly mean zonal and meridional wind speed components at the sea surface. In order to study the effect of wind on the ocean, the wind stress, windstress curl and Ekman pumping were calculated from the climatology of the components of the wind speed.

4.2.1 Wind stress, windstress curl and Ekman pumping

The frictional force acting on the sea surface as a result of the surface wind is the wind stress (Brown et al., 1989), which was calculated in this study following the method of McClain and Firestone (1993):

$$(t_x, t_y) = r_a C_d |U_{10}| (u_{10}, v_{10}) \qquad (4.2)$$

Where t_x and t_y are the zonal and meridional wind stress components respectively. U_{10} is the absolute wind speed of either the zonal (u_{10}) or meridional (v_{10}) wind speed. ?$_a$ is the density of air and C_d is the drag coefficient, which is given by:

If, $0=U_{10}<11 m.s^{-1}$,

$$C_d = 0.0012 \quad (4.3)$$

If $U_{10}=11 m.s^{-1}$,

$$C_d = 0.00049 + 0.000065U_{10} \quad (4.4)$$

The net amount of transport of the ocean induced by surface winds depend not on the absolute value of wind stress, but rather on its torque, i.e. its tendency to cause rotation around the vertical (Brown *et al.,* 1989). This force ($curl_h$) is known as the 'windstress curl' and is calculated in the following way:

$$curl_h = \frac{\partial t_y}{\partial x} - \frac{\partial t_x}{\partial y} \quad (4.5)$$

Positive windstress curl is characterized by surface convergence and downwelling of the thermocline, while negative curl is associated with divergence and upwelling. For example, the downwelling signal of the subtropical gyre is a result of positive windstress curl, whereas areas of upwelling in the Benguela are partly a consequence of negative windstress curl. The curl is strongest at 30° where meridional motion dominates and is weakest at 15° and 45°, where flow is almost entirely zonal (Brown, 1989). There are difficulties in calculating Ekman processes at the equator as the coriolis parameter is zero there. Similarly one should separate contributions to upwelling, from 'windstress curl' and Ekman divergence at a coastal boundary. (Tomczak and Godfrey, 2003).

Wind fluctuations that occur on longer time-scales than one day result in a surface current that moves at an angle to the direction of the wind stress (to the left in the southern hemisphere and the right in the northern hemisphere). This flow is known as Ekman drift after its first investigator. The importance of Ekman transport is not confined to the surface horizontal flow, but extends into the deeper layers of the ocean and can also induce vertical motion. The vertical

motion comes about in places where Ekman transports converge or diverge resulting in downward or upward motion respectively. This process is known as Ekman pumping (Tomczak and Godfrey, 2003) and is defined as follows:

$$w_E = \frac{curl_h}{f\, r_w} \tag{4.6}$$

Where W_E is the vertical Ekman pumping velocity, f is the coriolis parameter* and ?$_w$ is the density of water (taken to be 1000kg.m^{-3}). Like windstress curl, Ekman pumping is not defined near the equator and along coastlines.

* f = 2Ω sinΦ, where Ω is the angular velocity of the Earth and Φ is the latitude.

CHAPTER FIVE:
RESULTS AND DISCUSSION

Whilst this research encompasses thermohaline and circulation features of the Angolan Basin in general, the primary objective is to gain a better understanding of the approximately circular-shaped cool feature within its realm as resolved by the OPA/TOTEM model output. Whether this feature is the Angola Dome, noted by Voituriez (1981) and Yamagata and Iizuka (1995) or the Angola Gyre, detected by Gordon and Bosley (1992), is not clear at this stage.

5.1 Thermohaline Characteristics

The monthly mean temperature and salinity fields of the Angolan Basin have been closely examined to a depth of 105m. A preliminary inspection of horizontal plots of each parameter at 10m intervals from a depth of 5m to 105m, gives an indication of the vertical structure of salient hydrographic features of the Angolan Basin such as the Angola Gyre and the ABFZ.

The convergence area of warm Angolan Current water and cool water of the Benguela Upwelling regime, the ABFZ, is situated at approximately 16°S and is present as a region of sharp meridional gradients of temperature and salinity. The strong meridional temperature gradient indicative of the ABFZ is most prominent at the surface, but is evident from the surface to a depth of about 35m, whereas the salinity front is well-defined from the surface to a depth of at least 55m. Both the temperature and salinity fronts of the ABFZ are progressively more diffuse at greater depths.

The main feature of interest is an isolated region of relatively cool water. It starts to become evident at 35m and is more distinct at 45m. Another aspect worth noting is a cool ‘ribbon’ of water that extends northwards at the coast and moves offshore at approximately 2.5°S. It is present from the surface to at least 45m and gets progressively wider and extends further offshore with greater depth. This

cold tongue was also noted by Yamagata and Iizuka (1995), who associated it with the cyclonic Angola Gyre.

Because the clearest signal is at 45m depth, the next section presents an analysis of the temperature and salinity fields at this depth. Details of the horizontal extent and seasonal variations of the cool feature are discussed.

5.1.1 Monthly mean composites at 45m

Temperature

Figures 5.1a-f and 5.2a-f are twenty-one year monthly mean composites of temperatures at 45m, from 10°N to 20°S and from 10°W to the African coast. They reveal the presence of a well-defined, cool feature that is 2-3° cooler than the surrounding water and is particularly distinct between September and November and also in January and February, centered at approximately 5°S, 5°E. In all instances the feature has an elongate shape, oriented in a NW-SE direction, spanning about 10 degrees (1100km) of latitude and 5 degrees of longitude (550km). During all other months of the year, a tongue of cool water extends in a north-westerly direction from the southwest African coast. The temperature output from the OPA/TOTEM model agrees well with the 45m temperature plots of Yamagata and Iizuka (1995), which made use of a model with meridional and zonal resolution of 0.5°. A more detailed description of the seasonal variation of the temperature signal at the 45m depth level follows.

Appendix 1 shows plots of the temporal variation of temperature between successive months at a depth of 45m and are calculated by subtracting the temperatures of the previous month from the present month. As a result, positive (negative) values occur where temperatures increase (decrease) in a particular region between consecutive months. The temperature variations from month to month are plotted from 10°N to 20°S and from 10°W to the African coast (Appendix 1). These images were created in order to more clearly visualize the

variation of temperature from month to month. They also serve to aid the analysis of possible associations between the monthly variation of temperature and the size and position of the cool feature that is situated at approximately 5°S 5°E at the 45m depth level.

Between May and July (Figures 5.1e-f & 5.2a) a tongue of cool water extends northwards, bends offshore from about 5°S and spreads in a zonal band across the equator to at least 10°W. Plots of the temperature variation between consecutive months (Appendix 1) unambiguously show that the equatorial zone from about 2°N to 3°S experiences most intense cooling between the successive months. Less extreme cooling extends progressively northward and southward from the equatorial region with greater proximity to the coast. The fairly extreme regime of cooling in the equatorial zone and along the coast is separated from cooling to the south (south of a NW-SE oriented line from 6°S to 17°S) by a NW-SE oriented band (±5° width) of progressively warmer water. The general cooling at this time may be a result of seasonal cooling, while the more intense cooling in the region of the equator may be induced by a localized upward displacement of the thermocline (the structure of the thermocline is analyzed in more detail in section 5.1.2). Similarly, the band that experiences repeated warming each month between May and July is perhaps a result of a deepening of the thermocline in this region.

Between July and August, although cooling occurs in the majority of the study region (Appendix 1), temperatures in August are consistently warmer in a narrow zonal band, spanning about 1.5°N to 2°S, as well as in a narrow coastal strip that extends as far south as 14°S. It is probable that the equatorial region that is significantly warmer in August than in July corresponds to a southward movement of the thermocline ridge, which was situated in the equatorial region between May and July. The warming along the coast may be related to a deepening of the thermocline in this region, resulting in the better-defined, more

circular shape of the cool feature (NW-SE oriented and centered on ± 3°S 5°E) in August.

In September (Figure 5.2c) the cool feature is well-defined and is distinctly separate from the coast, with its centre situated at approximately 5°S 5°E. The isolation of the cool feature in September is likely to be associated with the intense warming along the coast that may be related to a continued downward displacement of the thermocline there. In October this cool feature appears slightly further south- and eastward (±6.5°S 7°E) and as an even more distinct and isolated feature (Figure 5.2d). The fact that the feature appears more well-defined in October is perhaps due to continued warming to the east of it (Appendix 1), while the warming to the north of it is probably related to the southward movement of the cool feature.

In November (Figure 5.2e), a zonal equatorial band, broadening gradually from about 2° near 10°W to 10° at the coast is cooler than during October. South of the region of cooling is an area dominated by warming, particularly along the coast, north of and within the northern limb of the cool feature that was present during October. A region of slight cooling exists south of the band of intense warming. In terms of thermocline structure, this pattern of warming and cooling can be explained as follows; the upward doming of the thermocline that results in the cool feature evident in the 45m sections shifts southward and deepens, thus explaining the relatively weak cooling that occurs south of very intense warming. The smaller horizontal extent of the cool feature (centered near 7°S 5°E) at the 45m-horizon in November can be explained by the deepening of the ridge in the thermocline. The cooling near the equator is possibly related to the generation of a new cool feature evident in Figure 5.2e (at 2.5°E on the equator) by an upward displacement of the thermocline in that region.

The pattern of spatial warming and cooling that occurs between November and December is very similar to the temperature variation between October and

November, implying that similar processes continue to influence the thermal structure in this area. The upward displacement of the thermocline near the equator intensifies, while the comparable feature to the south moves further southward and deepens somewhat. The temperatures at 45m (Figure 5.2f) reflect this process by the almost complete dissolution of the cool feature that was centered near 7°S 5°E in November and the initiation of a cool, tongue-like feature with its temperature minimum centered near 2°S 7°E.

By January (Figure 5.1a), the tip of this cool tongue evolves into a cool feature that is isolated from the coast, with its centre situated at approximately 5°S 8°E. The formation of the isolated cool feature may be associated with intense warming in the equatorial region and, more especially, along the coast between December and January. A deepening of the thermocline along the coast and the southward movement of the thermocline ridge in the equatorial region are likely processes resulting in the relative warming between December and January in these regions. The smaller and less distinct nature of the cool feature, centered near 6.5°S 7.5°E, in February is perhaps a result of general seasonal warming.

From March through to April (Figures 5.1c-d) general warming occurs throughout the region of study, though during April warming is limited to a region south of a line extending from about 10°S at the coast to 2°S at 10°W. North of this line is a band of cooling, broadening toward the coast. The general warming trend results in the diminishing of the distinct cool feature. In March, only a cool tongue, extending in a north-westerly direction from 15°S to 5°S, to which the feature seems to be related remains. In April the tongue begins to retreat in a south-easterly direction, toward the region of the ABFZ.

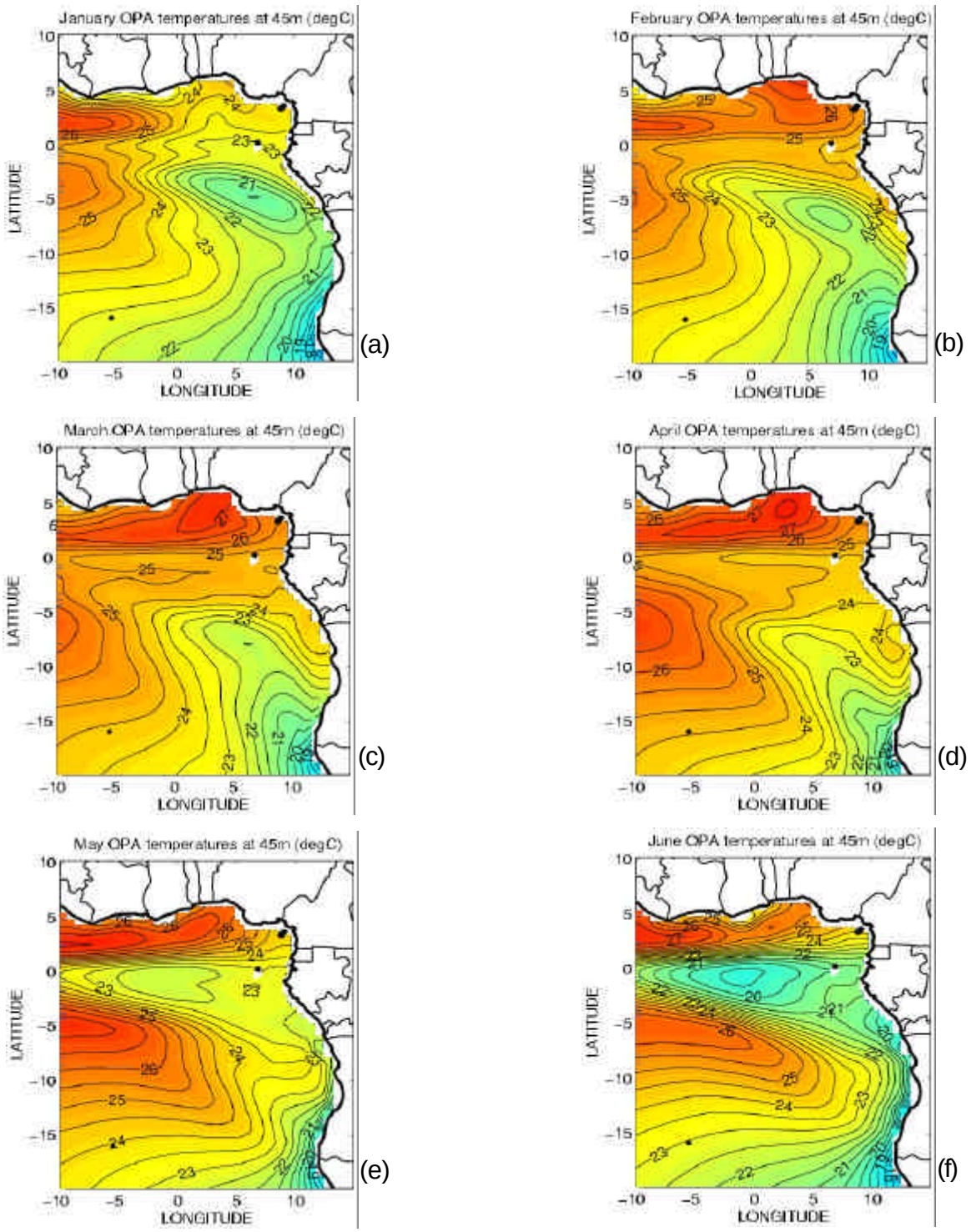

Figure 5.1(a-f): Monthly mean OPA/TOTEM temperatures (°C) at a depth of 45m (January to June). The contour interval is 0.5°C.

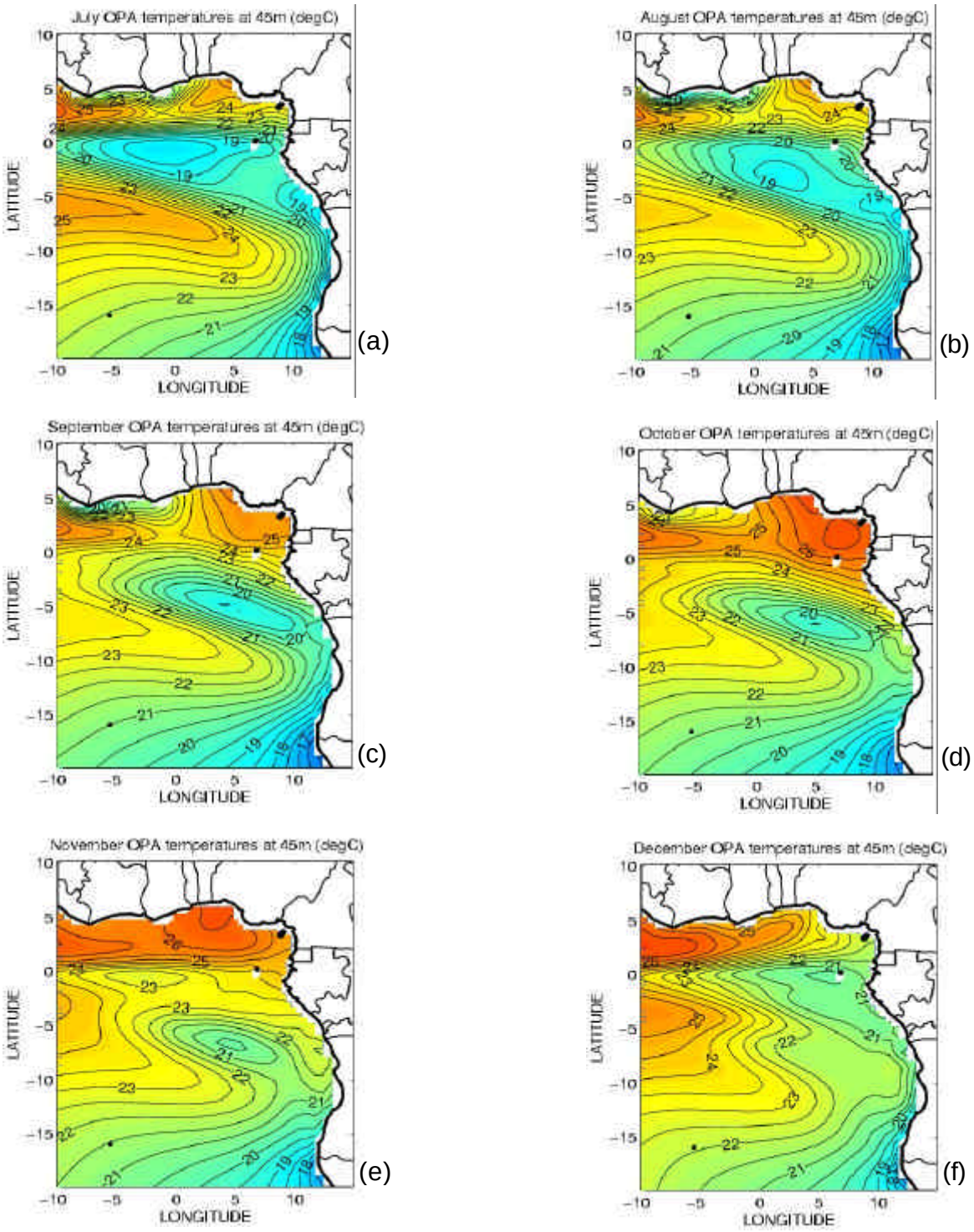

Figure 5.2(a-f): Monthly mean OPA/TOTEM temperatures (°C) at a depth of 45m (July to December). The contour interval is 0.5°C.

The slight cooling near the equator in April (Appendix 1) is likely to be the forerunner of the more intense cooling in this region from May to July. The progressive cooling is tied to a successive upward displacement of the thermocline, which presents a region of significantly cool water in the equatorial region during winter at the 45m depth level. The southward movement of the upward displacement of the thermocline in spring is therefore reflected by the southward shift of the isolated cool feature. The cool feature disappears in December and is replaced by a similar, though less distinct, feature to the north, which gradually moves southward in January and February when its signal at a depth of 45m is a pseudo-circular region of relatively cool temperatures.

Salinity

Horizontal plots of monthly mean salinities at 45m (Figures 5.3 & 5.4) show that between May and August (Figures 5.3e-f & 5.4a-b) a relatively narrow tongue of fresh water extends offshore in a north-westerly direction from about 10°S at the coast. The northern boundary of the fresh tongue forms a relatively intense salinity front with a zonal band of highly saline waters in the equatorial region. This front coincides with the zonal cross-section of the large cool feature that is situated near the equator between May and August. The lower salinity tongue that exists slightly south of the gyre probably originates from the low salinity upwelling regime at the coast and perhaps from Congo River discharge and precipitation. The implication of this is that fresher water advects offshore and saline water moves onshore at the positions of the southern and northern limbs of the cool feature respectively.

In September and on until November (Figures 5.4c-e) when the circular-shaped cool feature is most distinct and moves southward, the salinity front once again zonally crosses the cool feature approximately at its centre and is also oriented in a NW-SE direction. This reinforces the idea that an onshore flow exists at the northern limb of the cool feature and an offshore flow at its southern limb.

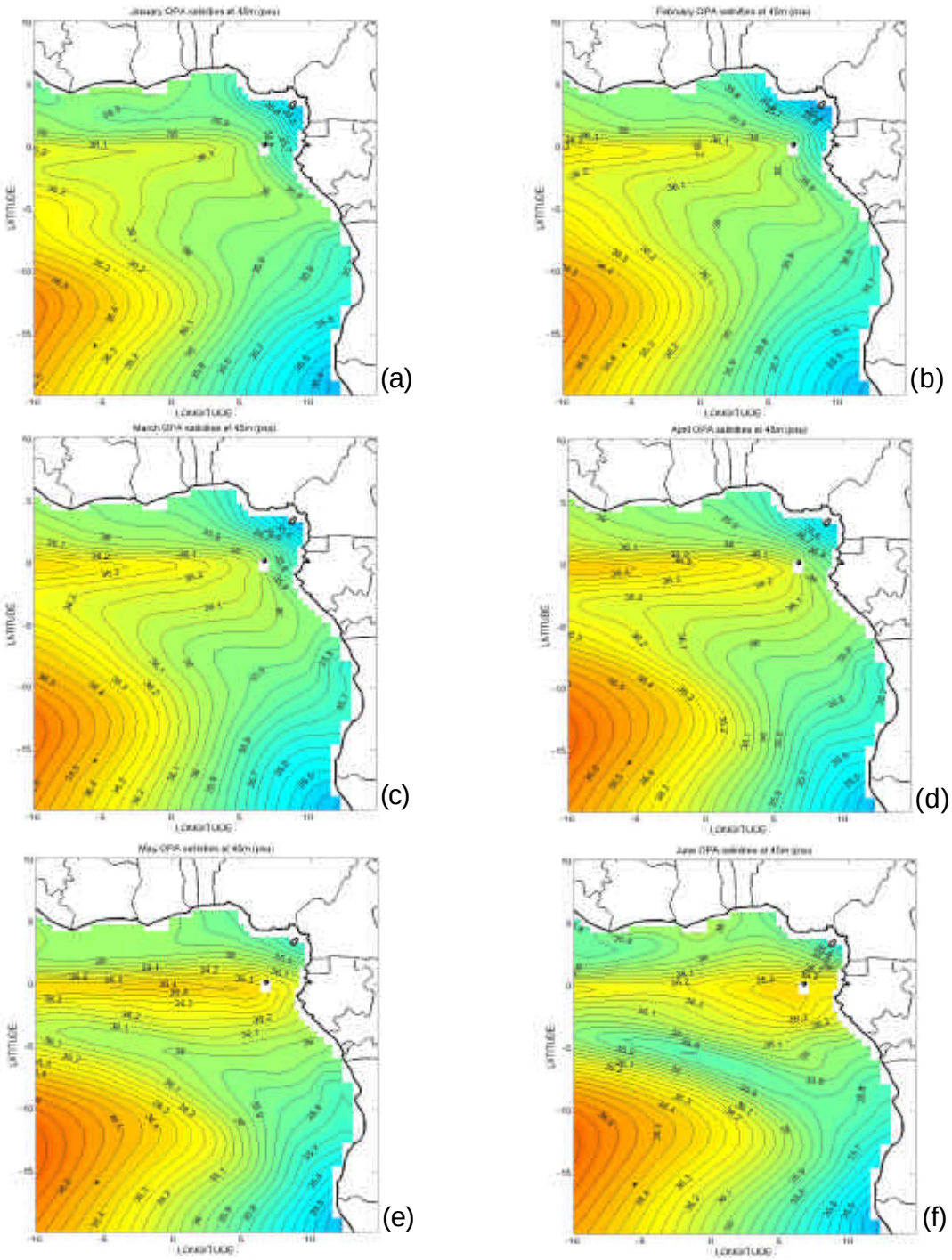

Figure 5.3(a-f): Monthly mean OPA/TOTEM salinities (psu) at a depth of 45m (January to June). The contour interval is 0.05psu.

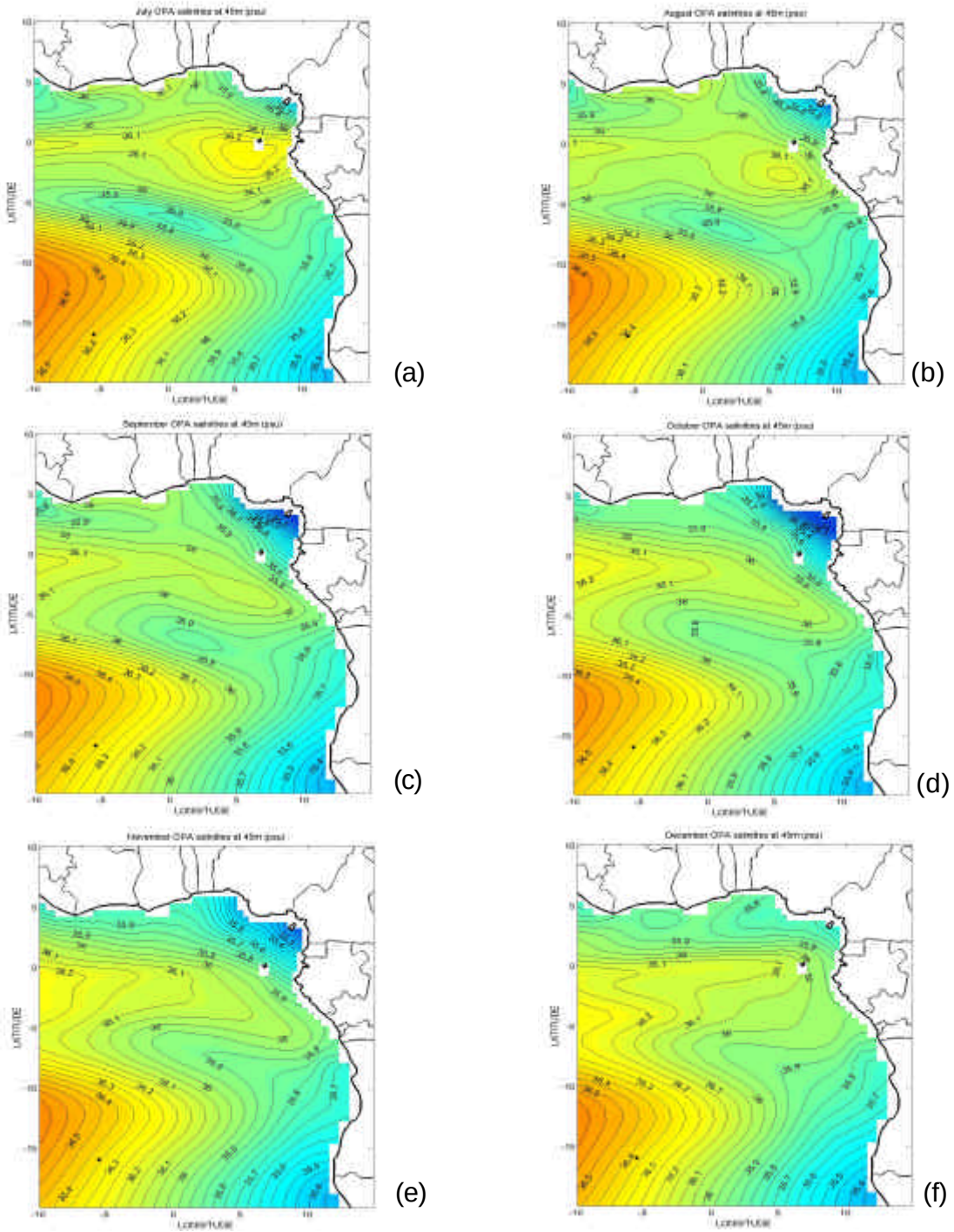

Figure 5.4(a-f): Monthly mean OPA/TOTEM salinities (psu) at a depth of 45m (July to December). The contour interval is 0.05psu.

As the cool feature becomes progressively smaller between September and November, the high salinity tongue at its northern limb becomes saltier and the lower salinity tongue at its southern limb gets fresher and retreats toward the coast.

Between December and February (Figures 5.4f & 5.3a-b) the saline tongue in the equatorial zone splits into two branches; one near the equator and another between 3-5°S (these are perhaps associated with the EUC and SEUC respectively). The branch near the equator is more distinct (i.e. narrow and more saline) and extends zonally across the equator to at least 5°E. The southern branch is more diffuse and west of 5°E it bends slightly southward. It is the southern branch of this high salinity tongue that is situated at the northern limb of the cool feature in December, January and February. The lower salinity region that defines the southern limb of the gyre is not as significant and retreats toward the coast slightly between December and February.

In March and April (Figures 5.4c-d) the cool tongue that extends in a north-westerly direction from the coast is associated with a similarly positioned tongue of lower salinity. The high salinity tongue in the equatorial zone intensifies (i.e. it narrows and the salinity increases), while the temperatures in that region drop. This could be a result of two processes; an upward displacement of the thermocline in that region and a continued (and perhaps, strengthening) eastward current, carrying more saline water toward the coast.

5.1.2 Vertical configuration

In order to investigate the vertical structure of the cool feature, meridional and zonal sections (5°E and 5°S respectively) of monthly mean temperatures have been plotted to a depth of 100m. The positions of the sections were chosen to best intersect the centre of the gyre at all times of the year. As well as the sections, three-dimensional plots of the thermocline depth were created,

accommodating a more complete image of the upward displacement of isotherms, characteristic of the cool feature. The depth of the thermocline was identified as the depth of the steepest temperature gradient in the vertical.

Thermocline structure

Three-dimensional plots of thermocline depth (Figures 5.5 & 5.6; refer to Appendix 2 for a contour plot) reveal and, to an extent, verify the manner in which the vertical thermal structure of the Angola Basin is related to the cool feature evident in the monthly mean temperature plots at 45m. Most conspicuously they show that throughout the year a general trend seems to be the shoaling of the thermocline from west to east. They also reveal a zonally oriented, ridge- trough-ridge structure superimposed on this during certain months of the year.

Two distinct ridges of the thermocline are evident in January, February and March (Figures 5.5a-c). In January the shallower and latitudinally broadest ridge lies in a NW-SE orientation, centered on about 5°S. Between ±45-60m, the eastern edge of the thermocline-ridge deepens, effectively resulting in an elongate, isolated cool feature, with its centre at approximately 5°S 8°E. This doming results in the cool feature evident in the horizontal temperature plots at 45m. A narrower ridging of the thermocline is cantered at 3°N and is separated from the ridge to the south by a shallow, zonally oriented, trough at the equator. In February the two distinct ridges are still present, however both are significantly smaller and move slightly southward. In March the thermocline deepens and the peak of the ridge at approximately 7.5°S is situated deeper than 45m and therefore does not appear on the horizontal temperature plots in the previous section.

In April (Figure 5.5d) the thermocline ridge to the south deepens somewhat and is not characterized by a distinct peak, whereas the ridge to the north remains distinct and its peak is 5m shallower than during March. The two ridges are only

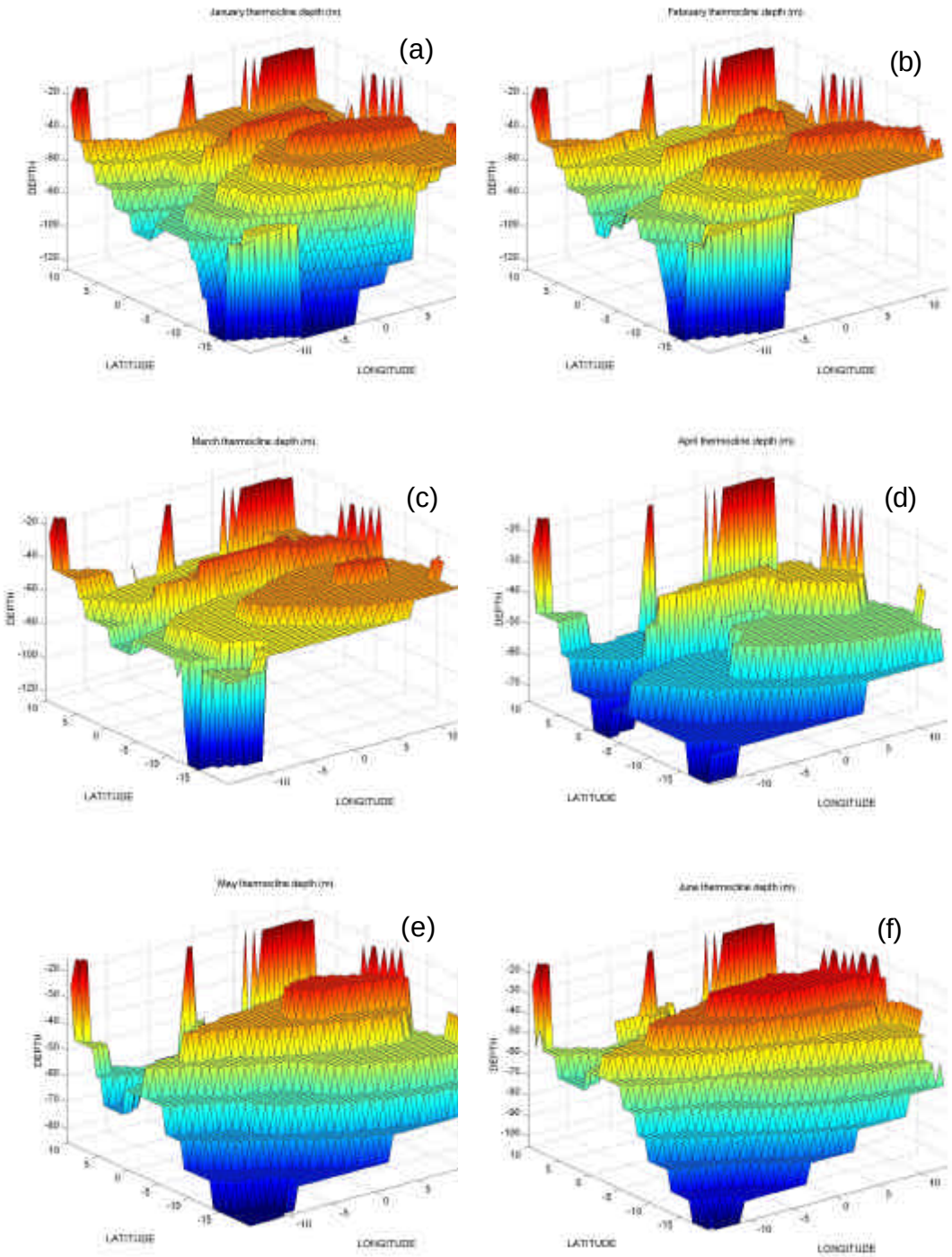

Figure 5.5(a-f): Monthly mean thermocline structure in the Angola Basin derived from OPA/TOTEM temperatures (January to June).

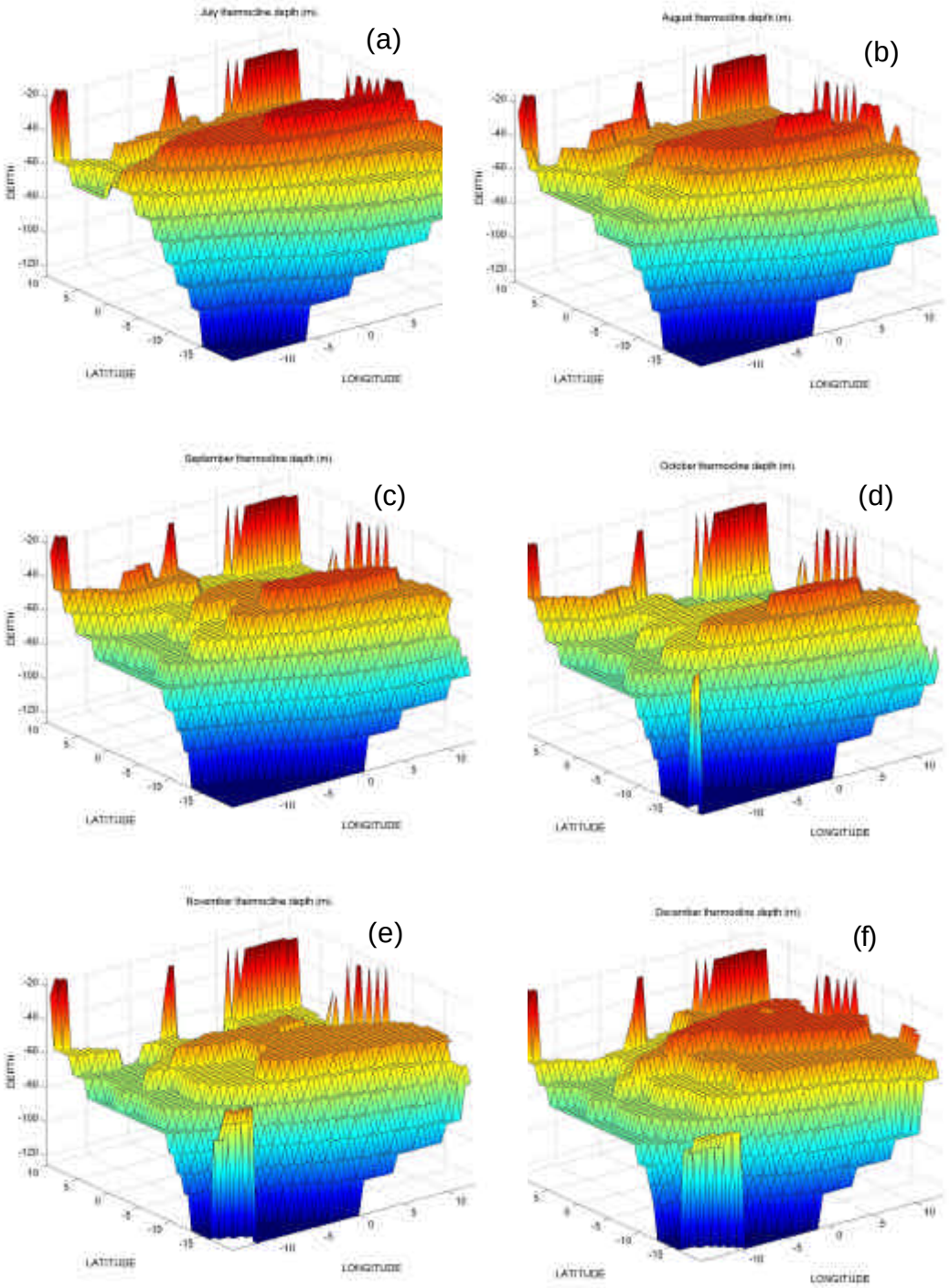

Figure 5.6(a-f): Monthly mean thermocline structure in the Angola Basin derived from OPA/TOTEM temperatures (July to December).

partially separated by a trough situated at about 2°S that extends eastward only as far as about 5°E. From May to August (Figures 5.5e-f, 5.6a-b) a single, steep ridge at approximately 2.5°S dominates the structure of the thermocline and moves slightly southward throughout this period. In August, the peak of the thermocline ridge is smaller, but exists as an isolated feature due to a slight deepening of the thermocline toward the coast.

In September and October (Figures 5.6c-d) the ridge deepens and moves southward to 5°S and 6.5°S respectively. During both months the upper 10m of the ridge exists as an isolated feature due to a deepening of the thermocline at the easternmost edge of the peak.

The isolated peak is not evident in November (Figure 5.6e), despite a distinct cool feature evident in the horizontal 45m temperature plots. This may be due to the fact that in November the upward doming of the isotherms is situated as far south as the ABFZ and the vertical temperature gradient calculations do not take into account the surfacing of isotherms at the ABFZ. In December (Figure 5.6f), a distinct ridging of the thermocline is situated to the north; it is most zonally extensive across the equator and toward the south it wedges coastward. The temperature and monthly temperature variation plots at 45m (Figures 5.2 and Appendix 1 respectively) provide compelling evidence that this ridge is in fact a 'new' upwelling of the thermocline and that the ridge associated with the cool feature between May and November all but disappears as it moves southward toward the ABFZ.

The southward migration of the thermocline-ridge between May and November approximately mirrors the situation in the Northeastern Equatorial Atlantic identified by Hastenrath and Merle (1987), whereby the shallowest mixed layer moves northwards. Furthermore, they observed that the poleward displacement of the thermocline-ridge is concordant with the seasonal migration of ITCZ, i.e.

the northward displacement of the ITCZ results in a poleward movement of the thermocline-ridge in both hemispheres.

The three-dimensional plots reveal that the isolated cool feature (evident in January, February, September, October and November) is indeed related to a doming of the thermocline, which comes about due to a deepening of the eastern edge of a ridge in the thermocline. The cool tongues present during all other months of the year are similarly related to the thermocline ridge. The difference being that the easternmost edge of the ridge does not deepen and therefore a cool feature, separate from the cool water regime at the coast is not generated at the 45m depth level.

Meridional and zonal temperature sections

The meridional sections at 5°E (Figures 5.7 & 5.8) reveal the upward doming of the isotherms that is associated with the ridge-like structure of the thermocline described in the previous section. The sections recapitulate the growth of the thermocline ridge (i.e. the shoaling of closely-spaced isotherms) at the equator during winter, its southward migration in spring and the initiation of another, smaller ridge-like structure near the equator in November, which persists until March.

A deeper doming feature, associated with an upward displacement of the isotherms, is present in the vertical sections and extends to a depth of at least 300m. It is offset southward of the more intense feature in the thermocline and is situated approximately beneath the ABFZ. As the thermocline ridge moves southward from August to November, the upward doming of the isotherms beneath the ABFZ becomes more asymmetrical, with its crest shifting slightly northwards. However, when the doming within the thermocline lies furthest north (between May and July) the doming beneath the ABFZ resumes its symmetrical nature. The implication of this is that the two features are formed by different

processes, but that when the shallower feature is furthest south it partially merges with the deeper one.

Beneath the ABFZ the thermocline deepens considerably toward the south, corresponding with the southern limb of the dome-like feature beneath the front. The southward slope of the thermocline beneath the ABFZ is steepest from August to November. During this time, the thermocline ridge moves southward, effectively merging the southern limbs of the shallow and deep features, resulting in the steeply sloping thermocline toward the south. The fact that the shallow doming is not evident south of the ABFZ implies that the front essentially acts as a barrier to the southward migration of the shallow dome-like feature in the thermocline.

The zonal temperature sections at 5°S (not shown) illustrate the shoaling of the thermocline toward the east and, during certain months, a slight deepening near the coast. This deepening is in accordance with the isolated dome-like feature evident in the three- dimensional plots of the depth of the thermocline as well as the horizontal temperature sections. At greater depths, a broad (± 10°W to 5-10°E) region characterized by upward-bending isotherms, roughly intersecting the crest of a similar feature observed in the meridional sections approximately beneath the ABFZ, confirms that it is in fact a dome-feature and of a relatively large-scale (of the order of 1000-2000km).

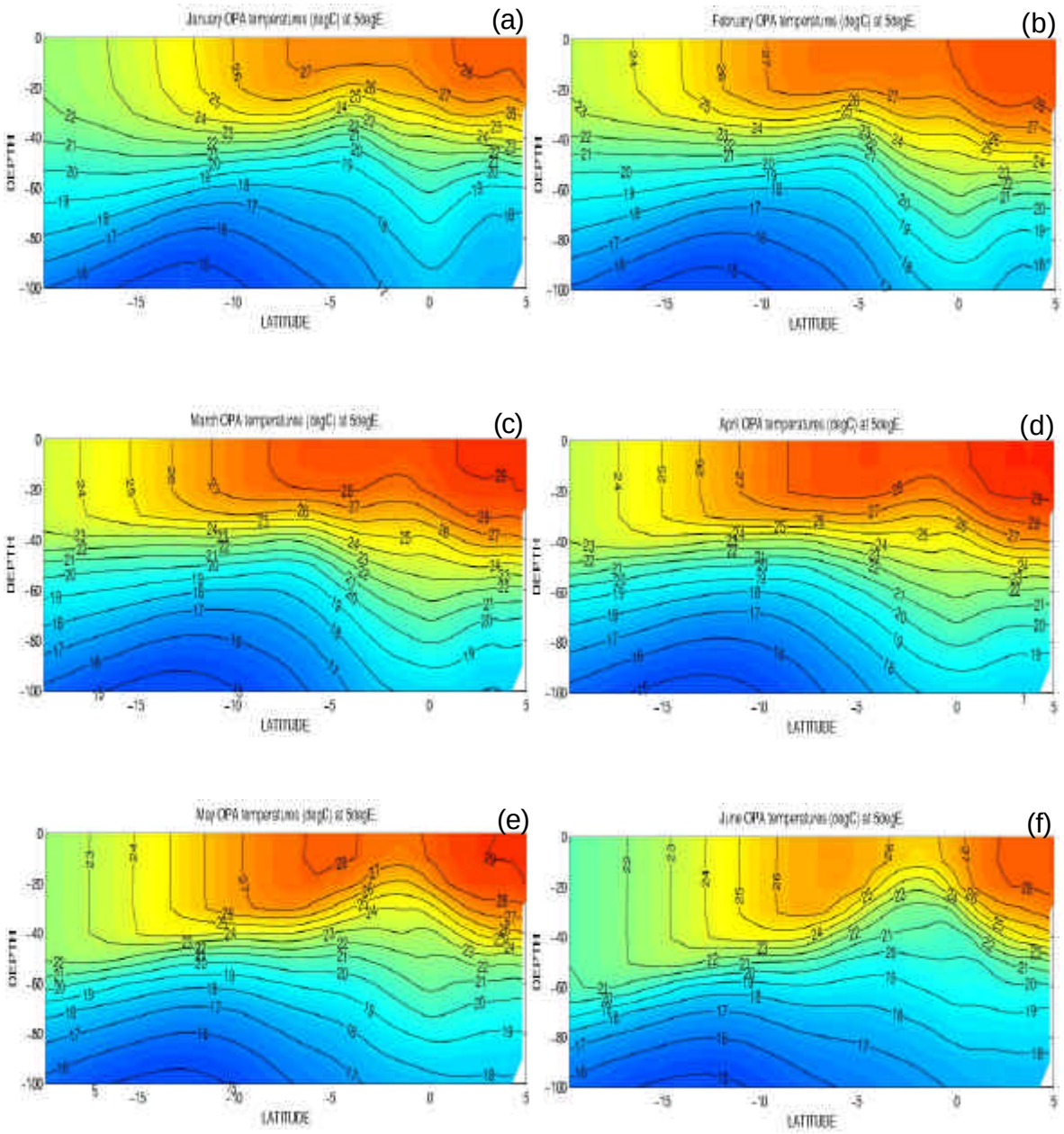

Figure 5.7(a-f): Monthly mean OPA/TOTEM temperature sections along 5°E (January to June).

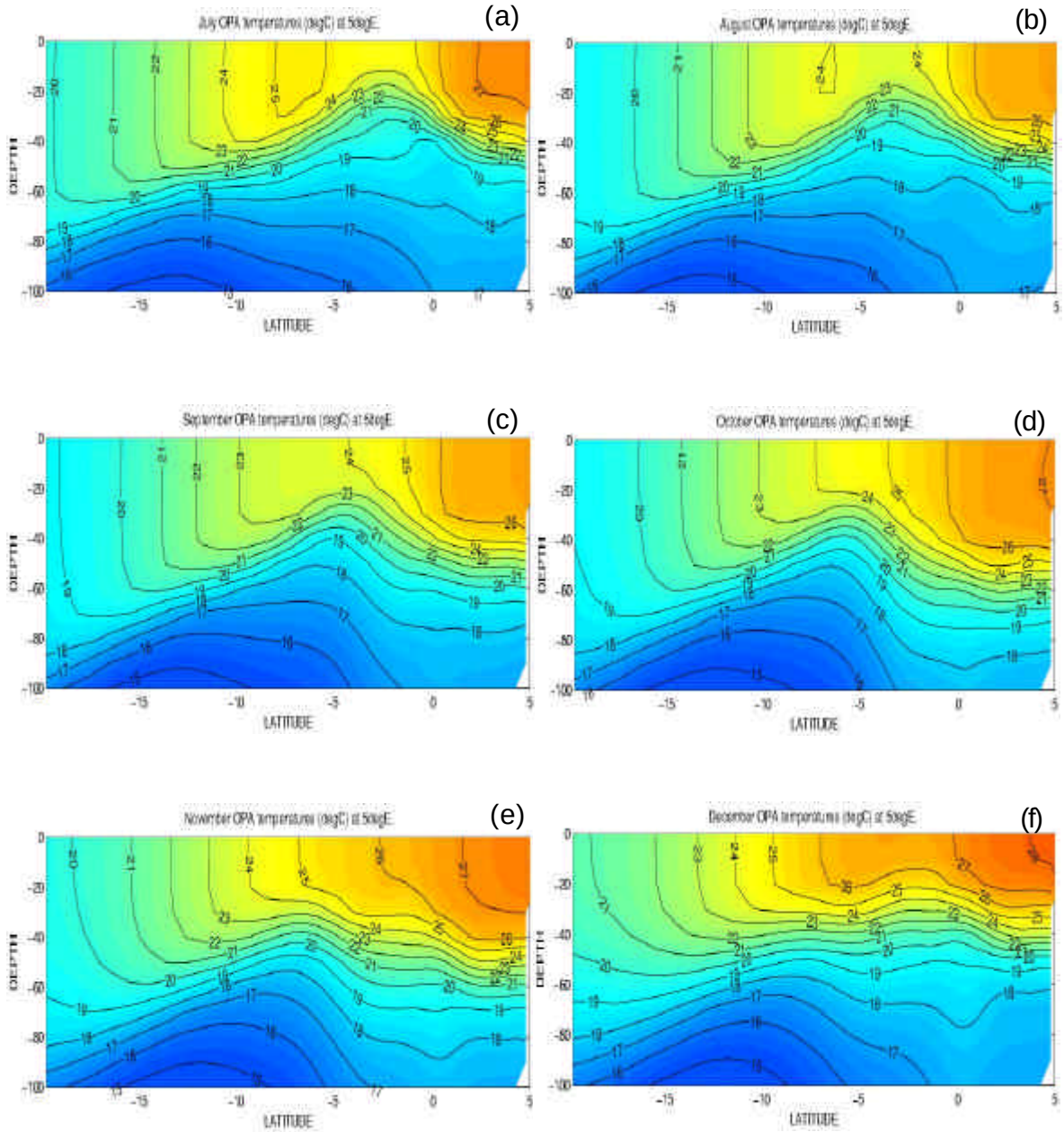

Figure 5.8(a-f): Monthly mean OPA/TOTEM temperature sections along 5°E (July to December).

5.1.2.1

Monthly mean salinity sections

The monthly mean salinity sections at 5°E (Figures 5.9 & 5.10) intersect the seaward edge of the fresh water influence of the Congo River plume as well as the relatively low salinity water that prevails in the Bight of Biafra. According to Berrit (1969), the region of permanent low salinity in the Bight of Biafra is a result of heavy rains, freshwater runoff and a weak evaporation rate.

Like the temperature sections at 5°E, the salinity plots reveal an upward doming of the isohalines beneath the ABFZ, which is also resolved, but in this case as a salinity front. Zonal salinity sections at 5°S (not shown) reveal that the doming of the isohalines occurs both meridionally and zonally. Again, this reflects the finding in the temperature sections. However, the upward displacement of the thermocline evident in the temperature sections is not clearly resolved in the salinity plots. This is perhaps a result of the influence of the massive fresh water input* from the Congo River and, to an extent, the relatively low salinity water in the Bight of Biafra (±35.2 psu).

At 5°E, some 750km from the coast, the fact that the relatively shallow, less saline water (±35.2-35.4 psu), north of about 6°S, is related to the Congo River plume is substantiated by the finding of van Bennekom and Berger (1984) who observed the plume to extend up to 800km offshore. The zonal sections at 5°S reveal that the plume deepens from approximately 5m at the coast to a maximum depth of about 30m at its seaward boundary. At 5°E, the fresher water generally extends northwards from 5- 6°S, this is consistent with the wind-driven, north-westerly orientation of the plume throughout much of the year (Eisma and van Bennekom, 1978). Evidence of the plume at 5°E is most distinct between April and May and in December and January, concurrent with the maximum rates of discharge (Eisma and van Bennekom, 1978).

---

* According to Eisma and van Bennekom (1978) an annual mean discharge of ±40 000$m^3.s^1$ flows into the South East Atlantic Ocean.

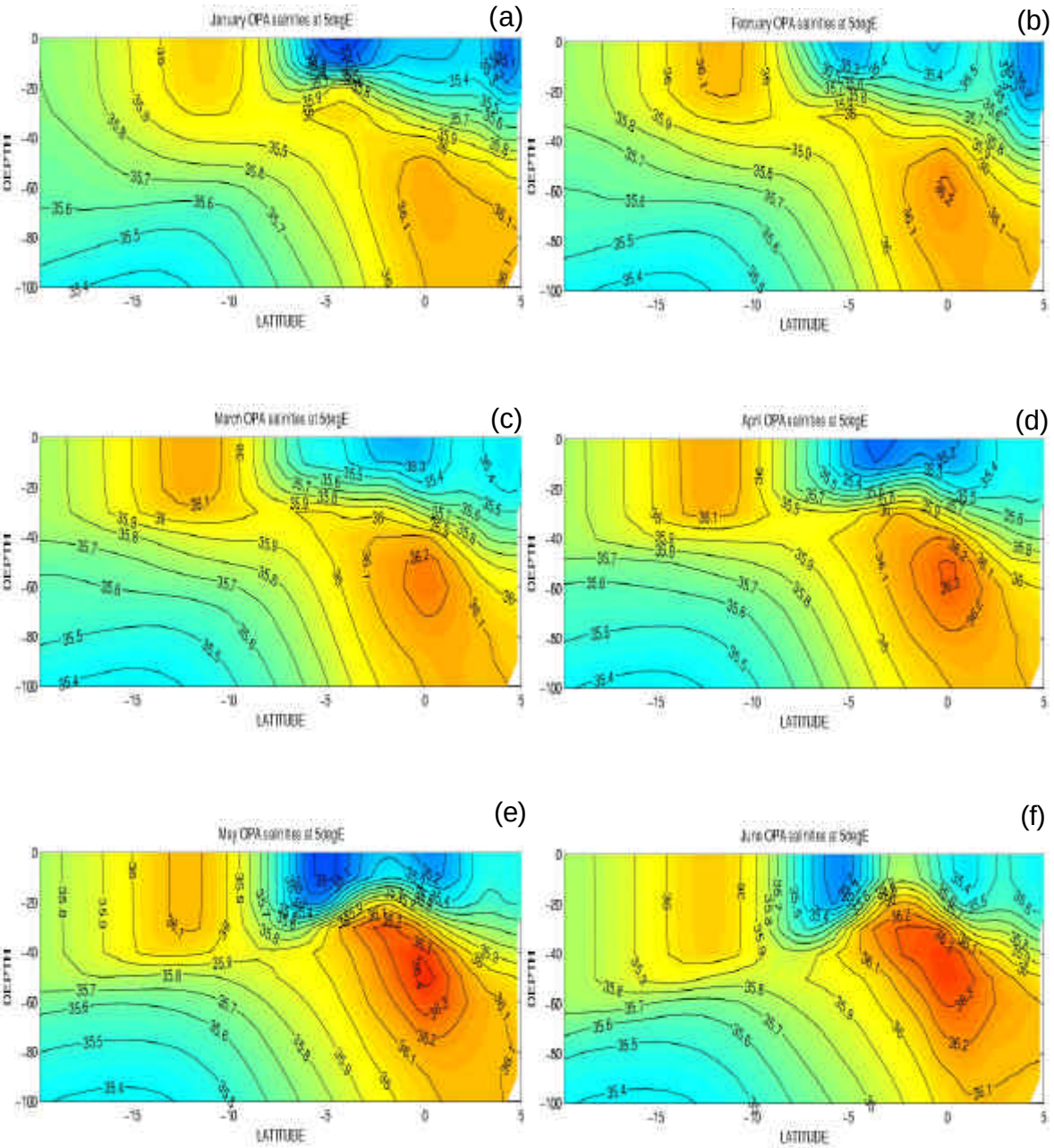

Figure 5.9(a-f): Monthly mean OPA/TOTEM salinity sections along 5°E (January to June).

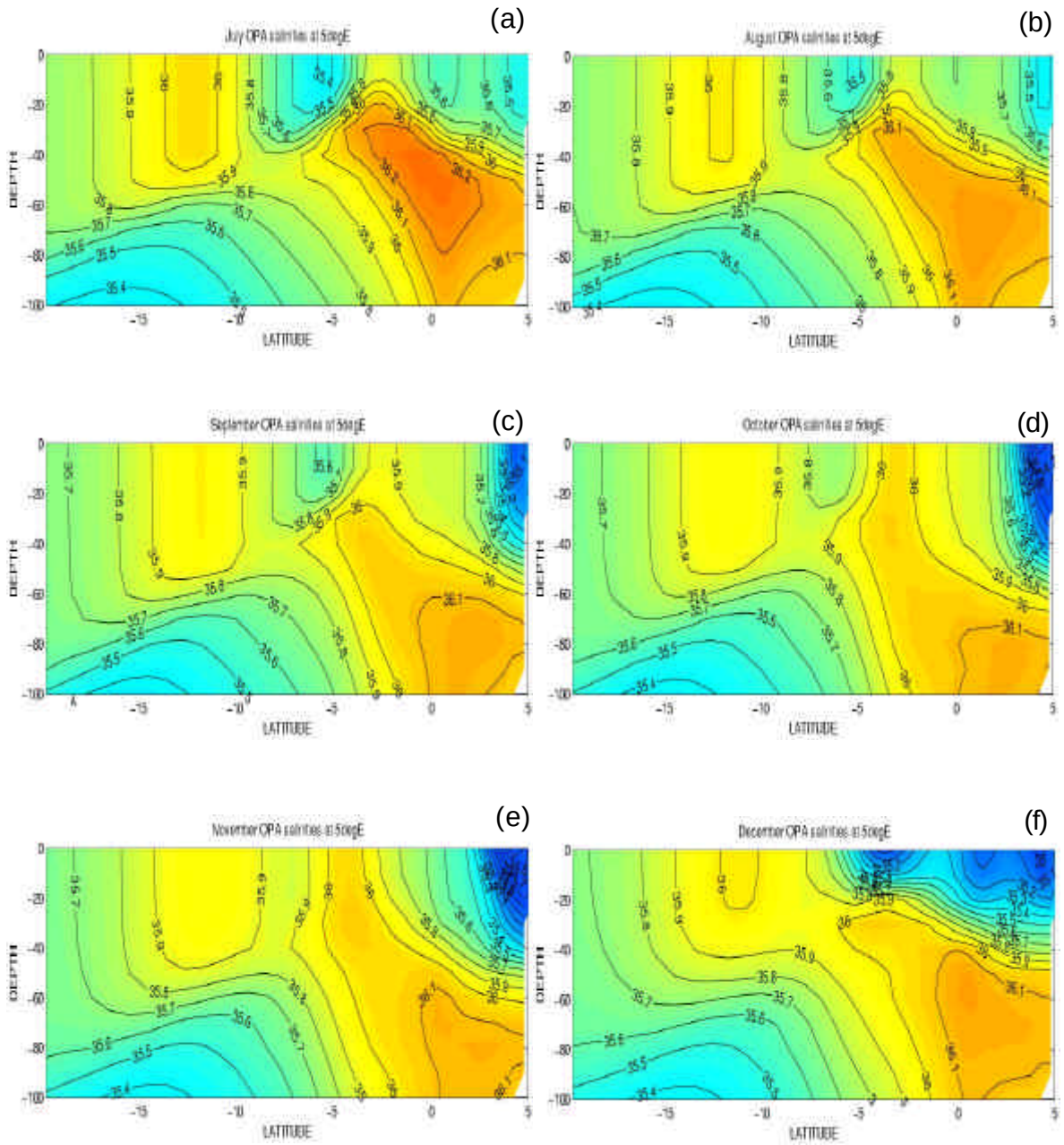

Figure 5.10(a-f): Monthly mean OPA/TOTEM salinity sections along 5°E (July to December).

The relatively low salinity signal of the plume is weakest in September, October and November, lagging the minimum discharge rate (in July and August) by a couple of months. From December to April the low salinity signal of the Congo River plume merges with that of the Bight of Biafra.

Nevertheless, throughout the year (excluding September to November), although slight, a suggestion of the thermocline-ridge exists in the meridional salinity sections, whereby deeper water, more saline (±36-36.3 psu) than that influenced by the Congo River discharge, is displaced toward the surface. Concurrent with the development of the distinct ridge-like feature of the thermocline and its southward movement from June to August, the two low salinity regimes of the Congo River plume and the Bight of Biafra exist as distinctly separate features. During September, October and November the little evidence of the dome-like feature may be a result of a weakening of the low salinity signal of the Congo River plume as well as the southward migration and deepening of the ridge.

5.1.3 Synopsis

The analysis of the thermohaline output parameters of the OPA/TOTEM model has allowed for the following significant observations to be made:

- A cool feature becomes distinct at a depth of 45m, extending as a tongue-like feature offshore in a north-westerly direction during most months of the year.
- In January, February, September, October and November the cool feature at 45m is present as an elongate, NW-SE oriented, circular region, which is separated from the cool regime along the coast. Its horizontal dimensions are of the order of 1000km (zonally) x 500km (meridionally), with a centre located at approximately 5°S 5°E.
- The cool feature is directly related to a ridge-trough-ridge structure of the thermocline and its shoaling toward the east. A deepening of the thermocline at the African coast occurs only during months when the cool

feature is isolated and situated some distance from the cool coastal regime.

- The cool feature seems to be related to a semi-annual upwelling (which commences around March and December) of the thermocline in the equatorial region, which becomes more distinct as it moves southward between June and November (for a visualization of this southward migration refer to the hoffmöller plot in Appendix 3).
- The southward migration is associated with the seasonal migration of the ITCZ.
- The ABFZ acts as a barrier to the southward movement of the thermocline-ridge.
- A permanent, upward-doming of the isotherms exists beneath the ABFZ.
- The salinity signal of the cool feature is weak and may be a result of the massive fresh- water input from the Congo River.
- The salinity signal at 45m suggests onshore and offshore motion at the northern and southern boundaries of the cool feature respectively.

The cool feature identified in the OPA/TOTEM model output is of a much larger scale than the Angola Dome identified by Mohrholz *et al.* (2001), which was less than about 250km in diameter. Using model data Lien (2004) located the dome at about 10°S 12°E with dimensions of 100-300km. Historical investigations of the Angola Dome have also placed it further south and east of the feature evident within these data. Mazeika (1967) found that the Angola Dome is only present between January and April, whereas the cool feature described in this section appears to be present throughout the year, but is most distinct as an isolated cool feature at a depth of 45m between September and November and in January and February. On the basis of these comparisons, the cool feature investigated in this section is probably commensurate with the large-scale 'Angola Gyre'. The permanent upward doming of the isotherms beneath the ABFZ can be linked to the southward-shift of the Angola Gyre with depth, noted by Gordon and Bosley

(1991). The Angola Gyre is therefore present throughout the year, but its shallow expression in the thermocline shows strong seasonal variability.

The next section is an analysis of the three-dimensional velocity fields obtained from the OPA/TOTEM model. The primary objective is to resolve the cyclonic circulation of the Angola Gyre and to establish its relationship to the equatorial current system.

5.2 Circulation Features

Circulation features in the Angola Basin are investigated using the horizontal and vertical velocity output of the OPA/TOTEM model. The main purpose of this section is to determine whether the cool feature at the 45m horizon, identified in the previous section as the Angola Gyre, is indeed associated with a distinct cyclonic circulation. The flow regimes that constitute the limbs of the Angola Gyre are identified and their seasonal fluctuations will be described, particularly with respect to their influence on the structure of the gyre.

5.2.1 Monthly mean composites of zonal and meridional velocity

The zonal and meridional components of the horizontal velocity field are initially plotted and analyzed separately in order to resolve the zonal equatorial currents and the poleward coastal currents that define the boundaries of the gyre with greater clarity. The mean resultant horizontal velocities at a depth of 45m are then investigated, aiding a more thorough understanding of the circulation connected with the gyre.

The northern and southern limbs (zonal velocity sections)

The monthly mean zonal velocities along a meridional transect at 5°E (Figures 5.11 & 5.12) reveal three prominent eastward flowing currents in the southern hemisphere that are related to the equatorial system of currents; the EUC, the SEUC and the SECC. These currents are generally (though not exclusively) limited to subsurface layers, with westward flow dominating the surface layers.

The EUC exists as a narrow, subsurface jet, spanning the equator by approximately 3° of latitude. At its shallowest and most intense (±0.2 $m.s^{-1}$), in February, it is situated between 40-80m depth. From May to August it is deepest (>60m) and least distinct, with weakest velocities (±0.06 $m.s^{-1}$). The depth of the EUC evident in Figures 5.11 and 5.12 agree with the results of Peterson and Stramma (1991) and Schott *et al.* (1998) and the seasonal deepening is consistent with the finding of Waconge and Piton (1992).

The SEUC is situated between about 2-5°S and at least within the upper 100m, contrary to the findings of Molinari *et al.* (1981) who observed the SEUC to be situated between 100m and 150m. It is strongest (±0.14$m.s^{-1}$) and outcrops at the surface in January and February and between September and November. The seasonal surfacing of the SEUC observed between January and February and between September and November verifies the speculation of Waconge and Piton (1992). The fact that the surfacing of the SEUC corresponds to times when the cool feature at the 45m horizon is most distinct, implies a direct relationship. A natural assumption would be that the SEUC forms the northern limb of the Angola Gyre. For this reason, the seasonal variability of the SEUC will be described in greater detail.

South of the SEUC is the subsurface SECC, which is centered at approximately 10°S and is 20m at its shallowest and extends to depths of greater than 100m. It is larger but much weaker (±0.01$m.s^{-1}$) than both the EUC and the SEUC. A shallow westward flow exists between the SEUC and the upper-most layers of the SECC, effectively separating them at depths shallower than about 50m. However, during certain months of the year no such shallow westward flow distinctly separates the two eastward currents and, in consequence, the SEUC and SECC merge in shallow water as well as at depth.

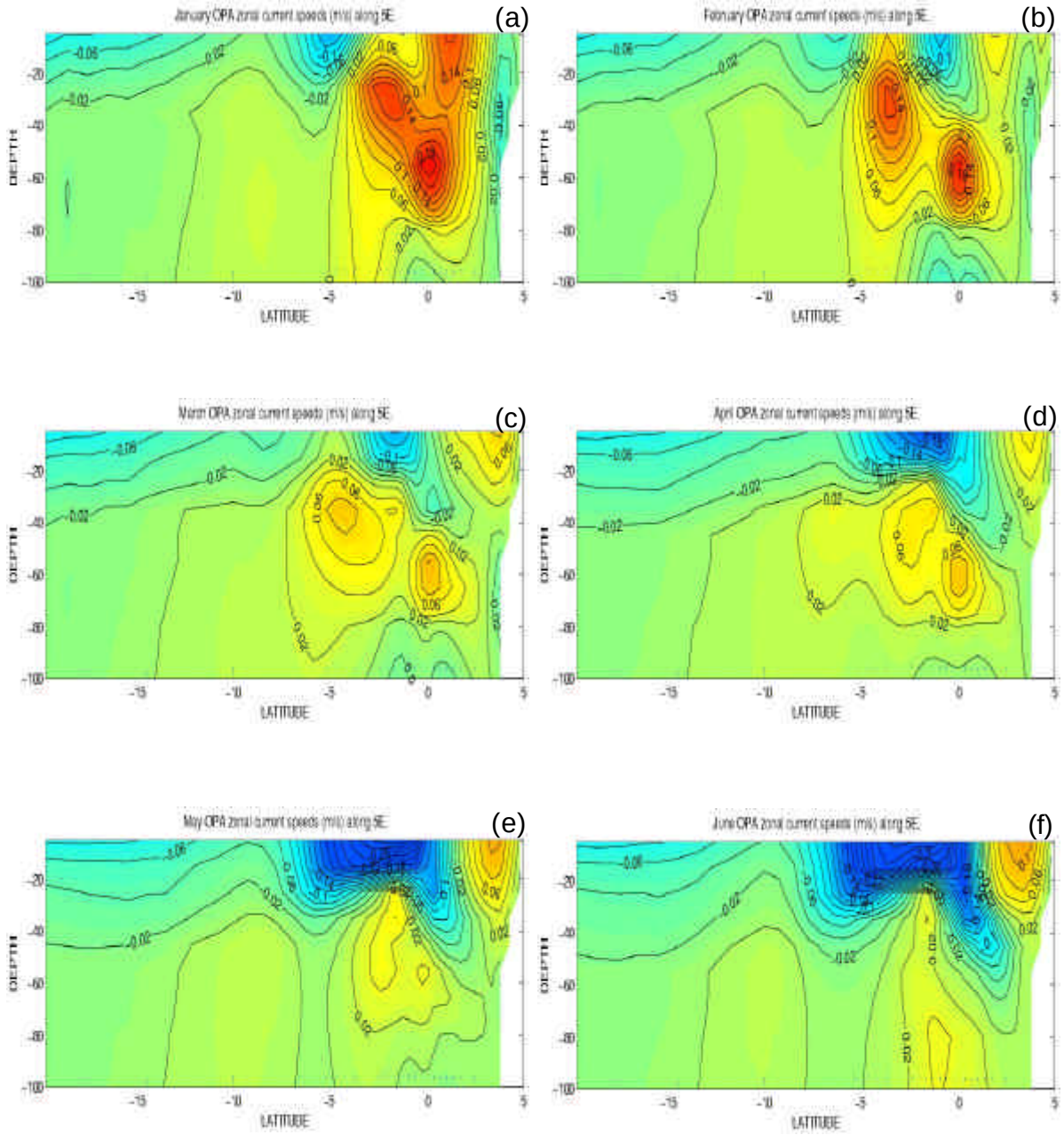

Figure 5.11(a-f): Monthly mean zonal velocity sections at 5°E (January to June). Positive and negative velocities correspond to eastward and westward flow respectively. Contour Interval is 0.02m.s^{-1}.

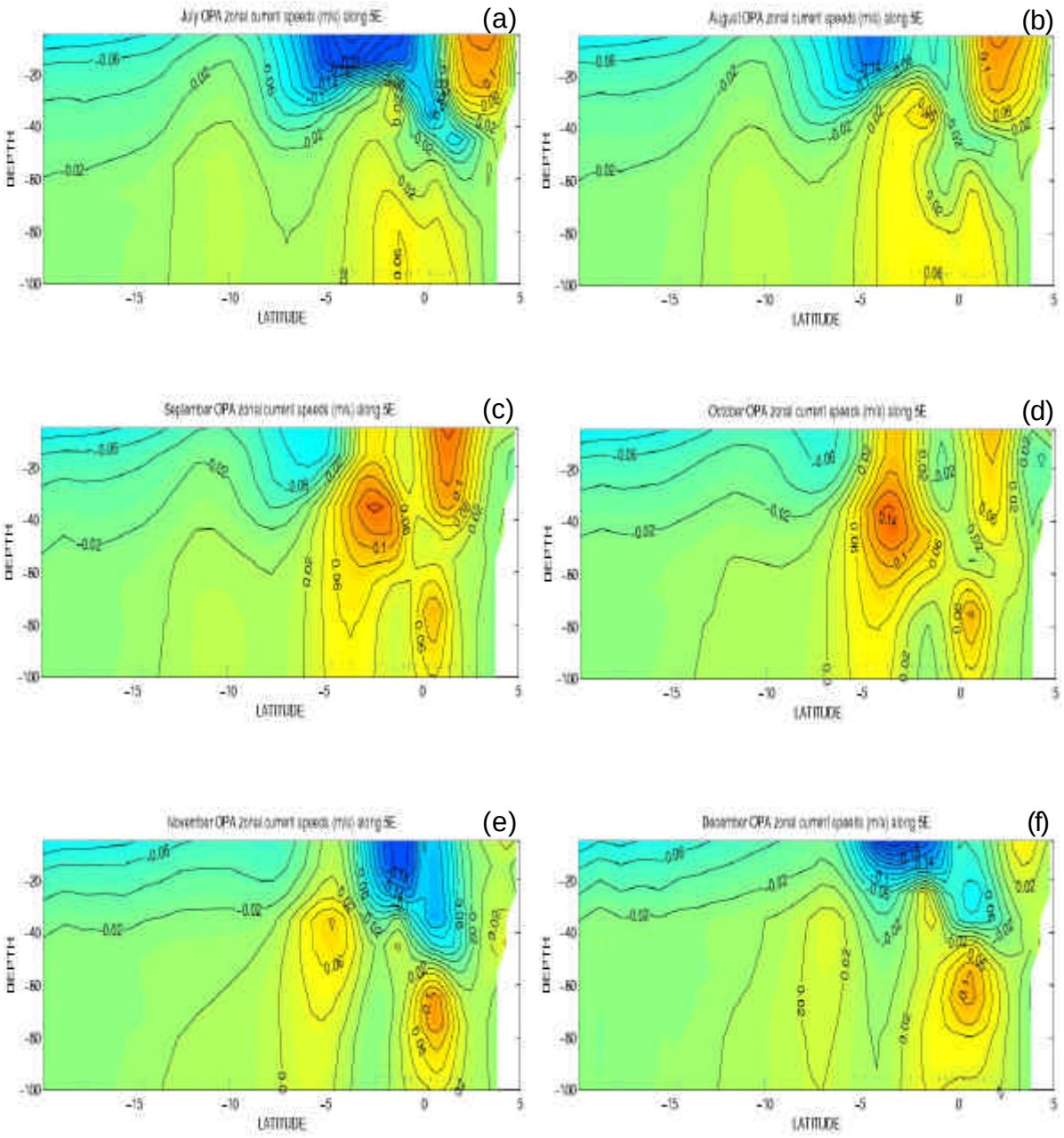

Figure 5.12(a-f): Monthly mean zonal velocity sections at 5°E (July to December). Positive and negative velocities correspond to eastward and westward flow respectively. Contour Interval is 0.02m.s^{-1}.

This occurs during March, April and November. The merging of the SEUC and the SECC implies that the SECC is also associated with the northern limb of the Angola Gyre, particularly at greater depths, where the gyre is situated further south. Next is a detailed analysis of both of these equatorial currents.

In January and February (Figure 5.11a & 5.11b) the SEUC outcrops at the surface and is particularly strong, spanning 2-5°S. The SECC is present as shallow as 20m, but is separated from the SEUC by a westward flowing current that extends from the surface to a depth of about 45m. The eastward flow of the SECC extends as far south as approximately 13°S during both months, at which point the flow becomes weakly westerly. The flow regime in January and February confirms that the northern (the SEUC) and southern limbs of the cool feature at 45m flow onshore and offshore respectively. The deeper counterpart of the cool feature, positioned approximately beneath the ABFZ is similarly associated with a cyclonic motion (although weaker); the deeper, 'merged' SECC and SEUC as its northern limb.

In March and April (Figure 5.11c & 5.11d) no clear separation exists between the SEUC and the SECC. However, at about 4°S and 2°S for March and April respectively, a latitudinally narrow stream of the SEUC is present at depths of about 20-40m. This stream broadens with depth and is widest and most intense at a depth of about 50m. Because the SEUC is not paralleled by a strong, westward countercurrent to the south, it does not induce strong upwelling and therefore distinct regions of cooling at shallower depths (i.e. no cool feature is present in the temperature plots at 45m). The deeper- reaching SECC remains evident, constituting the northern limb of the cool feature that exists permanently beneath the ABFZ.

From May until August (Figures 5.11e-f & 5.12a-b) the eastward currents are weakest, while the westward surface currents are strongest (±0.2-0.26 $m.s^{-1}$) and

deepest, reaching from the surface to 40-50m. During this time, a relatively weak eastward velocity component is present in the equatorial zone and it is unclear whether it is the EUC, the SEUC or remnants of both. This weak eastward current situated approximately between 2°N and 5°S is separated from the SECC by a weak westerly current that extends to a depth of at least 100m. The SECC is weaker and less zonally extensive, yet seems to form the northern limb of the ever-present cool feature approximately beneath the ABFZ. Therefore, it seems that the Angola Gyre is not associated with a cyclonic flow during austral winter, whereas the deep cool feature beneath the ABFZ appears to be connected to a very weak cyclonic circulation during this time.

In September and October (Figures 5.12c-d) when the cool feature is distinct at a depth of 45m, the SEUC strengthens considerably and shifts southward, to some extent merging, at depth, with the SECC. This is consistent with idea of a southward shift of the Angola Gyre at greater depths. Also, the strong SEUC at depths of between 20-60m and a westward flow of ±0.06 $m.s^{-1}$ immediately to the south of it explains the intense and distinct cool feature evident at 45m as the shallow, northward counterpart of the Angola Gyre. At greater depths the weaker SECC corresponds to the southward shift and less distinct expression of the Angola Gyre.

In November and December (Figures 5.12e-f) the SEUC and the SECC appear to have completely merged, in water as shallow as 45m as well as at depth. This 'merged' eastward flow moves southward in December, whilst the re-initiation of the SEUC just south of the EUC that occurs in November, strengthens. This southward movement and re-generation of the SEUC corroborates the finding in the previous section that a 'new' gyre is formed between November and December as the old one shifts southward and eventually disappears.

The zonal velocity plots reveal that the Angola Gyre is indeed bounded by an onshore current at its northern boundary and an offshore current at its southern

boundary, thus suggesting cyclonic circulation. However, during austral winter there is little evidence of a cyclonic flow around the cool feature. The northern boundary of the gyre is most clearly defined and is associated with the SEUC. The southern limb of the gyre, associated with offshore motion is not as apparent. At depths of greater than about 60m, south of the SECC the offshore limb is related to a weak, but sizeable westward current regime. This may be related to the upwelling regime south of the ABFZ. The westward current south of the SEUC is much stronger and more variable and is likely to be related to wind-induced offshore Ekman flow.

The eastern and western limbs (meridional velocity sections)

Figures 5.13 and 5.14 are monthly mean plots of meridional velocities at approximately 5°S. The position of 5°S was chosen to best represent the center of the outcropping of the dome-like structure of the thermocline at a depth of 45m. This upwelling feature is likely to be the result of a cyclonic circulation pattern associated with the Angola Gyre. The aim of this section is to resolve the eastern and western limbs of the Angola Gyre.

The meridional velocity sections reveal that a strong southward velocity component exists from the coast to about 5°E during months when the Angola Gyre is most distinct (January, February, September and October), becoming weaker at greater depths. The eastern limb is commensurate to this southward flowing current, which is known as the Angola Current. The western limb of the Angola Gyre is not characterized by an unambiguously northward current. Rather, the western limb is made up of a meridional velocity component that is weakly southward to approximately the position of the Greenwich Meridian, at which point the meridional velocity component is weakly northward (at depths greater than about 40m).

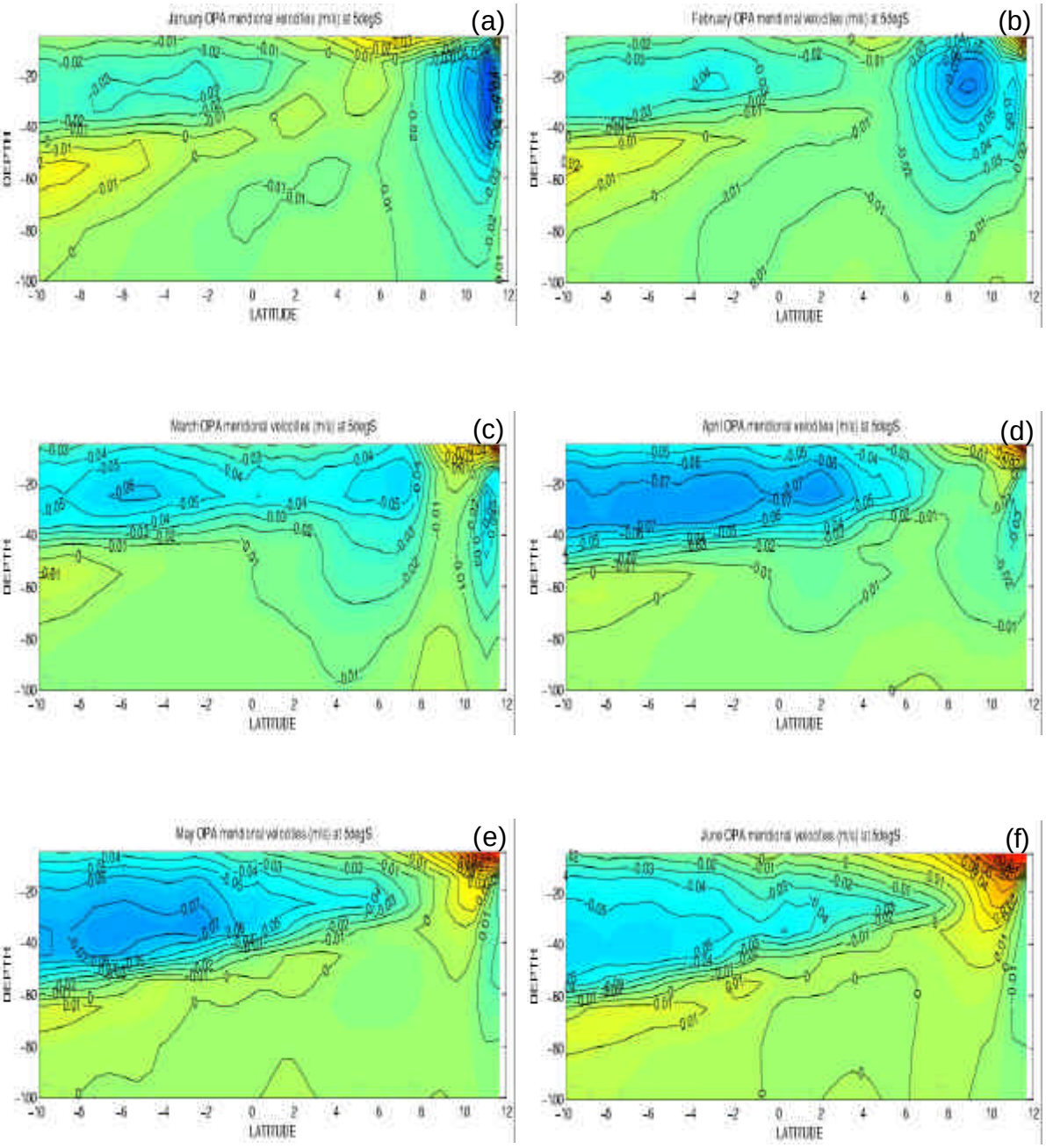

Figure 5.13 Monthly mean meridional velocity sections at 5°S (January to June). Positive and negative velocities correspond to northward and southward flow respectively. Contour Interval is 0.01m.s^{-1}.

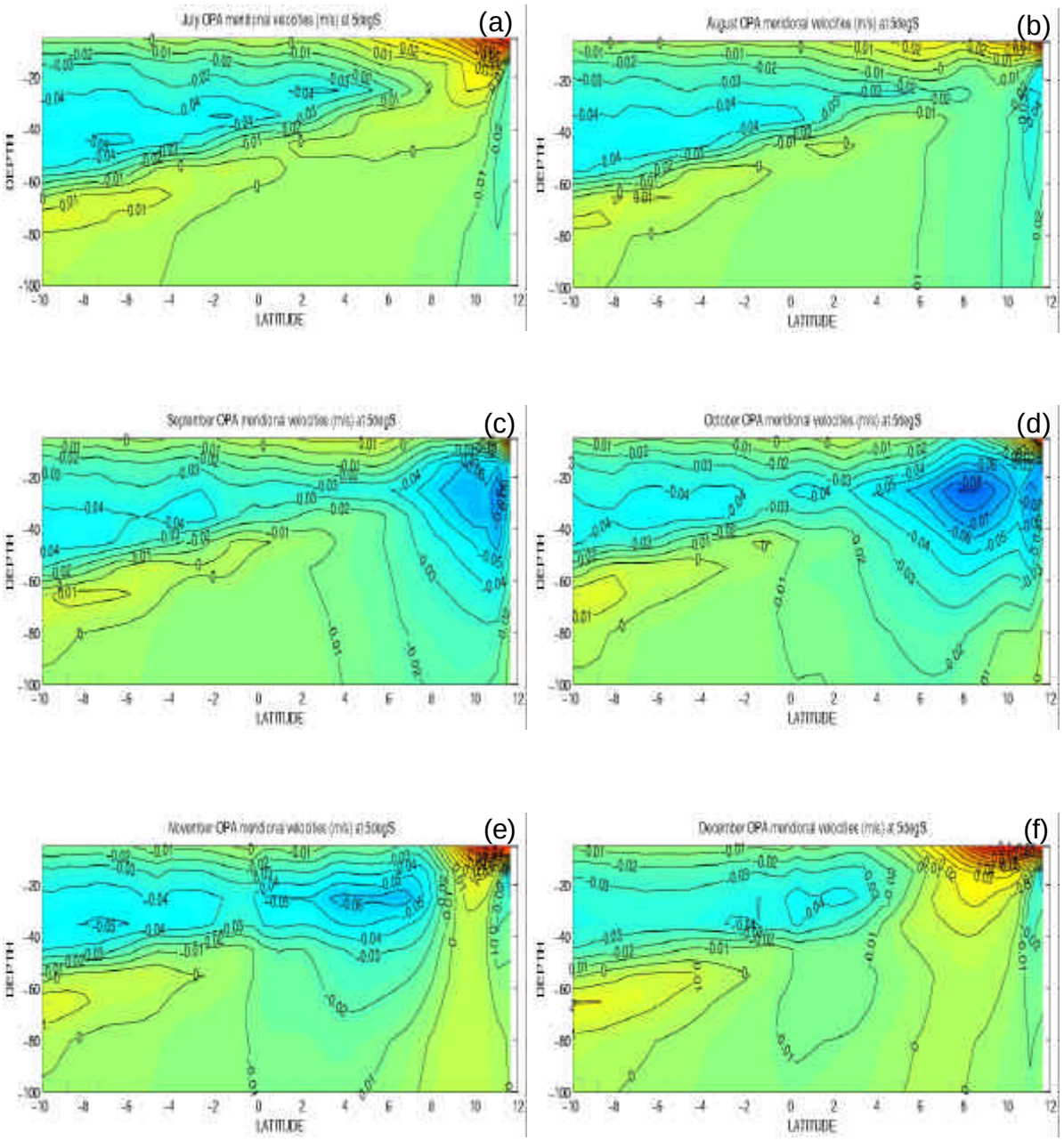

Figure 5.14 Monthly mean meridional velocity sections at 5°S (July to December). Positive and negative velocities correspond to northward and southward flow respectively. Contour Interval is $0.01 m.s^{-1}$.

The Angola Current that constitutes the eastern limb of the gyre weakens considerably from a maximum of about $0.1m.s^{-1}$ in January to less than $0.01m.s^{-1}$ in winter. This is consistent with the findings of Shannon and Agenbag (1987), who observed the Angola Current to be weakest in winter and spring. The large cool feature that exists during winter months is present in the equatorial zone, therefore possible meridional flow around them is not resolved in these sections.

The eastern and western limbs of the gyre show a strong inequality in their southward and northward transports respectively. This disparity may be related to the NW-SE orientation of the gyre and the corresponding asymmetry of the cool feature evident in the temperature plots at 45m

Resultant horizontal flow at 45m

Figures 5.15 and 5.16 are plots the monthly mean current direction and magnitude from the equator to 15°S and from the Greenwich Meridian to the west- African coast at a depth of 45m. Overlaid on these plots are the isotherms that define the boundaries of the cool feature when it is present at 45m depth. The plots give an indication of the complexity of the currents surrounding the Angola Gyre and demonstrate that the cyclonic circulation associated with it is not conspicuous, particularly at its southern and western limbs.

During months when the Angola Gyre is most distinctly separate from the coast (January, February, September and October), a southeastward current that originates at the equator is strongest. This strong current ends somewhat abruptly, zonally bisecting the NW-SE oriented cool feature, giving way to a much weaker southeasterly current to the south of it. To the east of the cool feature the flow bends southward forming the Angola Current. Evidence of a weak westward flow is present at the southern limb of the gyre in September, October and November whereas only vestiges of it remain in January and February. The western limb of the cool feature during these months is not defined by a

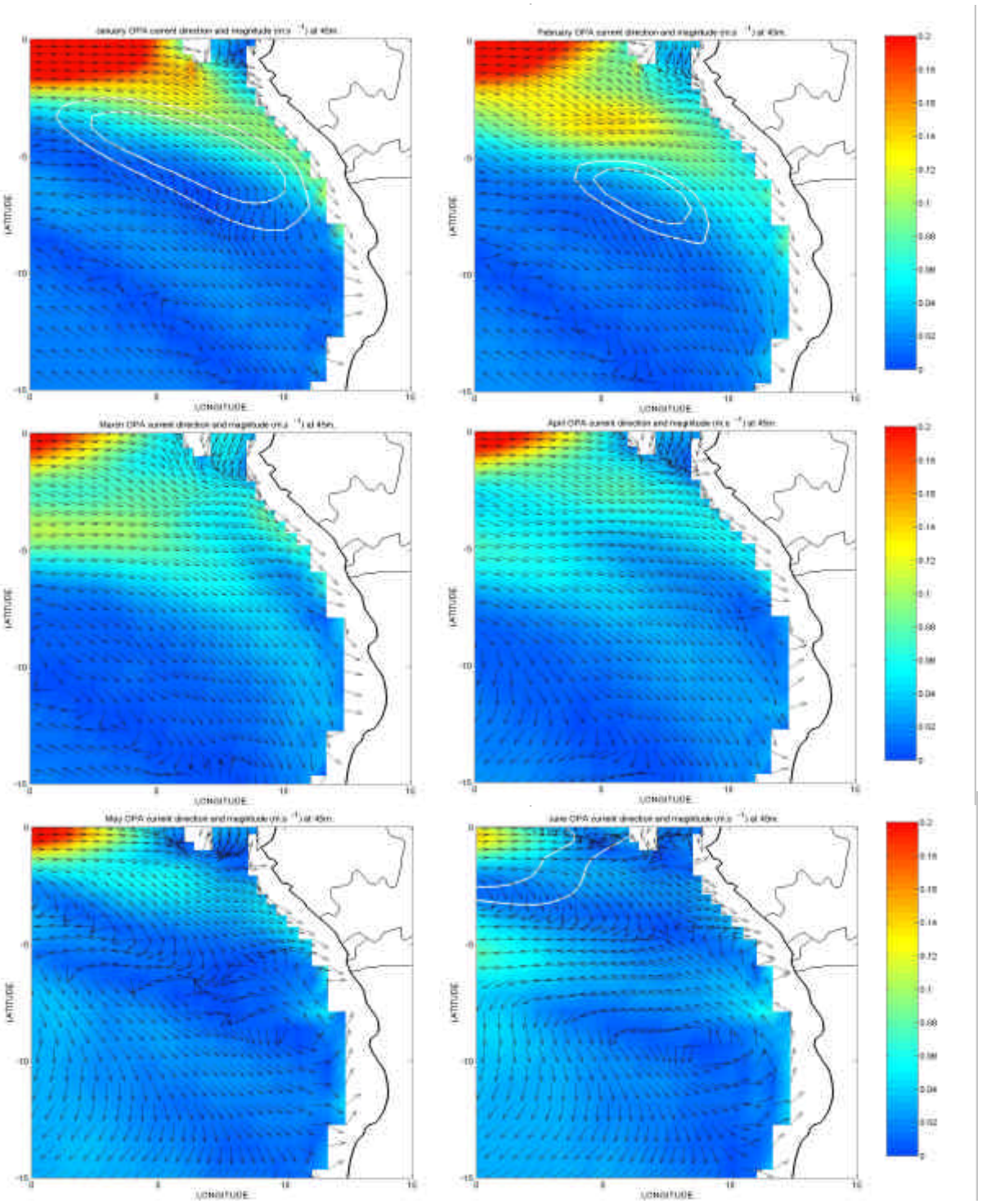

Figure 5.15: Monthly mean resultant horizontal flow pattern and magnitude at 45m (January to June). Overlaid is an outline of the cool feature at 45m for January, February and June, as defined by the bounding isotherms.

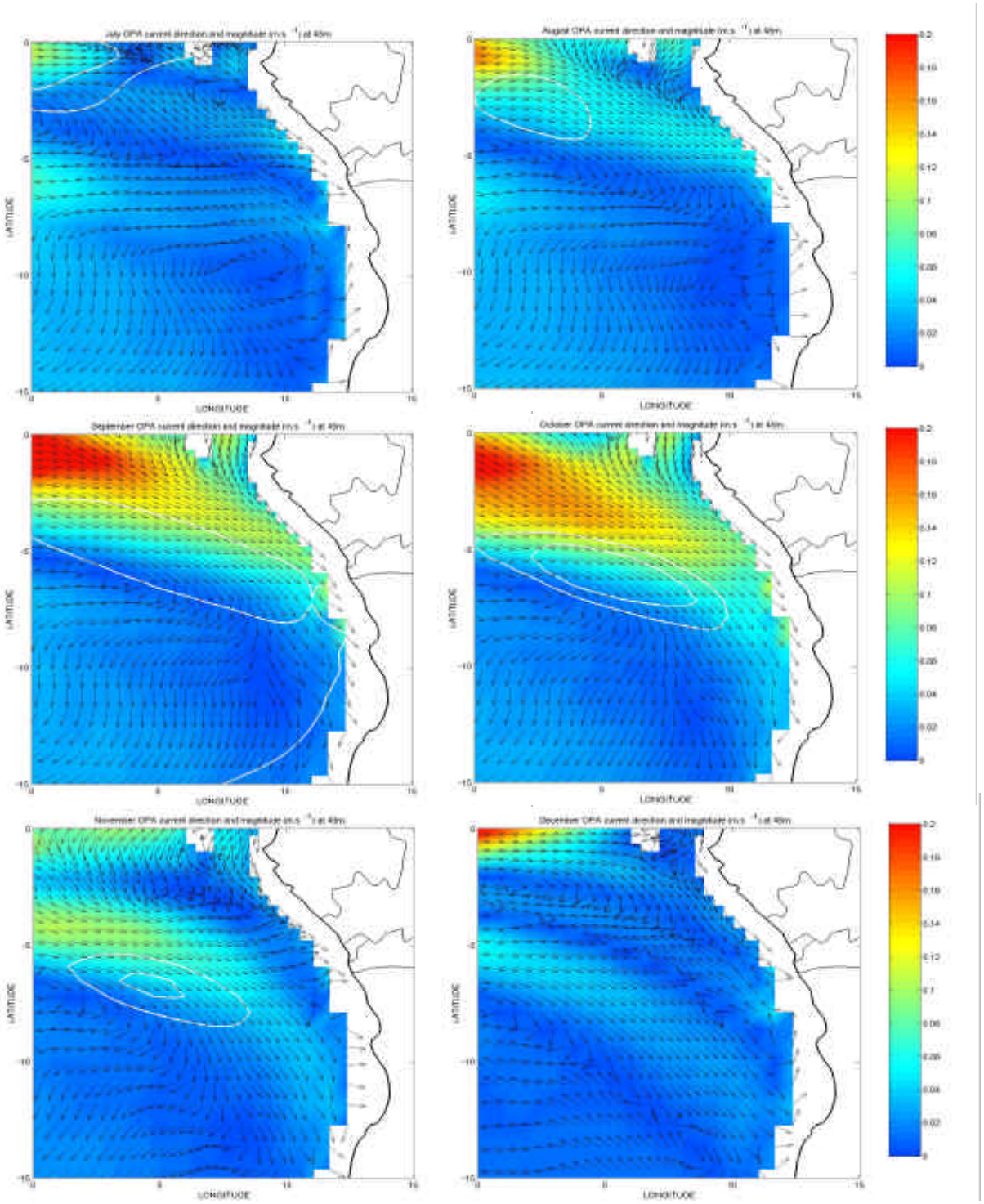

Figure 5.16: Monthly mean resultant horizontal flow pattern and magnitude at 45m (July to December). Overlaid is an outline of the cool feature at 45m for July – November, as defined by the bounding isotherms.

northward current as might be expected. Instead, it is characterized by a rapid change from southeasterly to southwesterly flowing currents, particularly in September and October.

In November the southeasterly current weakens slightly and moves southward, in accord with the southward motion of the Angola Gyre. Again, the current veers southward and then slightly toward the west, east and south of the cool feature respectively. The strong easterly and southeasterly equatorial currents do not prevail at 45m depth during November. A southwesterly flow exists between the equator and about 3°S, at which point it rapidly changes direction toward the southeast.

An easterly flow returns to the equatorial region in December, veering toward the southeast at about 5°E. This southeasterly current extends all the way to the African continent and is paralleled to the south by the current that formed the northern limb of the cool feature in November. The two southeasterly currents are separated by a northwesterly current, which bends distinctly towards the west by 5°E. It is this system of alternating southeasterly and northwesterly currents that is likely to be a major contributor to the dissipation of the cool feature evident at 45m and to the initiation of a region of slightly cooler temperatures at approximately 2°S during November and December.

During winter months (May to August), the equatorial flow regime from about 5°E to the African coast is predominantly westerly to southwesterly. This is perhaps related to a seasonal, wind-induced weakening of the eastward equatorial currents.

Figures 5.15 and 5.16 therefore show that the Angola Gyre is not associated with a well-defined cyclonic motion, but that it certainly seems closely-tied to the eastward equatorial currents.

Divergence of the horizontal velocity fields

The fact that the cool feature, indicative of the Angola Gyre, is not delineated by conspicuous cyclonic circulation negates the idea that it is solely a result of subsequent coriolis-induced upwelling. However, it is likely that the strong variability of current speed and direction within the cool feature leads to regions of horizontal current divergence resulting in upward vertical motion. Figure 5.17 shows plots of the monthly mean temperatures at 45m overlaid on plots of the current divergence, calculated from the horizontal velocity fields, for selected months. Including both the temperature and divergence parameters in a single plot aids the analysis of a possible relationship between the two fields.

The plots of divergence and temperature at in Figure 5.17 are for the months during which the cool feature is shallow and distinctly separate from the coast, namely January, February, September, October and November. It is striking that the cool feature intersects almost precisely with a region of current divergence. The diverging currents result in an upward displacement of deeper, colder water in order to satisfy the conservation of mass theorem. On the other hand, the divergence may, in fact, be the consequence of the upward motion of deeper waters. Therefore, the cause or effect of the diverging current field is a significant process governing the seasonal cycle of the Angola Gyre. Meridional sections at 5°E of fields of divergence (not shown) reveal that the divergence associated with the Angola Gyre persists at least to a depth of 100m in January, February, September, October and November.

The large cool feature that is evident during winter months near the equator does not correspond to a region of horizontal current divergence at 45m. It is perhaps formed by equatorial upwelling. From May to July a southwesterly current crosses the equator from 5°E to the coast and the change in sign of the coriolis parameter across the equator results in a divergence and upwelling of cooler, deeper waters. A southwesterly current also crosses the equator during November, resulting in divergence and upwelling in the same manner. During all

other months of the year, the flow regime across the equator is south to south-easterly, resulting in a zone of convergence.

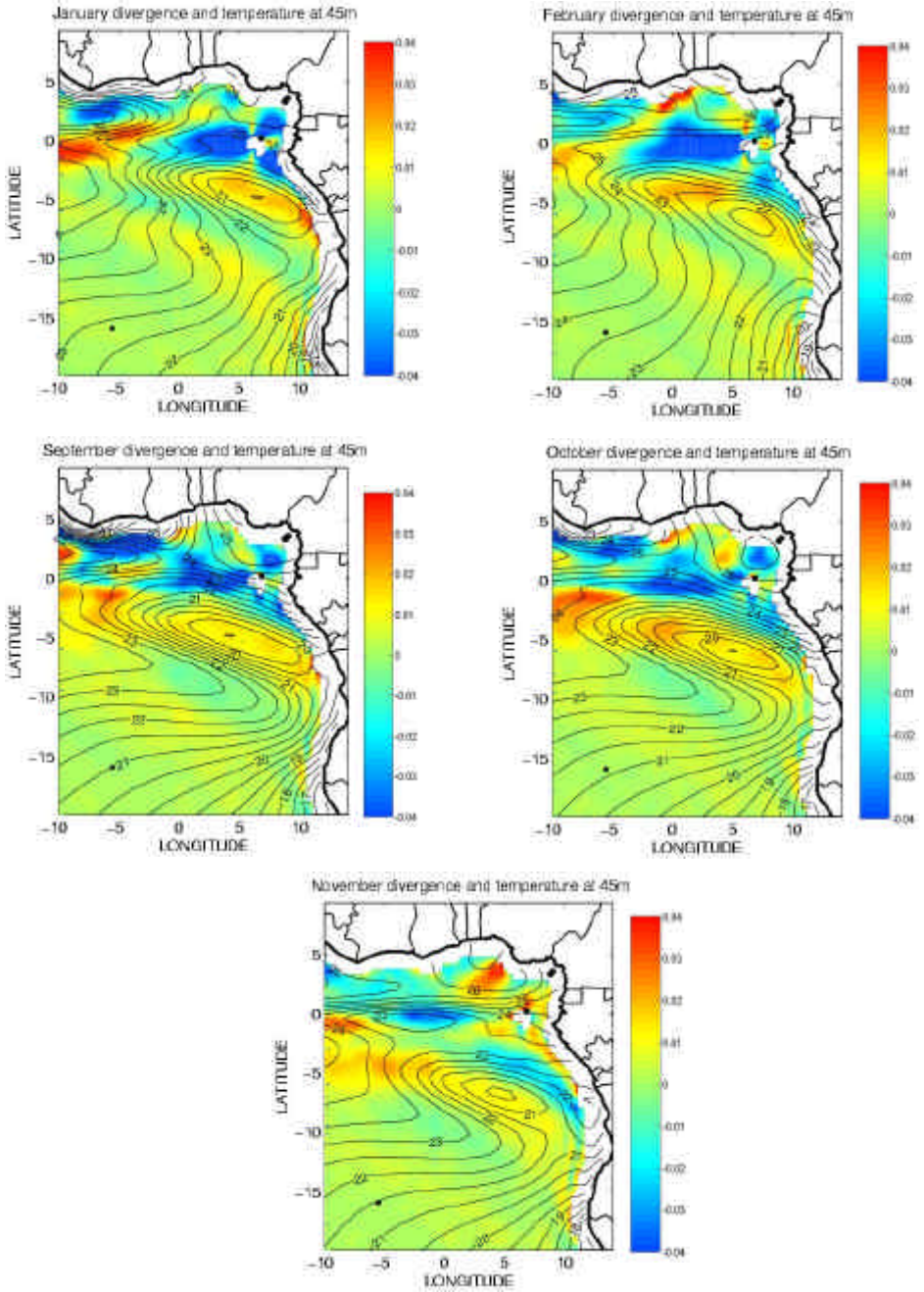

Figure 5.17: Monthly mean horizontal current divergence and temperatures at 45m for months during which the cool features is most distinct (January, February, September, October and November).

5.2.2 Vertical velocity field

The vertical velocity fields along the 5°E meridian (Figures 5.18 & 5.19) reveal a relatively intense upward motion in the equatorial region between April and July and in November of the order of 0.12-0.2x10^{-4}m.s^{-1} (or 1-1.7m.d^{-1}). This motion is consistent with the initiation and development of equatorial upwelling during these months and is in accord with assumption made in the previous section. The positive vertical velocity near the equator in November corresponds with a previous observation that the thermocline, once again, domes upwards at approximately 2°S due to equatorial upwelling instigated by a predominantly southwesterly current flowing across the equator.

The vertical velocities in the equatorial region between April and July and in November are of the order of the seasonal uplift of isohalines observed by Stander (1964) (cited in Nelson and Hutchings, 1983). At strong upwelling sites in the Benguela upwelling regime such as the Lüderitz upwelling cell, Stander (1964) noted the uplift of isohalines to be approximately 1.9m.d^{-1}.

Between August and October and in November, as the cool feature moves southward and the currents in the equatorial region are south-easterly, the upwelling and associated upward motion near the equator ceases.

A careful comparison is made between the temperature and vertical velocity sections at 5°S. The comparison reveals that the upward doming of the isotherms within the Angola Gyre between September and November is consistently characterized by weak upward motion south of its crest and weak downward motion north of it. Though somewhat unexpected for a region of divergence, this motion is a result of the interplay between horizontal current divergence and the southward movement of the dome-like structure of the thermocline (indicative of the Angola Gyre) and is illustrated in Figure 5.20.

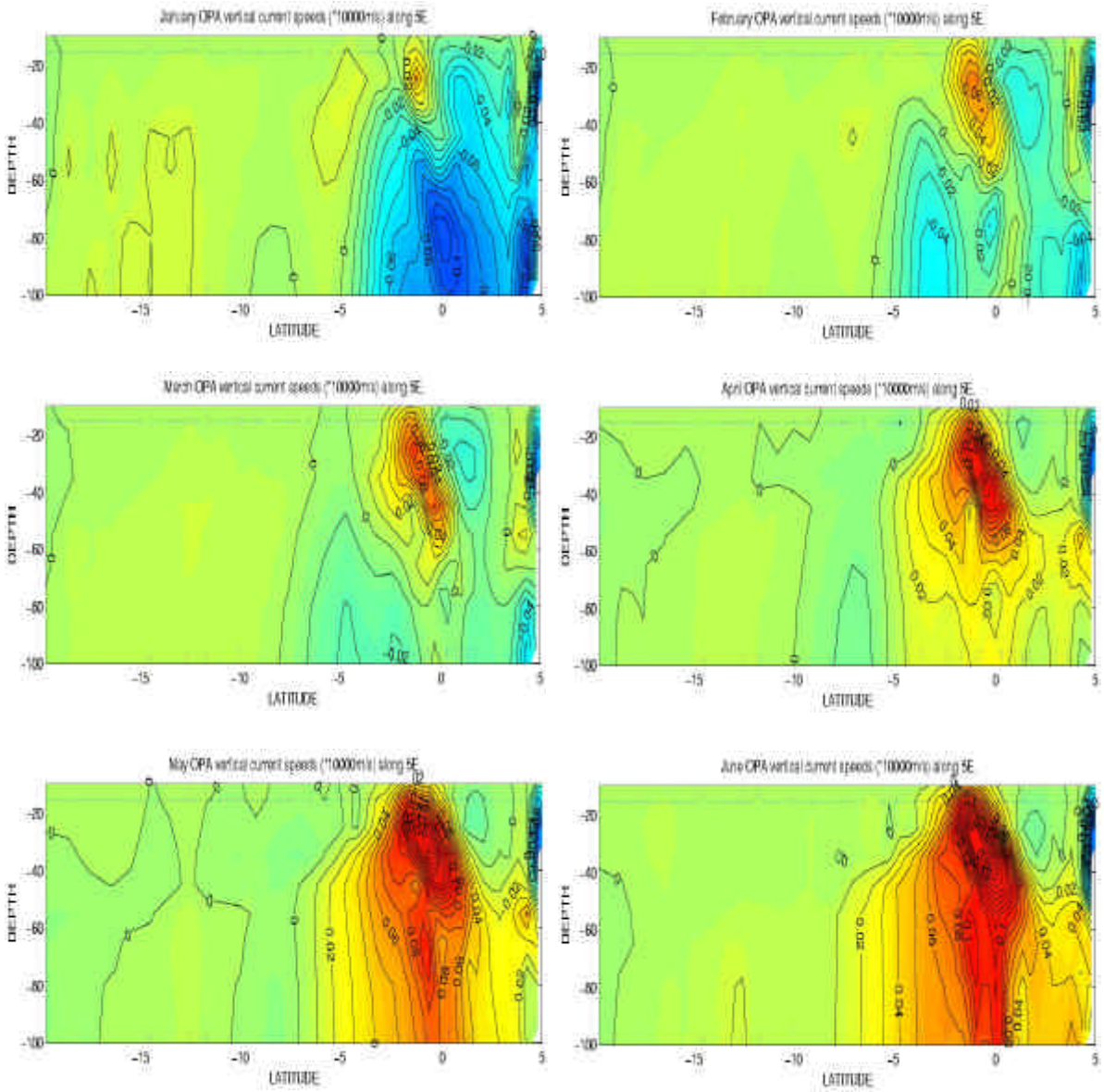

Figure 5.18: OPA/TOTEM vertical velocities of a section at 5°E (January to June). Positive and negative velocities correspond to upward and downward velocities respectively.

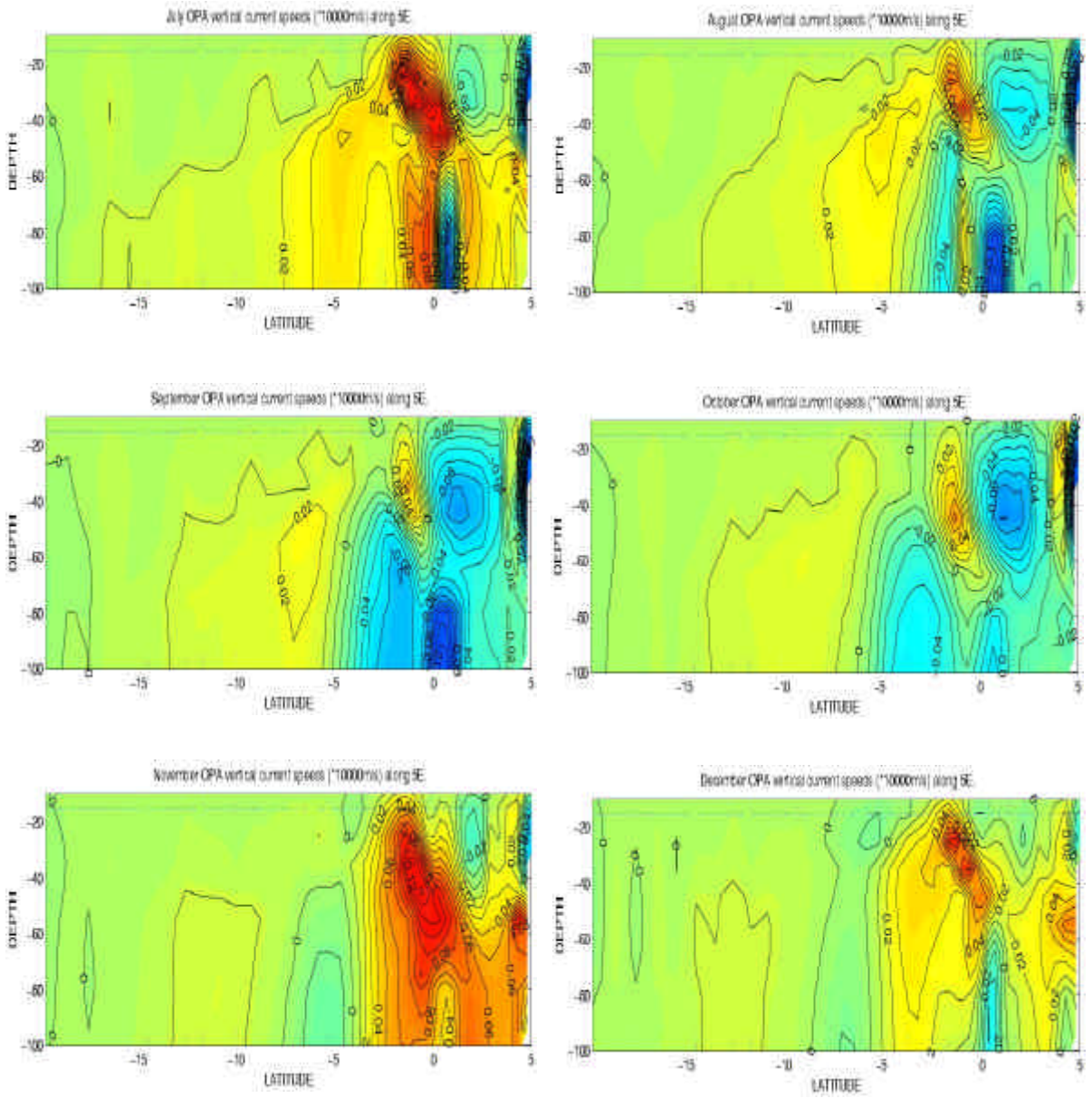

Figure 5.19: OPA/TOTEM vertical velocities of a section at 5°E (July to December). Positive and negative velocities correspond to upward and downward velocities respectively.

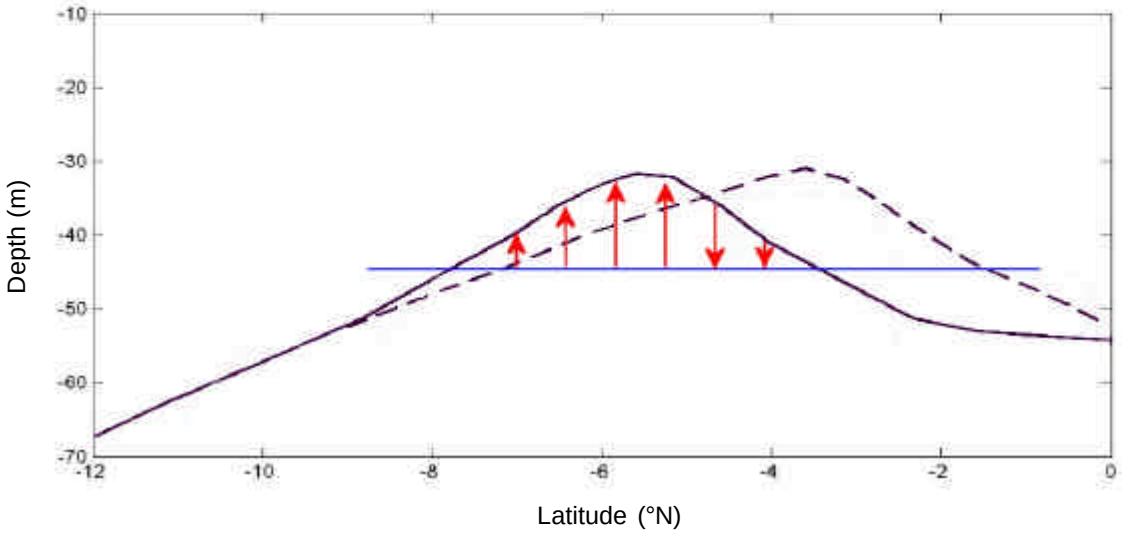

Figure 5.20: Sketch of the southward movement of the thermocline-ridge that results in the pattern of downward and upward motion within its cool, circular expression at 45m (approximately the position of the blue line). The dashed and solid lines represent the position of the thermocline in September and October respectively.

5.2.3 Synopsis

The velocity fields obtained from the OPA model have not only provided insight into the circulation associated with the Angola Gyre, but have also revealed the evolution of the gyre from its origin in the zone of equatorial divergence to its dissipation near the ABFZ. The following observations have been made:

- The northern limb of the upper portion of the Angola Gyre (upper-Angola Gyre) is unambiguously associated with the SEUC.
- The southern limb of the gyre is not as distinctly defined and is associated with a weak westerly component of the zonal velocities, which may be related to wind-induced Ekman transport.
- The eastern limb of the gyre seems to be unambiguously related to a strong, yet fairly narrow, poleward coastal current namely the Angola Current ($\pm 0.05 m.s^{-1}$).

- The western limb of the gyre is not clearly apparent. Instead, it is related to a marked weakening of the strong south-easterly current that forms the northern and eastern boundaries of the gyre.
- The SEUC is strongest (±0.14m.s^{-1}) in January, February, September and October when the gyre is a distinctly isolated cool feature at 45m. On the other hand, the SEUC is weakest (0.02-0.06m.s^{-1}) when it is least distinct (from April to June and, to a lesser extent, in November and December).
- The southward migration of the upper-Angola Gyre between September and November and again between January and April matches the southward displacement of the core of the SEUC.
- A south-westerly current that crosses the equator from 5°E to the coast between May and July and in November causes equatorial divergence (due to a change of sign of the coriolis parameter) and upwelling, which initiates the ridge-like structure of the thermocline.
- During the other months of the year, flow across the equator is dominated by a south-easterly current, thereby ceasing equatorial divergence and upwelling.
- From August to November and from December to April, the thermocline ridge moves southward in conjunction with the SEUC and the thermocline-expression of the Angola Gyre. Thus, the idea of a close relationship between these three features is strengthened.
- As the ridge moves southward, it appears to be maintained by a strong horizontal divergence.
- The northern limb of the deep, southward portion of the Angola Gyre beneath the ABFZ is related to the weak SECC. The deep counterpart of the gyre is a permanent feature, like the SECC which is situated at about 10°S throughout the year, with magnitudes of less than 0.02m.s^{-1}. The southern limb is linked to a weak westerly component, which may be a result of the offshore current induced by the Benguela upwelling regime.

The Angola Gyre can be thought of as having very distinct upper and lower portions, neither of which is connected with a distinct cyclonic motion. However, both are characterized by an upward doming of isotherms. The deep counterpart of the Angola Gyre is permanent and is situated approximately beneath the ABFZ with the SECC as its northern limb. The shallow counterpart is more distinct, but also more transient. It is generated by a semi-annual equatorial upwelling and shifts southward as the SEUC intensifies and moves similarly southward.

The next section investigates the effect of the local and remote wind fields on the equatorial currents and, in turn, their relationship to the Angola Gyre. Direct effects of wind forcing on the gyre, such as Ekman pumping and windstress curl, are also considered.

5.3 The Atmospheric Connection

Climatologies of various parameters calculated from 8 years of ERS satellite-derived wind data are used to assess the extent to which circulation features in the Angola Basin are forced by local and/ or remote wind fields.

This section provides a brief discussion of the spatial and temporal variability of the windstress field of the south Atlantic, with particular emphasis on correlations between the wind stress and circulation features and thermal structure in the Angola Basin. For a more explicit analysis of the wind forcing of the eastward equatorial currents, the monthly mean zonal wind stress component is calculated for a 10° x 10° box in the western and eastern Atlantic oceans: from the equator to 10°S, 20°W to 30°W and the Greenwich meridian to 10°E respectively (box A and B). The monthly mean zonal current component and thermocline depth in box B is compared to the monthly mean zonal wind stress component in both box A and box B, in order to ascertain whether the forcing mechanism is primarily remote or local. Finally, the local effects of windstress curl and Ekman pumping are briefly evaluated in terms of their contribution to the upward doming of the thermocline.

5.3.1 Wind stress variability in the south Atlantic.

The southeasterly tradewinds that prevail in the tropical and subtropical south Atlantic are closely related to the South Atlantic subtropical high, which is centered at approximately 32°S 5°W in austral summer and 27°S 10°W in winter (Peterson and Stramma, 1991). The northward movement of the high pressure system in the south Atlantic in winter matches the northward migration of the ITCZ and, ultimately results in a strengthening of the southeasterly tradewinds. Conversely, the tradewinds are weakest in summer when the ITCZ and the south Atlantic high pressure system are furthest south.

Figure 5.21 is a plot of the windstress magnitude and direction for the southeast Atlantic during mid-summer (January) and mid-winter (July) (refer to Appendix 4 for the mean wind speeds in January and July). They agree well with the results of Chelton *et al.* (1991), who calculated windstress from wind data obtained from the Seasat scatterometer. The plots confirm that the southeasterly tradewinds are weaker in summer than during winter in the south Atlantic.

The southeasterly tradewinds are consistently strongest (±0.08 $N.m^{-2}$ or 7-8 $m.s^{-1}$) in a band stretching from the southern African coast to the promontory of Brazil. A plot of the standard deviation of wind stress magnitude from a climatology of the windstresses in the south Atlantic (Figure 5.22) reveals that seasonal variability of wind stress generally increases toward the western Atlantic, with a maximum near the equator. Another pocket of high wind stress variability is situated at the African coast, south of about 20°S and extending to approximately 10°E.

Wind stress in the region of the Angola Basin is relatively low throughout the year (approximately 0.02-0.03 $N.m^{-2}$) and experiences only a small amount of seasonal variability (refer to Figure 5.22). However, south of about 15°S, is a zone of much higher wind stress that persists throughout the year. The zonal and meridional

extent of this region of higher wind stress varies throughout the year, resulting in the pockets of high variability that exist at about 15°S and between 25°S to 30°S.

Superimposed on Figure 5.22 is box A, in the west, and box B, in the east. The monthly mean zonal wind stress is calculated for each of these boxes and is used in the following section to investigate the link between the zonal current speed and thermocline depth in the Angola Basin and local and/or remote zonal wind stress variability. The zonal wind stress has been specifically chosen to assess the connection between the atmosphere and circulation in the Angola Basin as it has been shown to be a major driving force of the eastward equatorial currents due to the eastward pressure gradient force brought about by the southeasterly tradewinds (Picaut, 1985). Furthermore, it has been noted that the thermocline structure in the eastern Atlantic is also closely related to the zonal winds along the equator (McPhaden, 1984 and Hastenrath and Merle, 1986).

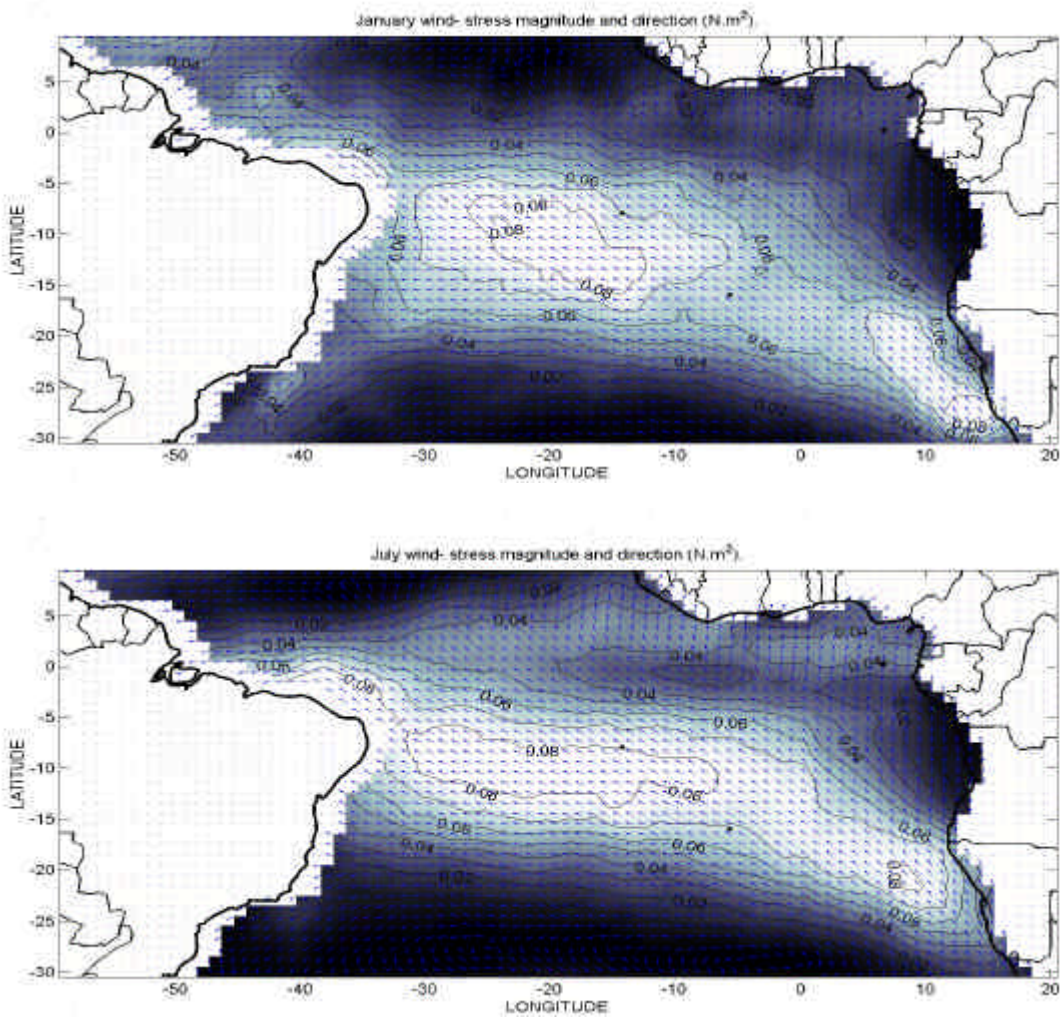

Figure 5.21: Plot of wind stress magnitude (unit: $N.m^{-2}$, contour interval: 0.01 $N.m^{-2}$) and direction of the South Atlantic Ocean for January (top) and July (bottom).

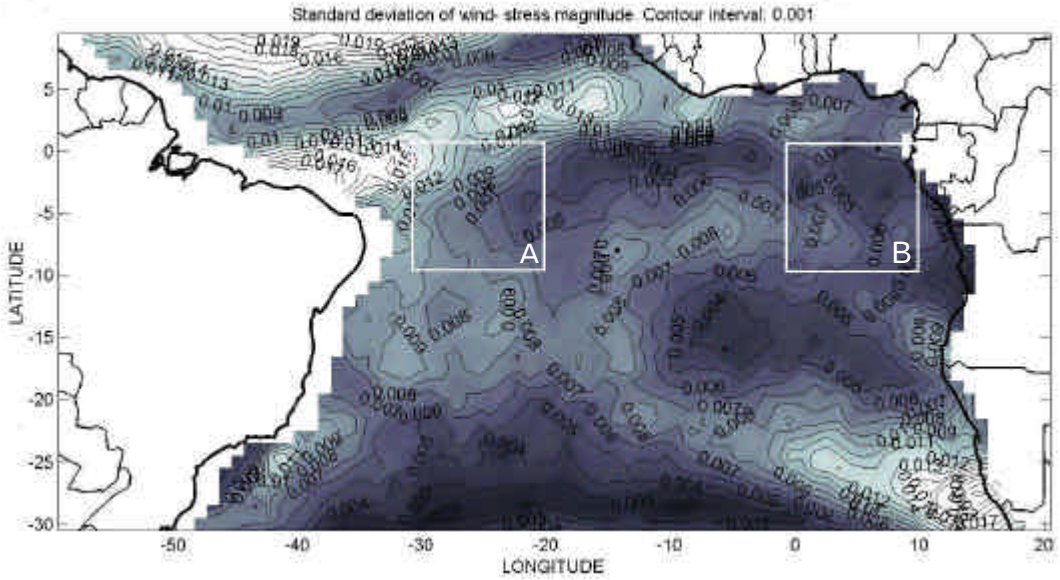

Figure 5.22: Standard deviation of wind stress magnitude in the south-east Atlantic Ocean. Superimposed are boxes A (20°W-30°W, equator - 10°S) and B (Greenwich meridian - 10°E, equator - 10°S).

5.3.2 Local vs. remote forcing

Figure 5.23 is a plot of the monthly mean zonal windstress components in the eastern and western equatorial Atlantic (box B and A respectively). The negative values correspond to the continuous tradewinds that blow toward the west, therefore the more negative the velocity, the stronger the southeasterly tradewind.

A conspicuous difference between the wind stress variability in the eastern and western equatorial Atlantic is that a somewhat semi-annual signal typifies the east, whereas an annual signal is present in the western equatorial Atlantic. In the eastern equatorial Atlantic, windstress peaks in May (0.018 $N.m^{-2}$) and to a lesser extent in November (0.013 $N.m^{-2}$). On the other hand, zonal windstress in the east is weakest from December until February (±0.011-0.009 $N.m^{-2}$) and in September (0.012 $N.m^{-2}$).

Windstress in the western equatorial Atlantic is approximately four times stronger and is more seasonally variable than in the eastern Atlantic. In the west, wind stress is at a maximum between June and October and exerts forces between 0.06N.m^{-2} and 0.065N.m^{-2} on the sea surface during this time. The wind stress begins to wane in November and is at its minimum between February and May (0.05-0.055 N.m^{-2}).

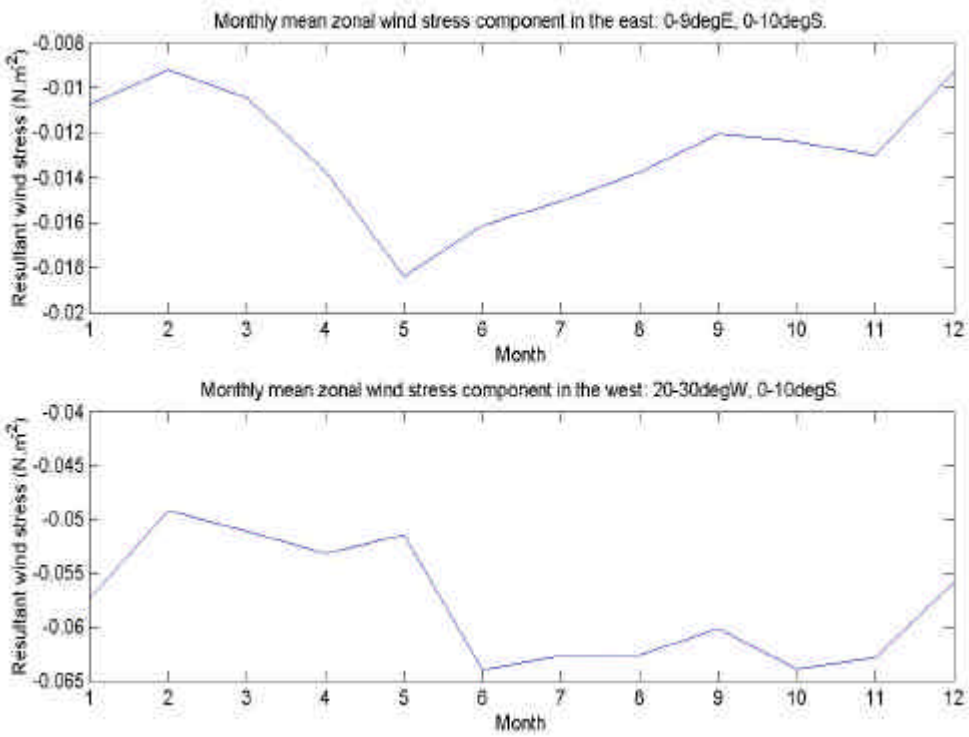

Figure 5.23: Monthly mean zonal wind stress component in the eastern equatorial Atlantic (box B, top) and the western equatorial Atlantic (box A, bottom).

The zonal component of currents in the region of the Angola Basin (Fig. 5.24) at a depth of 45m has a very distinct semi-annual signal and is eastward throughout the year, except for June when it is weakly westward. Eastward velocities are strongest in October (±0.047m.s^{-1}) and February (± 0.037m.s^{-1}) and weakest in June (±-0.0025 m.s^{-1}) and December (±0.0025 m.s^{-1}). These results support the finding made in section 5.2.1, that the SEUC is strongest in January and February and between September and November.

Although the seasonal signals of the zonal wind stress and zonal current velocity in the eastern equatorial Atlantic are somewhat out of phase, the fact that they are both semi-annual implies that a relationship might exist between them. Also based on a comparison of their seasonal signals, windstress variability in the western portion of the Atlantic Basin seems to have little influence on the seasonal fluctuation of currents in the eastern equatorial Atlantic. Despite the implications of these findings, the exact dynamics involved in the relationship between the zonal wind and the equatorial currents in the Angola Basin are beyond the scope of this investigation.

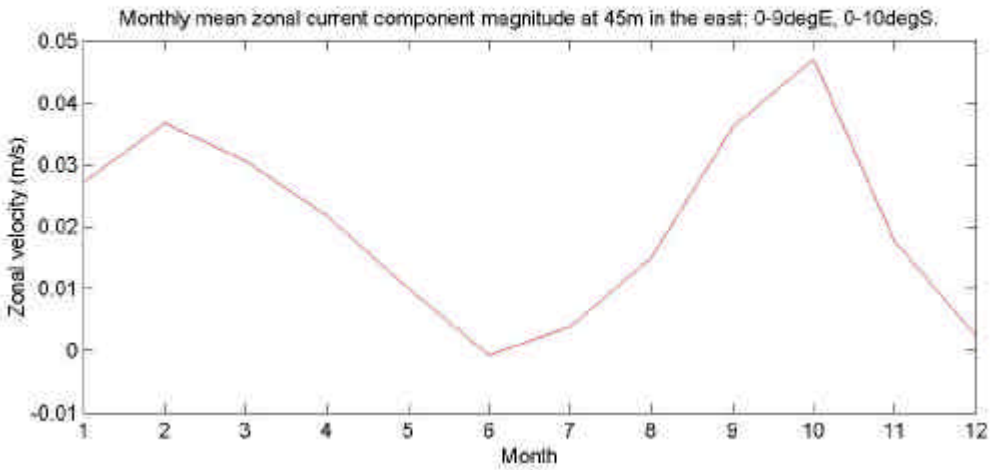

Figure 5.24: Monthly mean zonal velocity component in the eastern equatorial Atlantic (box B).

The monthly mean thermocline depths in box B (Figure 5.25) reveal that the thermocline in the Angola Basin, also with a distinct semi-annual signal, is deepest in February and October and shallowest in July. The seasonal fluctuation of the depth of the thermocline supports the findings of Busalacchi and Picaut (1983), who's model investigation revealed similar results. The seasonal signal of the thermocline depth is in phase with the eastward equatorial currents

whereby the strongest eastward equatorial currents at 45m coincide with the deepest thermocline (February and October). Conversely, the thermocline is shallowest in June and December when the eastward currents are weakest. The close relationship between the thermocline structure and the equatorial system of currents in the eastern equatorial Atlantic is noted by Katz (1981) and Hastenrath and Merle (1987) concluded that the inherent mass and pressure distribution induced by the ridging thermocline is associated with the eastward equatorial currents.

The above analysis provides evidence that the equatorial currents are closely tied to the thermocline structure across the equatorial Atlantic Ocean. Furthermore, it confirms the fact that in the eastern equatorial Atlantic both the thermocline depth and the equatorial currents are forced by the local zonal wind stress component.

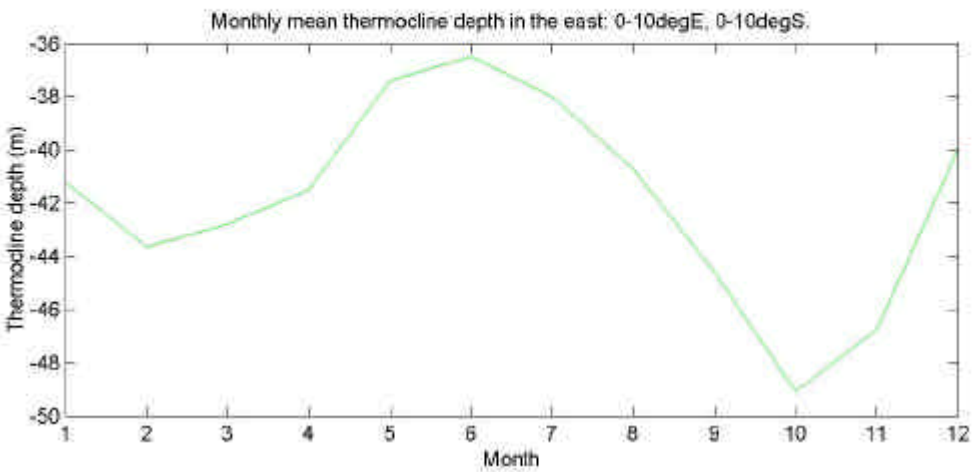

Figure 5.25: Monthly mean thermocline depth in the eastern equatorial Atlantic (box B).

5.3.3 Windstress curl and Ekman pumping

This section investigates the possible effects of Ekman pumping on the thermal structure of the Angola Basin. The horizontal shear of windstress (windstress

curl) induces a negative (positive) vorticity on the ocean, resulting in cyclonic (anticyclonic) motion in the southern hemisphere. Ekman pumping responds to the cyclonic and anticyclonic motion by an upward or downward motion of the thermocline respectively. Figure 5.27 (a & b) are plots of the Ekman pumping velocities for January and July and Figure 5.27 (c) is a timeseries of the monthly mean Ekman pumping velocities in box B (i.e. 2-10°S 0-10°E).

Negative windstress curl (around -0.7 x 10^{-7} N.m^{-3}) prevails throughout the year in a wedge-shaped area that extends in a northwesterly direction from the African coast south of 30°S (Figure 5.26). The windstress curl calculated using the ERS wind field is in agreement with the curl of the 25km-resolution QuikSCAT wind speeds computed by Chelton *et al.* (2004). The seasonal signal of the windstress curl is unequivocally semi-annual, inducing strongest negative vorticity on the ocean during April and August. The negative windstress curl in the Angola Basin is weakest in July and December. The perpetually negative windstress curl in the Angola Basin implies that the local wind forcing always tends to induce cyclonic circulation and an upward motion of the thermocline (positive Ekman pumping).

The region of positive Ekman pumping mirrors that of the negative windstress curl, extending in a northwesterly orientation from the African continent (Figure 5.27 a & b). The wedge of positive Ekman velocities that extend from the African continent in a northwesterly direction are in approximate agreement with those calculated by McClain *et al.* (1993) who used satellite-derived surface winds obtained from the Fleet Numerical Oceanography Center (FNOC). The upward Ekman pumping velocity is most intense during April and August (2 x 10^{-6} m.d^{-1} and 2.5 x 10^{-6} m.d^{-1}) and weakest in July and December (0.3 x 10^{-6} m.d^{-1} and 0.2 x 10^{-6} m.d^{-1}). Despite an unambiguous semi-annual signal, the difference between the maximum and minimum Ekman pumping velocities is only about 2.3 x 10^{-6} m.d^{-1} and is therefore unlikely to be the primary forcing mechanism of the doming of the thermocline ridge in the eastern equatorial Atlantic where the seasonal range of thermocline depth is about 13 m.

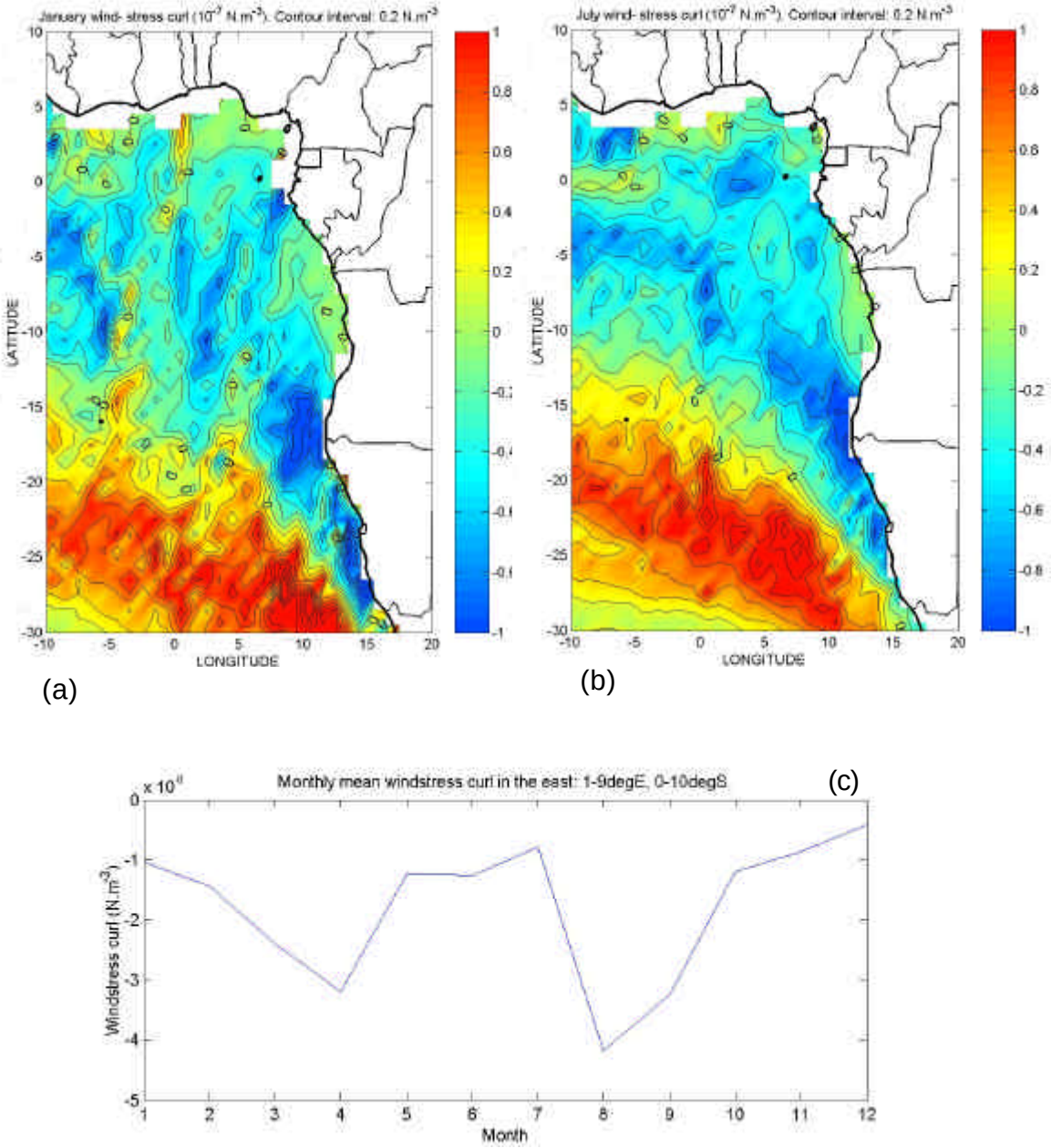

Figure 5.26(a & b): Windstress curl for January and July. Contour Interval is 0.2 N.m^{-3}. **Figure 5.26(c):** Monthly mean windstress curl in the eastern equatorial Atlantic (box B).

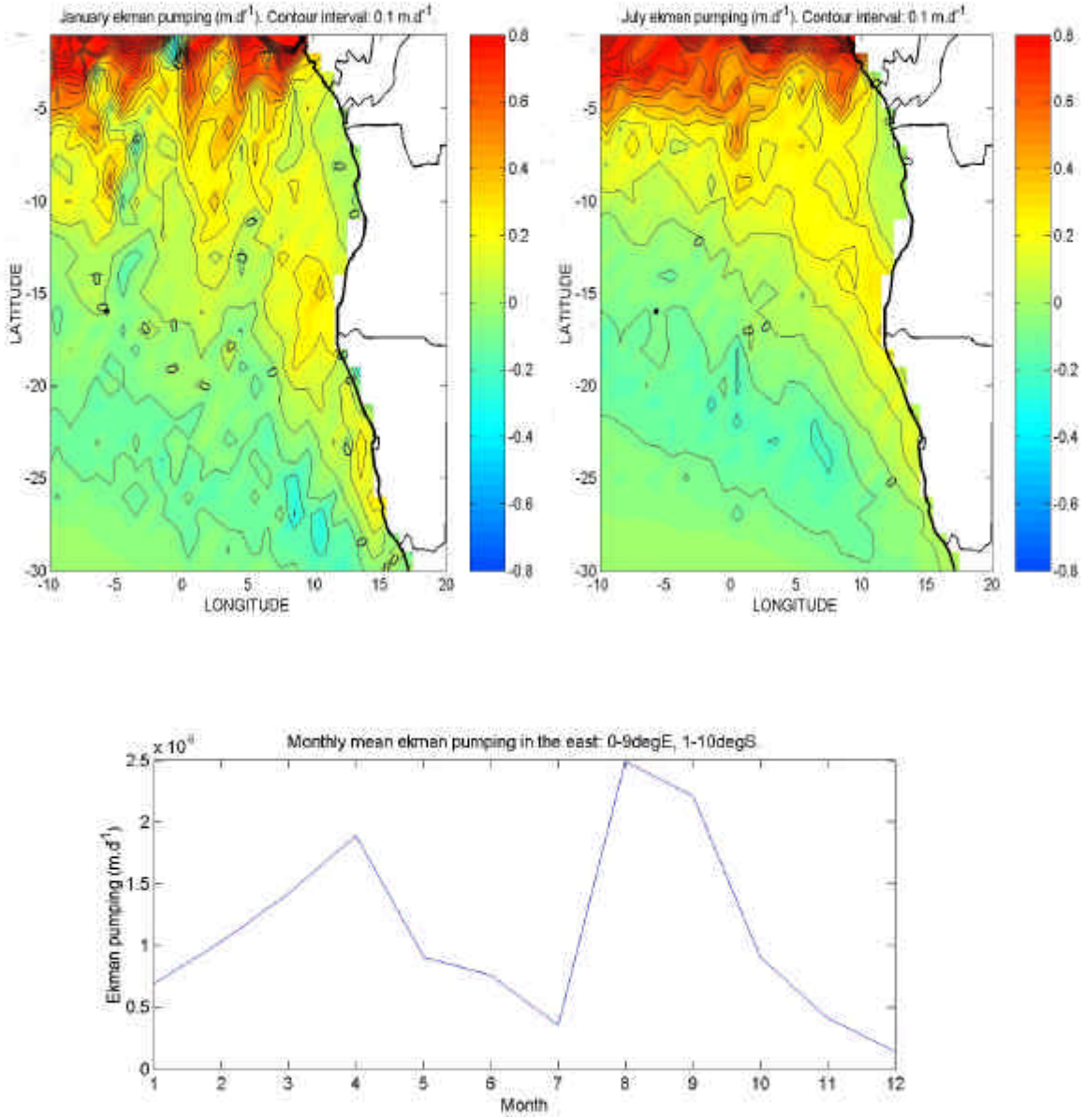

Figure 5.27(a & b): Ekman pumping velocities for January and July. Contour Interval is 0.1 $m.d^{-1}$.

Figure 5.27(c): Monthly mean Ekman pumping velocity in the eastern equatorial Atlantic (box B).

Further indication that the doming of the thermocline ridge in the eastern equatorial Atlantic is not primarily a result of local Ekman pumping lies in the fact that their semi-annual seasonal signals are out of phase in the following manner: when the upward Ekman pumping is most intense in April and August, the thermocline is approximately two months from its shallowest and deepest positions respectively.

The small influence that Ekman pumping has on the doming of the thermocline supports the finding of Busalacchi and Picaut (1983). From numerical studies, they concluded that Rossby waves determined the seasonal cycle of the doming in the Angola Basin and that the effect of Ekman pumping is small.

5.3.4 Synopsis

Though brief, this analysis of the influence of winds on the circulation and thermal characteristics of the Angola Basin has allowed for the following conclusions to be made:

- The seasonal cycle of the eastward equatorial currents is likely to be more influenced by local winds than by the remote wind field.
- The depth of the thermocline is closely tied to the intensity of the eastward equatorial currents and hence to the local winds.
- Throughout the year, windstress curl and Ekman pumping in the Angola Basin are conducive to cyclonic circulation of the sea surface and upwelling of the thermocline.
- The role of Ekman pumping in the seasonal cycle of thermocline depth in the Angola Basin is small.

5.4 Finer-scale structures resolved by the CLIPPER-ATL6 model

Only after the analyses of the OPA/TOTEM model output had been completed did the higher resolution output of the CLIPPER model become available. The CLIPPER model is based on the same primitive equation code as the OPA model, but has a higher resolution (1/6°) and is therefore eddy-permitting. This section briefly highlights the differences brought about by the higher resolution model and pays particular attention to a region of intense mesoscale variability in the region of the so-called 'Angola Dome'.

5.4.1 The Angola Gyre

Figure 5.28 shows the temperature output of both the CLIPPER and OPA/TOTEM models at 42m and 45m respectively for the month of October. The large-scale (1000-2000km) cool feature previously observed in the OPA/TOTEM temperature analysis, centered at approximately 6.5°S 7°E, and identified as the Angola Gyre remains a prominent feature in the CLIPPER temperature output, though narrower and centered more to the northwest (4°S 4°E). Furthermore, the seasonal cycle of the gyre observed in the OPA analysis is reproduced by the CLIPPER data (refer to Appendix 4 for the full climatology of the CLIPPER temperature output at 42m), despite mesoscale differences generated by the higher resolution model. The most conspicuous difference is that the margins of the cool feature at 42m are convoluted and therefore more ambiguous. Also, a tongue of relatively cool water (ranging from 19°C in winter to 22°C in summer) appears to be a permanent feature along the equator from the African coast to about 5°W, but is detached from the coast during spring (September to November).

The similarities between the OPA/TOTEM and CLIPPER model outputs are not surprising, bearing in mind that both are based on the same primitive equation code. The more detailed structure of the Angola Gyre resolved by CLIPPER is striking, yet insufficient to deem the investigation of the large-scale, seasonal fluctuations of the gyre using the OPA/TOTEM output invalid.

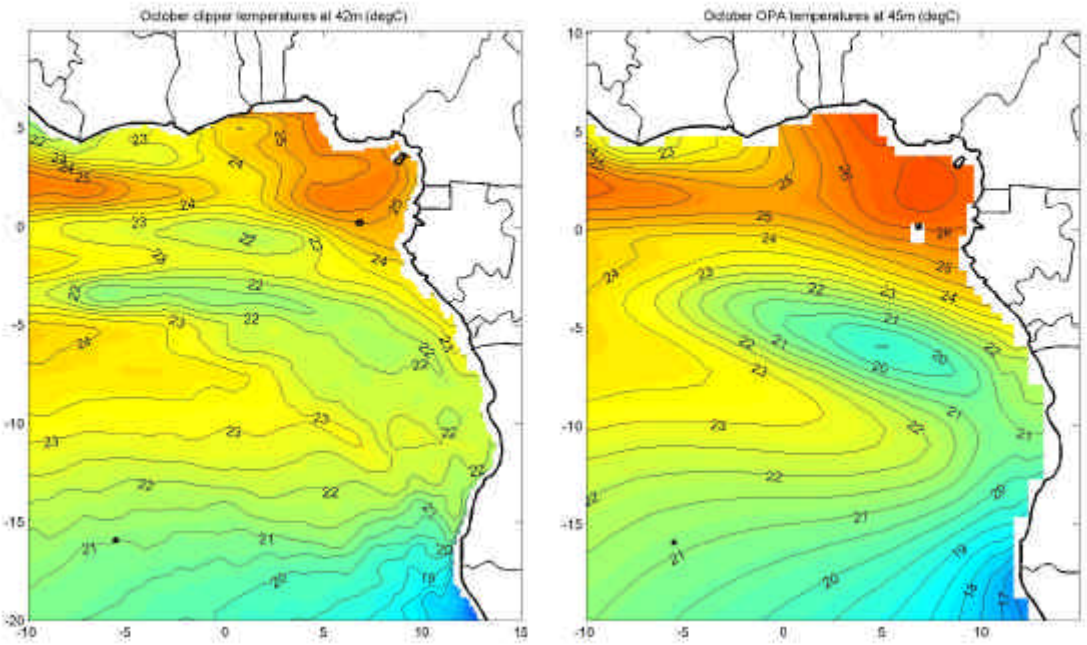

Figure 5.28: A comparison between the OPA/TOTEM (right) and CLIPPER (left) temperature output at 45m for the month of October.

5.4.2 The region of the Angola Dome

The somewhat elusive Angola Dome has been identified via *in situ* measurements periodically since 1967. Using hydrocast and bathythermograph measurements spanning 1902 to 1963, Mazeika (1967) located the dome at 9°S 9°E and observed that it was only present between January and April. *In situ* measurements collected in February 1977 enabled Voituriez and Herbland (1981) to locate it at 10°S 10°E. It was detected at approximately 12°S 12°E in April 1997 (Filipe, 1998) and at 9°S 8.5°E in April 2001 (Mohrholz *et al.* 2001), once again with *in situ* measurements. In all cases, the dome has been noted to be of mesoscale dimensions (i.e. of the order of 100-300km in diameter). The highly variable nature of the position of the dome is illustrated by the fact that since its discovery in 1967 it has not been observed in the same place twice. A further challenge in research of the dome thus far is that investigations have been based on *in situ* measurements, which despite obvious advantages, fail to

coherently resolve the spatial and temporal thermal structure in the region of the dome. For this reason, the use of the CLIPPER high resolution model might aid a better understanding of the mesoscale dynamics of the region of the Angola Dome.

Appendix 5 reveals that the region of the Angola Dome, ± 9-12°S 8.5-12°E, (based on the outcome of past *in situ* measurements), is a region of highly variable mesoscale activity, within the realm of the Angola Gyre. It is a region that is characterized by warm and cool filaments and eddies of the order of about 100-300km. At a depth of 42m the convoluted nature of the temperature structure in the area of the dome is most extreme in spring.

The seasonal mean current direction and magnitudes from 5°S to 15°S and 5°E to 15°E (Figure 5.29) as resolved by the CLIPPER horizontal velocity output reveals the highly variable nature of the horizontal current field, particularly south of 8°S and from about 8°E to the coast. The OPA/TOTEM horizontal velocity output (Appendix 6) resolves little of the finer-scale features present in Figure 5.29, other than a weak anticyclonic feature centered on 10°S 10°E in winter and a NW-SE oriented cyclonic feature at about 13°S 7°E in winter.

The convoluted nature of the horizontal current field of the CLIPPER model comprises a meandering poleward current at the coast and a more complex pattern of converging, diverging, cyclonic and anticyclonic structures further offshore. The intricate nature of the current direction is most evident during autumn and winter and least obvious in spring. Regions where cyclonic and anticyclonic features are most prominent correspond to weakest current magnitudes, whereas the strongest current is the poleward current at the coast. The poleward flow is fastest and extends furthest south in spring, deteriorating during summer and autumn and is at its weakest in winter.

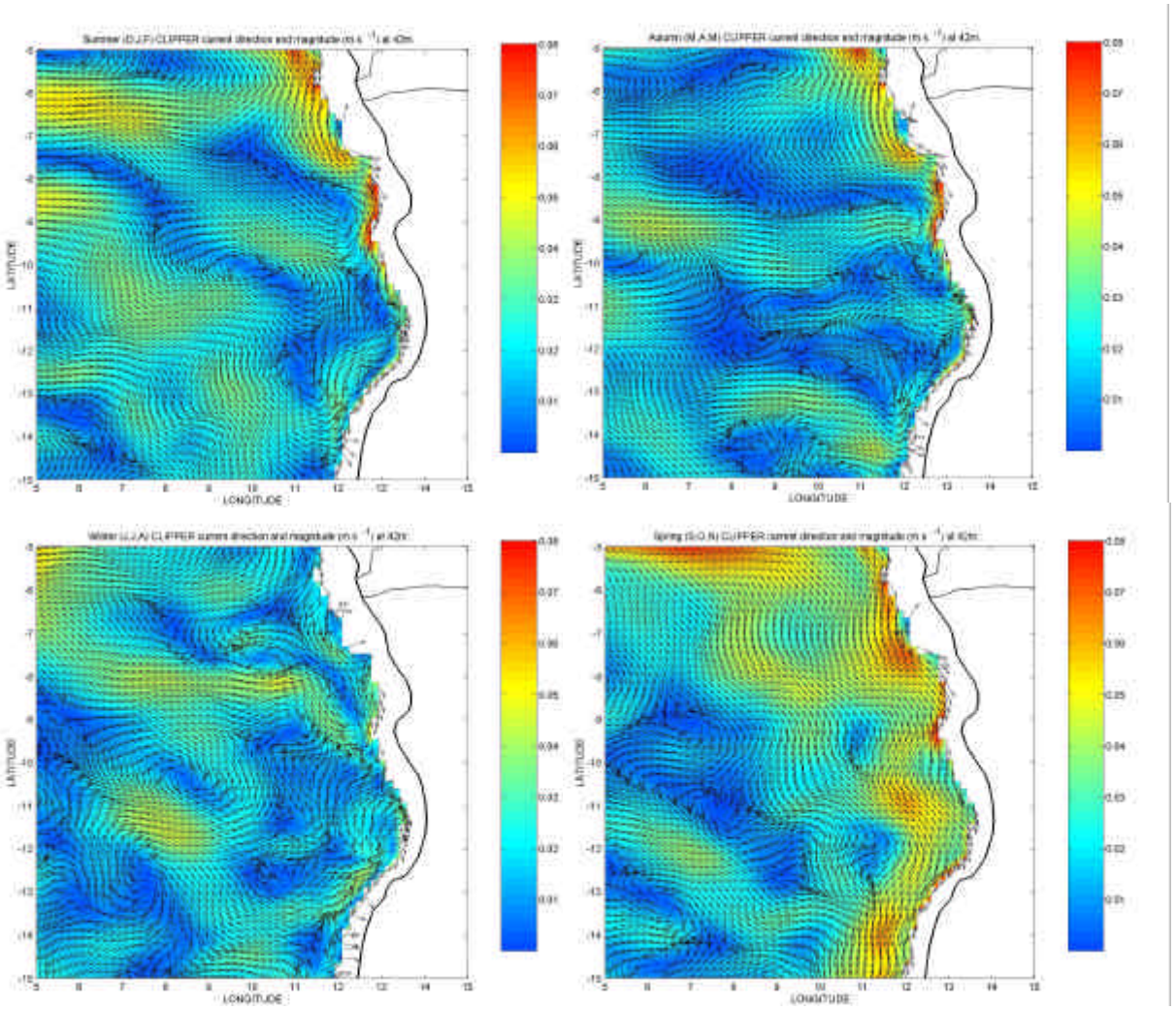

Figure 5.29: Seasonal mean resultant horizontal flow pattern and magnitude at 45m as resolved by the CLIPPER model.

The fact that mesoscale horizontal current features (e.g. eddies and patterns convergence and divergence) are most prevalent in the region of the dome during autumn and winter when the thermal structure is least convoluted is a somewhat surprising finding. However, in spring when cool and warm filaments and eddies are most apparent, the meandering poleward coastal current is strongest and extends well into the region of the dome. In consequence, a strong horizontal shear between the coastal flow and the much weaker offshore currents is most intense during spring. The intricate nature of the thermal structure between about 9-12°S and 8-12°E therefore appears to be related to the meandering nature of the poleward current and to the strong horizontal shear that exists between it and the offshore current field.

The highly convoluted nature of the region of the Angola Dome produces examination difficulties of its position, structure and seasonal signal, especially for investigations based on temporally and spatially incoherent *in situ* measurements. For this reason, it is conceivable that the characteristics of the dome, drawn from conclusions based on *in situ* data, have been somewhat misinterpreted. The findings of this brief analysis suggest that the Angola Dome, though perhaps indeed a cyclonic feature associated with an upward-doming of isotherms, is rather one of many such features within a highly dynamic area. This result is in support of the conclusion encountered by Mohrholz *et al.* (2001), who identified the Angola Dome as the largest of a number of mesoscale eddies within the area of the Angola Gyre.

5.4.3 Synopsis

This cursory comparison between the OPA/TOTEM and CLIPPER model output is simply a consideration of the smaller-scale features revealed by the higher resolution model. The outcome of this brief inquiry is summarized as follows:

- Similarities between the two models demonstrate that the lower-resolution OPA/TOTEM model is sufficient for the analysis of the large-scale circulation features of the Angola Basin, including the Angola Gyre.

- A significant finding revealed by the CLIPPER data is that the region of the Angola Dome is characterized by a convoluted temperature structure (i.e. cool and warm eddies and filaments) and highly variable currents.
- The Angola Dome is one of many such features between about 9-12°S and 8-12°E. Consequently, interpretations of *in situ* measurements leading to conclusions of the position, structure and seasonal signal of the Angola Dome may be somewhat inaccurate.

CHAPTER SIX
CONCLUSIONS

The primary objective of this thesis was to identify and investigate the most prominent circulation features of the Angola Basin from the output parameters of the OPA/TOTEM general circulation model, focusing particularly on the Angola Gyre and the Angola Dome. A key objective was the evaluation of the extent to which the OPA/TOTEM model resolves these features in terms of the seasonal variability of their vertical and horizontal thermal structures and associated circulation characteristics. Analyses of windstress, windstress curl and Ekman pumping were all computed from ERS satellite-derived wind speeds and were conducted with the intention of deciphering the link between the local and/ or remote wind field and circulation patterns in the Angola Basin.

The most conspicuous feature of the Angola Basin discerned in the thermohaline output of the OPA/TOTEM model is a ridge-like structure of the thermocline, which results in a cool feature that is most distinct at a depth of 45m. The feature is elongate in shape, with a NW-SE orientation and, at a depth of 45m, is centered at approximately 5°S 5°E with dimensions of the order of 1000x500km. While the cool feature at 45m is essentially an 'outcropping' of the thermocline-ridge at that depth, a deeper upward displacement of isotherms exists to the south and is situated approximately beneath the ABFZ (±16°S). This deeper feature may be interpreted as a southward shift of the thermocline-ridge at greater depths.

On the basis of these findings, the cool feature appears to be the 'so-called' Angola Gyre that has been identified and described by Moroshkin (1970) and Gordon and Bosley (1991), among others. From their *in situ* studies, the dimensions of the gyre have been determined as being of the order of 1000-2000km and the center of the gyre has been located within a degree of 13°S 5°E. The significant disparity between this position and the position discerned in the

OPA/TOTEM model output is a consequence of the fact that only the dome-like feature in the

upper, thermocline layers was taken into account in this analysis. If the permanent cool feature beneath the ABFZ had been included, the position of the gyre would have been taken to be considerably further south.

The distinct cyclonic circulation that one might expect to be associated with the Angola Gyre is not conspicuous in the OPA/TOTEM velocity output. However, the northern edge of both the shallow thermocline-doming and the deeper feature beneath the ABFZ are clearly coincident with major eastward currents; the SEUC (situated between 2-5°S) and the SECC (at around 10°S) respectively. If one were to consider the deeper feature as the southward expression of the Angola Gyre, these observations support the findings of Waconge and Piton (1992) who speculate that the northern limb of the gyre is delineated by both the SEUC and the SECC. In accord with the results of Moroshkin (1970), both these eastward currents are observed to bend southwards as they approach the African continent, contributing to the poleward Angola Current, which constitutes the eastern limb of the gyre. The southern and eastern limbs of the gyre are not as clearly defined and are associated with a weak westerly flow regime.

The seasonal cycle of the eastward equatorial currents are in accordance with the seasonal variability of both the shallow and deep portions of the Angola Gyre, thus recapitulating the close ties between them. The SEUC is strongest ($\pm 0.14 m.s^{-1}$) in January, February, September and October when the thermocline-ridge is deepest, resulting in a distinctly isolated cool feature at 45m. On the other hand, the SEUC is weakest ($0.02-0.06 m.s^{-1}$) when the thermocline-ridge is shallowest and its expression at 45m is least distinct (from April to June and, to a lesser extent, in November and December). Furthermore, the southward migration of the thermocline-ridge between September and November and again between January and April matches the southward displacement of

the core of the SEUC. The deep portion of the Angola Gyre shows little seasonal variability, other than a slight northward tilt of its vertical axis when the

thermocline-ridge is furthest south. Similarly, the SECC, which constitutes the northern limb of the deeper cool feature, is fairly consistent, in position and magnitude, throughout the year with velocities of less than $0.02 m.s^{-1}$.

The semi-annual nature of the gyre appears to be initiated by a south-westerly component of the equatorial flow regime from 5°E to the coast between May and July and again in November. Albeit weak, the south-westerly current component results in equatorial divergence due to the change in sign of the coriolis parameter across the equator. This results in an upwelling of the thermocline near the equator in austral winter and to some degree in November. During other months of the year, flow across the equator is dominated by a south-easterly current, thereby ceasing equatorial divergence and upwelling. As the ridge moves southward, it appears to be maintained by a strong horizontal divergence. The divergence is associated with strong SEUC, the much weaker westerly current that exists to the south of it and the shear between them.

The brief investigation of the ERS satellite-derived wind data showed that the seasonal cycle of the eastward equatorial currents is more probably related to the local than the remote windstress field. This is in support of the finding by Philander and Pacanowski (1986) who, from a model study, observed that the response of the tropical Atlantic Ocean was in phase and corresponded reasonably well with local winds. Throughout the year, windstress curl and Ekman pumping velocity in the region of the Angola Gyre are conducive to cyclonic circulation of the sea surface and upwelling of the thermocline. However, their scales of magnitude were found to be insignificant compared to the seasonal fluctuation of the thermocline depth.

The so-called Angola Dome has been identified as a mesoscale feature (100-300km) and is situated within a couple of degrees of 9°S 9°E (Mazeika, 1967; Voituriez and Herbland, 1982; Mohrholz, 2001; Lien, 2004). Thus defined, the Angola Dome is not resolved by the climatologies produced from the OPA/TOTEM model output due to its relatively small size and due to the fact that its position is quite variable. For this reason, a higher resolution model (CLIPPER) was briefly examined in an attempt to locate the Angola Dome. A significant finding revealed by the CLIPPER data is that the region of the Angola Dome is characterized by a convoluted temperature structure (i.e. cool and warm eddies and filaments) and highly variable currents. This supports the *in situ* investigation by Mohrholz *et al.* (2001) as well as the model-based study by Lien (2004); both found that the region of the dome was characterized by vigorous eddy activity. Mohrholz *et al.* (2001) identified the Angola Dome as the largest of the mesoscale eddies (± 200km in diameter) in this region, with its center at about 9°S 8.5°E. Lien (2004) hypothesized that the eddies in the region of the Angola Dome originate from baroclinic instabilities of the SECC that he observed to enter the Angola Basin at 10-12°S.

Unfortunately, the scope of this thesis did not include a thorough investigation of the Angola Dome and its forcing mechanisms. However, the somewhat superficial nature of the CLIPPER analysis has provided an understanding of the nature of the area in which the dome is thought to be positioned. The dome appears to be one of many mesoscale eddies in a highly dynamic area that is characterized by, not only eddies, but also meandering filaments. As such, the perception of the Angola Dome as a distinct and isolated feature within the Angola Basin is not supported by the model output.

A comparison of the Guinea and Costa Rica Domes with the Angola Dome and the Angola Gyre (defined as a mesoscale eddy and a large-scale cool feature respectively), reveals that the Angola Gyre is more similar to the Guinea and Costa Rica Domes than is the Angola Dome. For instance, both the Guinea and

Costa Rica Domes are located at the terminating edge of the east-west thermocline-ridge (Busalacchi and Picaut, 1983 and Fiedler, 2002 respectively) and both are of the order of 1000km in diameter. Furthermore, the Guinea Dome is positioned in a NW-SE orientation and is bounded to the south by the North Equatorial Undercurrent (NEUC) (Siedler, 1992). Therefore, the 'Angola Gyre' that is associated with an upward-doming of the thermocline and compares favourably with the Guinea and Costa Rica Domes is a misnomer and the term 'Angola Dome' more appropriately categorizes the feature.

REFERENCES

Asselin, R., 1972. Frequency filter for time integrations. *Mon. Wea. Rev.,* **100,** 487- 490.

Bentamy, A., Y. Quilfen, P. Queffeulou and A. Caranie, 1991. Calibration of the ERS-1 scatterometer C-band model. *IFREMER Technical report*, **DRO/OS-94-01,** IFREMER, Brest. 72pp.

Bentamy, A., Y. Quilfen, F. Gohin, N. Grima, M. Lenaour and J. Servain, 1996. Determination and validation of the of average wind fields from ERS-1 Scatterometer measurements. *The Global Ocean and Atmosphere System,* **4**, 1-29.

Berrit, G.R., Low salinity waters off the Gulf of Guinea. *Proceedings of the symposium on the oceanography and fisheries resources of the tropical Atlantic. Results of the ICITA and GTS. Review papers and contributions.* Abidjan, Ivory Coast, 20- 26 Oct. 1966.

Blanke, B. and P. Delecluse, 1993. Variability of the Tropical Atlantic Ocean simulated by a general circulation model with two different mixed- layer physics. *J. Phys. Oceanog.,* **23,** 1,363- 1,388.

Boyd, A. J., J. Salat, and M. Maso, 1987. The seasonal intrusion of relatively saline water on the shelf of northern and central Namibia. In *The Benguela and Comparable Ecosystems,* eds. A. I. L. Payne, J. A. Gulland and K. H. Brink. *S. Afr. J. mar. Sci,* **5,** 107- 120.

Brown, J., A. Colling, D. Park, J. Phillips, D. Rothery and J. Wright, 1989. Ocean Circulation. G. Bearman, ed, Pergamon Press in assoc. with the Open University, Milton Keynes, England, 238pp.

Busalacchi, A and J. Picaut, 1983. Seasonal variability from a model of the Tropical Atlantic Ocean. *J. Phys. Oceanog.,* **13,** 1,564-1,588.

Cane, M. A., 1979. The response of an equatorial ocean to simple wind stress patterns: II. Numerical results. *J. Mar. Res.,* **37,** 253-299.

Cane, M. A. and D. W. Moore, 1981. A note on low-frequency equatorial basin modes. *J. Phys. Oceanog.,* **11,** 1,587- 1,585.

Chelton, D.B. and A. M. Mestas- Nunez, 1991. Global wind stress and sverdrup circulation from the Seasat scatterometer. *J. Phys. Oceanog.,* **20,** 1175-1205.

Chelton, D.B., M.G. Schlax, M.H. Frielich and R.F. Milliff, (2004). Satellite measurements reveal persistent small – scale features in ocean winds. *Science,* **303 (5660),** 978-983;

Cury, P. and C. Roy. MS. Modélisation de l'abondance des espéces pélagiques côtiéres de Coté d'Ivoire integrant l'effort de péche et un indice d'upwelling. ORSTROM, 24 Rue Bayard, 75008, Paris, France.

Demin, Y. L., E. Hagen and A. M. Gurina, 1981. Large-scale currents in the upper layer of the Canary upwelling area in summer. *Oceanology,* **21,** 613- 618.

Delecluse, P., G. Madec, M. Imbard and C. Levy, 1993. OPA version 7 ocean general circulation model reference manual. *Internal Report, LODYC,* **93/05.** Available from LODYC, Université Paris VI, 75252 Paris cedex 5, France.

Eckhart, C., 1958. Properties of water. Part II: The equation of water and sea water at low temperatures and pressures. *Am. J. Sci.,* **256,** 225- 240.

Emery, W. J. and R. E. Thomson, 1997. Data Analysis Methods in Physical Oceanography, Chpt., 5. Pergamon, 1997.

Eisma, D. and A. J. van Bennekom, 1978. The Zaire River and estuary and the Zaire outflow in the Atlantic Ocean. *Neth. J. of Sea Res.,* **12 (3/4),** 255-272.

Farge, M., 1992. Wavelet transforms and their applications to turbulence. *Annu. Rev. Fluid. Mech.,* **24,** 395- 457.

Fiedler, F. C., 2002. The annual cycle and biological effects of the Costa Rica Dome. *Deep- Sea Res.,* **49,** 321- 338.

Filipe, V. L. L., 1998. The Angola Dome observed in April 1997. *Proceedings of the International Symposium on Environmental Variability in the South – East Atlantic, Swakopmund.*

Gordon, A. L. and K. T. Bosley, (1991). Cyclonic gyre in the tropical South Atlantic. *Deep-Sea Res., Suppl.,* **38**, S323- S343.

Hagen, E., (2001). Northwest African upwelling scenario. *Oceanologica Acta,* **24,** S113- S128.

Han, Y. J. and S. J. Lee, 1981. A new analysis of monthly mean wind stress over the global ocean. *Climate Research Institute, Oregon State University, Corvallis,* **Report 26,** 148 pp.

Hastenrath, S. and J. Merle, 1987. Annual cycle of subsurface thermal structure in the tropical Atlantic Ocean. *J. Phys. Oceanog.,* **17,** 1518- 1537.

Hay, W. W. and J. C. Brock, 1992. Upwelling off SW Africa. In: *Upwelling Systems: Evolution Since the Early Miocene,* C. P. Summerhayes, W. L. Prell and K. C. Emeis, eds. The Geological Society, London, pp. 463- 499.

Hellerman, S. and M. Rosenstein, 1983. Normal monthly wind stress over the World Ocean with error estimates. *J. Phys. Oceanog.,* **13,** 1,093- 1,104.

Henin, C., P. Hisard and B. Piton, 1983. Observations hydrologiques dans l'océan Atlantique equatorial (julliet 1982- août 1984). *FOCAL Vol. 1, Editions de l' O.R.S.T.R.O.M., Collection Travaux et Documents,* **No. 196,** *Paris.*

Isemer, H. -J. and L. Hasse, 1987. The Bunker Climate Atlas of the North Atlantic Ocean, Vol. 2: Air-sea interactions**.** Springer- Verlag, N. Y.

Katz, E.J., 1981. Dynamic topography of the sea surface in the equatorial Atlantic. *J. Mar. Res.,* **39,** 53–63.

Kostianoy, A. G. and J. R. E. Lutjeharms, 1999. Atmospheric effects in the Angola- Benguela frontal zone. *J. Geophys. Res.,* **104,** 20, 963- 20, 970.

Lass, H. U., M. Schmidt, V. Mohrholz and G. Nausch, 2000. Hydrographic and current measurements in the area of the Angola-Benguela Front. *J. Phys. Oceanog.,* **30,** 2,589- 2,609.

Levitus, S., (1982). Climatological atlas of the worlds oceans. *Tech. Rep., NOAA, Rockville, Md.*

Lien, V.S., 2004. The Angola Dome: structure and variability. *MSc thesis, Geophysical Institute, University of Bergen.*

Madec, G, P. Delecluse, M. Imbard and C. Levy, 1998. OPA version 8.1, Ocean General Circulation Model: Reference Manual. *Internal Report, LODYC.* Available at: *http://www.lodyc.jussieu.fr/opa/OPA_model.html.*

Maes, C., P. Delecluse and G. Madec, 1998. Impact of westerly wind bursts on the warm pool of the TOGA- COARE domain in an OGCM. *Clim. Dynamics,* **14,** 55-70.

Masson, S. and P. Delecluse. Influence of the Amazon River Runoff on the tropical Atlantic. *LODYC publication: http://www.lodyc.jussieu.fr/opa/Docu_Free/Publi_Online/Masson_Delecluse_PCE00.pdf*

Mazeika, P. A., 1967. Thermal domes in the eastern Tropical Atlantic Ocean. *Limnol. Oceanogr.,* **12,** 537- 539.

McClain, C. R. and J. Firestone, 1993. An Investigation of Ekman upwelling in the North Atlantic. *J. Geophys. Res.,* **98,** 12,327- 12, 339.

McCreary, J.P., J. Picaut and D. Moore, 1984. Effects of remote forcing in the eastern tropical Atlantic Ocean. *J. Mar. Res.,* **42,** 45- 81.

McPhaden, J. M., 1984. On the dynamics of equatorial subsurface countercurrents. *J. Phys. Oceanog.,* **14,** 1,216-1,225.

Meeuwis, J. M. and J. R. E. Lutjeharms, 1990. Surface thermal characteristics of the Angola- Benguela front. *S. Afr. J. Sci.,* **9,** 261- 279.

Mercier, H., M. Arhan and J.R.E. Lutjeharms, 2003. Upper-layer circulation in the eastern equatorial and south Atlantic ocean in January-March 1995. *Deep-Sea Res.,* **50,** 863- 887.

Merle, J. and S. Arnault, 1985. Seasonal variability of the surface dynamic topography in the tropical Atlantic Ocean. *J. Mar. Res.,* **43,** 267- 288.

Mohrholz, V., M. Schmidt and J.R.E Lutjeharms, 2001. The hydrography and dynamics of the Angola-Benguela Frontal Zone and environment in April 1999. *S.A.J.Sci.,* **97,** 199- 208.

Molinari, R. L., B. Voituriez and R. P. Bubnov, 1981. Observations in the subthermocline undercurrent of the equatorial South Atlantic Ocean: 1978-1980. *Oceano. Acta.,* **4,** 451- 456.

Moroshkin, K. V., V. A. Bubnov and R. P. Bulatov, 1970. Water circulation in the eastern South Atlantic Ocean. *Oceanology,* **10,** 27- 34.

Nelson, G. and L. Hutchings, 1983. The Benguela Upwelling Area. *Prog. Oceanog.,* **12,** 333-356.

Peterson, R.G. and L Stramma, 1991. Upper-level circulation in the South Atlantic Ocean. *Prog. Oceanog.,* **26,** 1-73.

Philander, S.G.H. and R.C. Pacanowski, 1980. The generation of equatorial currents. *J. Geophys. Res.,* **85,** 1,123- 1,136.

Philander, S.G.H. and R.C. Pacanowski, 1986. A model of the seasonal cycle in the tropical Atlantic Ocean. *J. Geophy. Res.,* **91,** 14,192-14,206.

Philander, S. G. H. and Y. Chao, 1991. On the contrast between the seasonal cycles of the equatorial Atlantic and Pacific oceans. *J. Phys. Oceanog.,* **21,** 1,399- 1,406.

Picaut, J., 1985. Major dynamics affecting the eastern tropical Atlantic and Pacific oceans. *CalCOFI Rep.,* **25,** 41- 50.

Piolle, J- F. and A. Bentamy, 2002. Mean Wind Fields (MWF Product) Volume 1- ERS-1, ERS-2 & NSCAT. *IFREMER User Manual,* **C2-MUT-W-05-IF, Vers. 1,** IFREMER, Brest 52pp.

Quilfen Y.,1993. ERS-1 scatterometer off-line products : calibration/validation results and case studies. *Proceedings of International Geoscience and Remote Sensing, Symposium IGARSS* 1993, Tokyo, Japan, pp. 1750-1752.

Reverdin, G., Y. Du Penhoat and Y. Gouriou, 1990. Vertical Structure of the Seasonal Cycle in the Equatorial Atlantic Ocean: XBT Sections from 1980 to 1988. *J. Phys. Oceanog.,* **21,** 277-291.

Risien, C., M, 2002. Windstress variability in the Benguela Upwelling Regime. *MSc. thesis, Department of Oceanography, University of Cape Town.*

Rothstein, L. M., 1984. A model of the equatorial sea surface temperature field and associated circulation dynamics. *J. Phys. Oceanogr.,* **14**, 1,875-1,892.

Schott, F.A., J. Fischer, L. Stramma, 1998. Transports and pathways of the upper-layer circulation in the western tropical Atlantic. *J. Phys. Ocean.* **28,** 1,904- 1,928.

Servain, J., J. Picaut and J. Merle, 1982. Evidence of remote forcing in the equatorial Atlantic Ocean. *J. Phys. Oceanog.,* **12,** 457- 463.

Shannon, L. V. and J. J. Agenbag, 1987. Notes on the recent warming in the south- east Atlantic, and possible implications for the fisheries of the region. *Colln. scient. Pap. int. Commn. SE Atl. Fish,* **14 (2),** 243- 248.

Shannon, L. V., J. J. Agenbag and M. E. L. Buys, 1987. Large- and meso-scale features of the Angola- Benguela Front. *S. Afr. J. mar. Sci.,* **5,** 11-34.

Shannon, L. V. and J. Agenbag, 1990. A large- scale perspective on interannual variability in the environment in the south- east Atlantic. *S. Afr. J. mar. Sci.,* **9,** 161- 168.

Shannon, L. V. and G. Nelson, 1996. The Benguela: large scale features and processes and system variability. In *The South Atlantic: Present and Past circulation,* G. Wefer, W.H. Berger, G. Siedler and D.J. Webb, eds. Springer-Verlag, Berlin Heidelberg, pp. 163- 210.

Shillington, F. A., 1998. The Benguela upwelling system off southwestern Africa. In *The Global Coastal Ocean,* A. R. Robertson and K. H. Brink, eds. John Wiley & Sons, New York, Chapter 20.

Sheng, Y., L. C. Smith, K. E. Frey and D. E. Alsdorf, 2002. A high temporal resolution data set of ERS scatterometer radar backscatter for research in Arctic and sub-Antarctic regions. *Polar Record,* **38(205),** 115- 120.

Siedler G., N. Zangenberg, R. Onken and A. Morliére, 1992. Seasonal changes in the tropical Atlantic circulation: observation and simulation of the Guinea Dome. *J. Geophys. Res.,* **97 (C1),** 703- 715.

Smith, W.H.F. and D.T Sandwell, (1997). Global Seafloor topography from Satellite Altimetry and ship depth soundings. *Science,* **277,** 1956-1962.

Stander, G.H. (1964). The Benguela Current off southwest Africa. *Investl. Rep. mar. Res. Lab. S.W. Africa,* **12.**

Stramma, L. and M. England, 1999. On the water masses and mean circulation of the South Atlantic Ocean. *J. Geophy. Res.,* **104 (C9),** 20,863-20,883.

Stramma, L. and F. Schott, 1999. The mean flow field of the tropical Atlantic ocean. *Deep-Sea Res.,* **46,** 279- 303.

Sverdrup, H. U., 1947. Wind- driven currents in a baroclinic ocean: with application to the equatorial currents of the eastern Pacific. *Proceedings of the National Academy of Science,* **33,** 318- 326.

Tomczak, M. and J. S. Godfrey, 2003. Regional Oceanography: an Introduction, 2nd edition. Daya Publishing House, Dehli, 390pp.

Torrence, C. and G. P. Compo, 1998. A practical guide to Wavelet analysis. *Bull. Amer. Met. Soc.,* **79, Vol. 1,** 61- 78.

Tsuchiya, M., 1986. Thermostads and circulation in the upper layer of the Atlantic Ocean. *Prog. in Oceanog.,* **16,** 235- 267.

Umatani, S. and Yamagata, T., 1991. Response of the eastern Tropical Pacific to meridional migration of the ITCZ: the generation of the Costa Rica Dome. *J. Phys. Oceanog.,* **21,** 346- 363.

Veitch, J.A., P. Florenchie and F. A. Shillington, 2003. Seasonal and interannual fluctuations of the Angola-Benguela Frontal Zone (ABFZ) using high resolution imagery from 1982 to 1999. Submitted to *Int. J. Remote Sensing.*

Voituriez, B., 1981. Les sous-courants equatoriaux nord et sud et la formation des domes thermiques tropicaux. *Ocean. Acta,* **4,** 497- 506.

Voituriez, B. and A. Herbland, 1982. A comparative study of the productive systems of the tropical East Atlantic: thermal domes, coastal upwelling and equatorial upwelling. *Rapports et Proces- Verbaux des Reunions. Conseil Permanent International pour l'Exploration de la Mer,* **180,** 114-130.

Waconge, S. and B. Piton, 1992. The near-surface circulation in the northeastern corner of the South Atlantic Ocean. *Deep-Sea Res.,* **39,** 1273-1298.

Weisberg, R. H. and C. Colin, 1986. Equatorial Atlantic Ocean temperature and current variations during 1983 and 1984. *Nature,* **322** (6076)**,** 240- 243.

Yamagata, T. and S. Iizuka, 1995. Simulation of the tropical thermal domes in the Atlantic: a seasonal cycle. *J. Phys. Oceanog.,* **25,** 2,129- 2,140.

http://www.eumetsat.de/en/
http://www.ifremer.fr/cersat
http://paos.colorado.edu/research/wavelets
http://www.ifremer.fr/lpo/clipper/result16/atl6

Appendix 1: Plots of temperature change between consecutive months at 45m: a positive (negative) value indicates an increase (decrease) in temperatures between successive months.

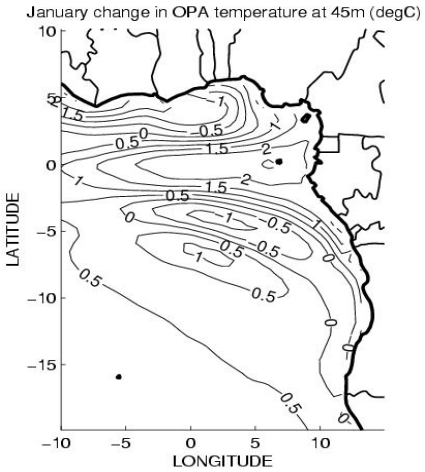

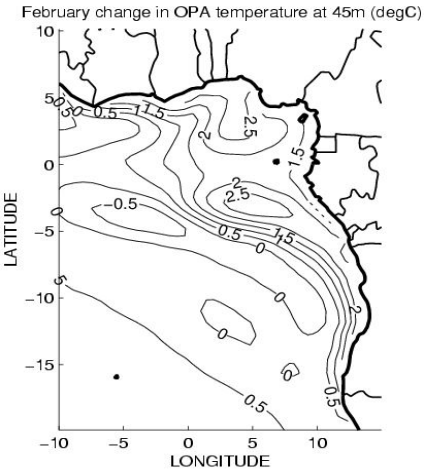

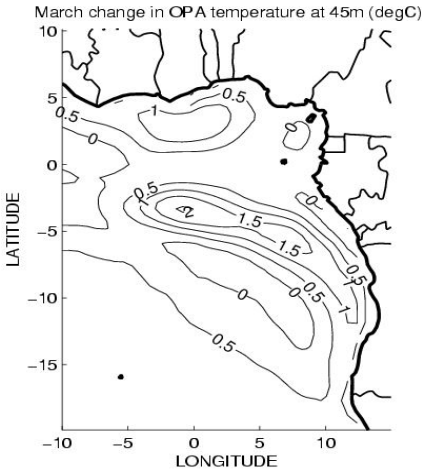

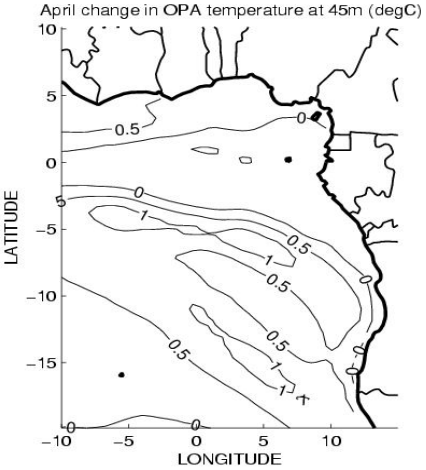

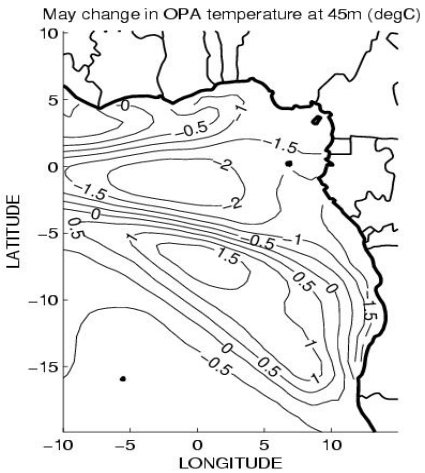

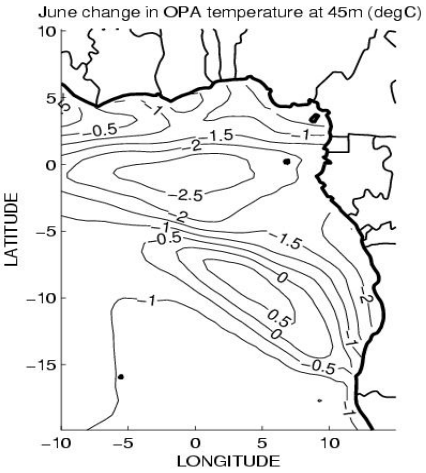

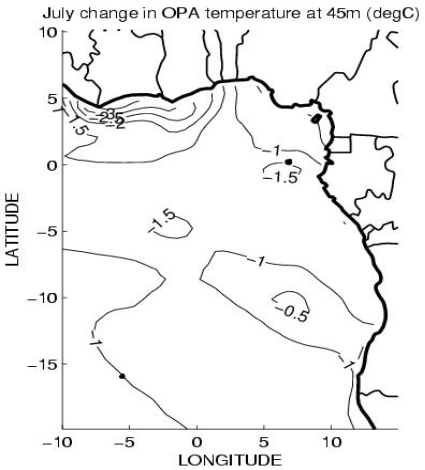
July change in OPA temperature at 45m (degC)
LATITUDE
LONGITUDE

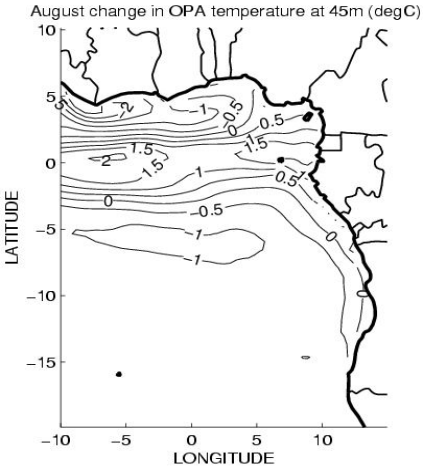
August change in OPA temperature at 45m (degC)
LATITUDE
LONGITUDE

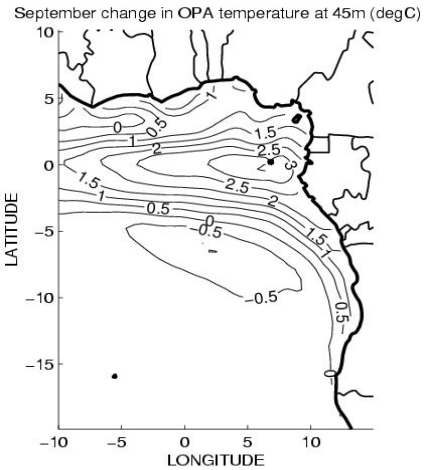
September change in OPA temperature at 45m (degC)
LATITUDE
LONGITUDE

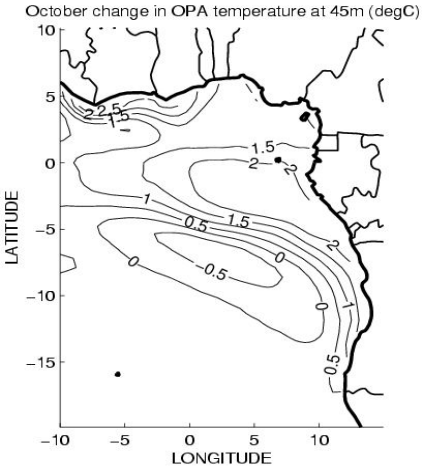
October change in OPA temperature at 45m (degC)
LATITUDE
LONGITUDE

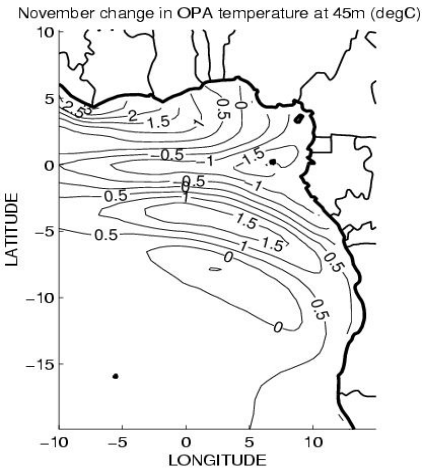
November change in OPA temperature at 45m (degC)
LATITUDE
LONGITUDE

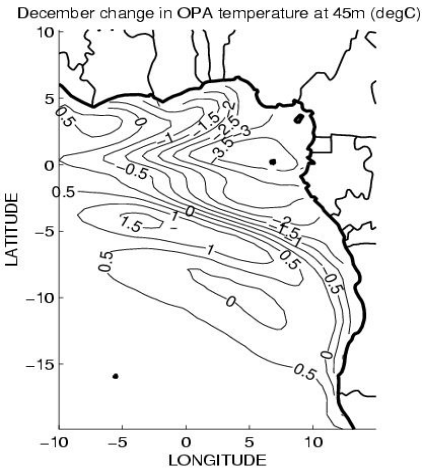
December change in OPA temperature at 45m (degC)
LATITUDE
LONGITUDE

Appendix 2: Monthly mean thermocline depth, calculated as the position of the most intense vertical temperature gradient.

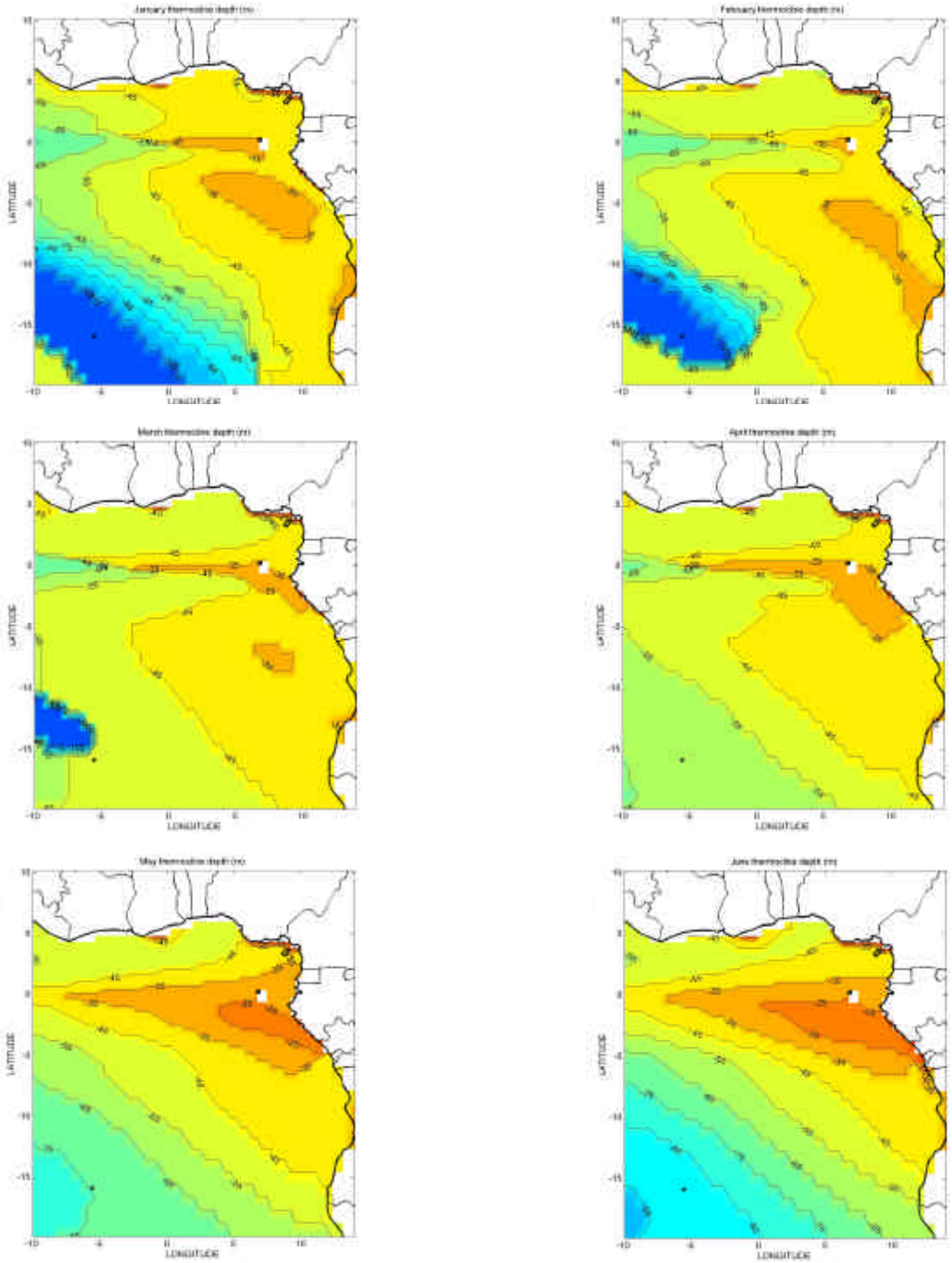

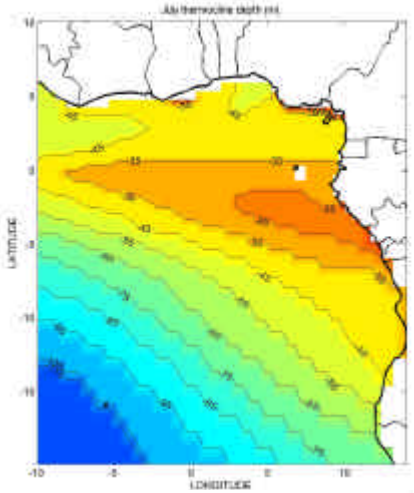
LATITUDE
LONGITUDE

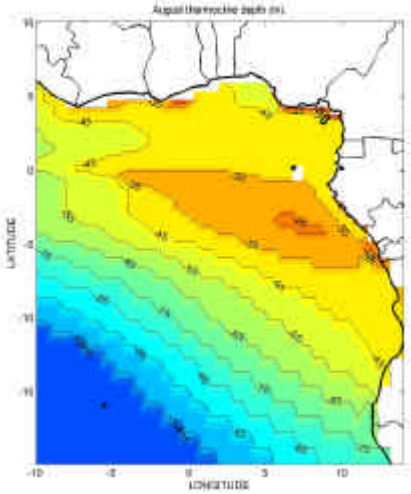
LATITUDE
LONGITUDE

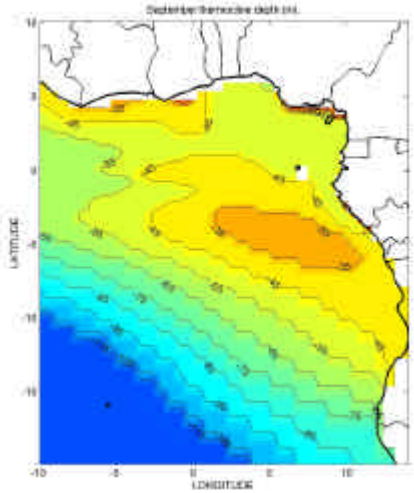
LATITUDE
LONGITUDE

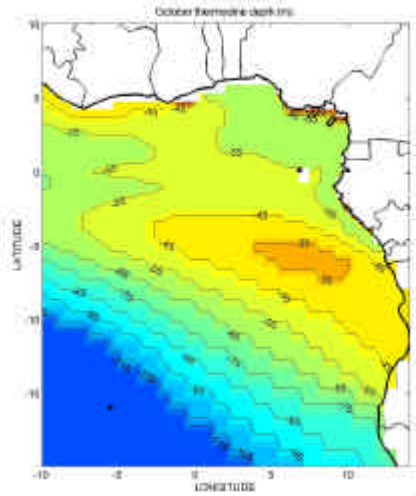
LATITUDE
LONGITUDE

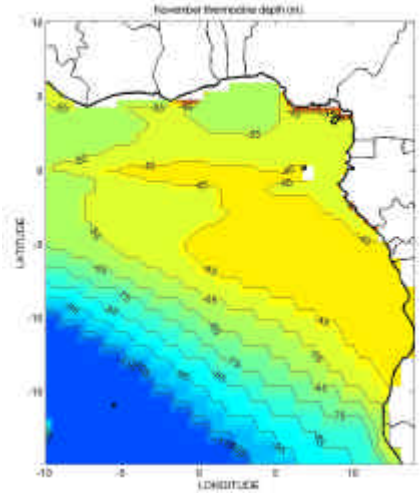
LATITUDE
LONGITUDE

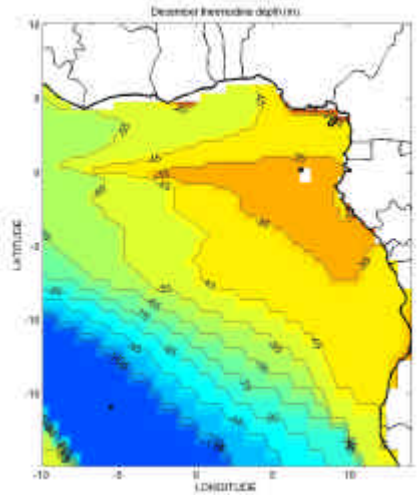
LATITUDE
LONGITUDE

Appendix 3: Hoffmöller plot of the monthly mean thermocline depth along 5°E. Note the southward migration of thermocline-ridge between May and October.

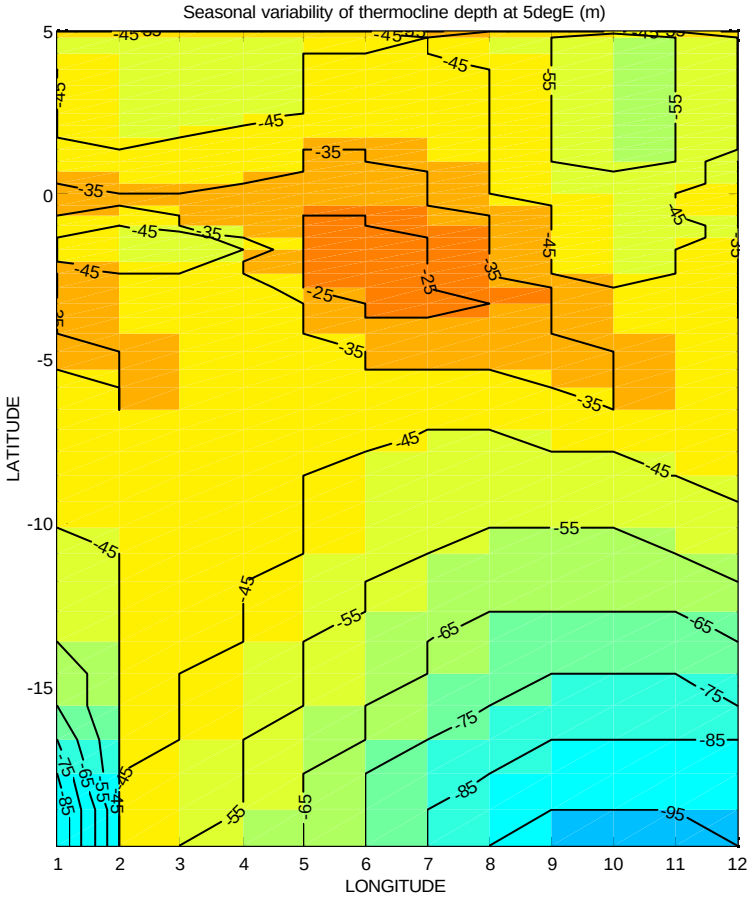

Appendix 4: Plot of wind speeds (unit: $m.s^{-1}$, contour interval: 0.5 $m.s^{-1}$) and direction of the South Atlantic Ocean for January (top) and July (bottom).

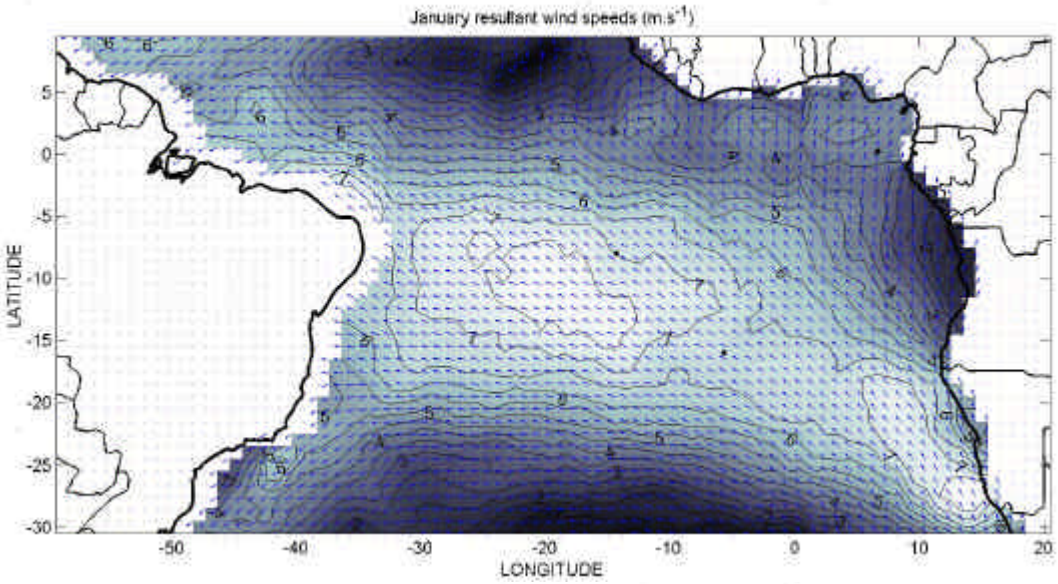

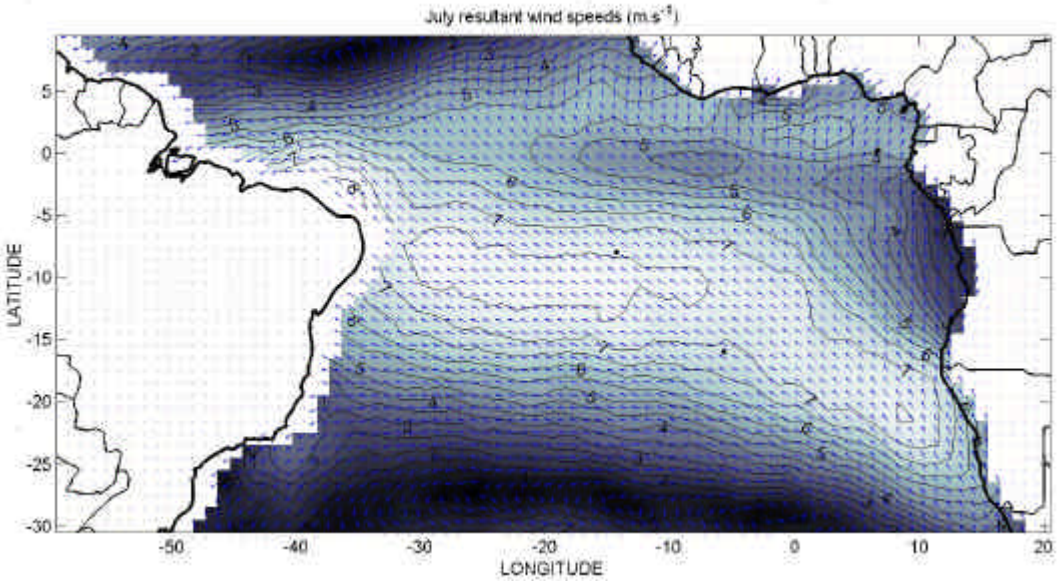

Appendix 5: Monthly mean CLIPPER temperatures at 42m.

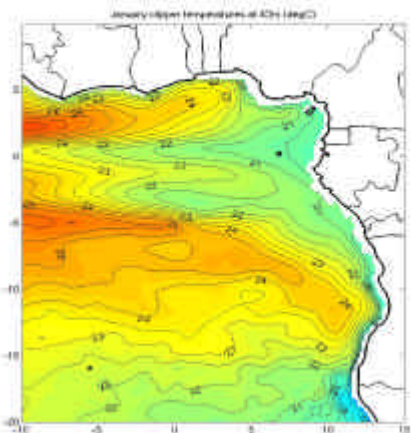

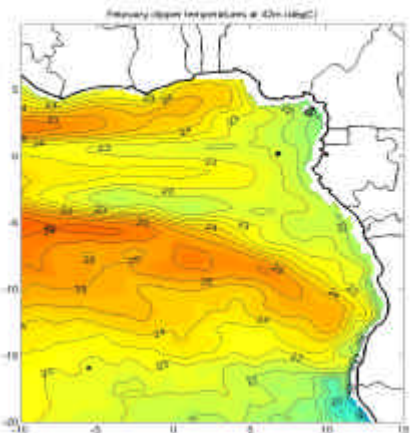

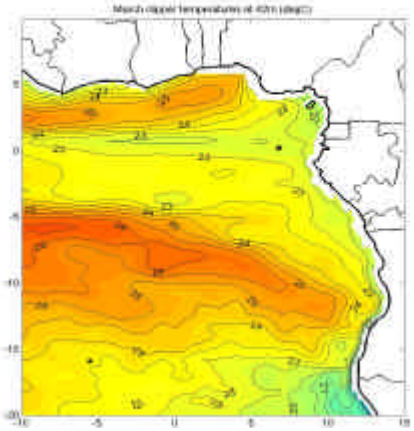

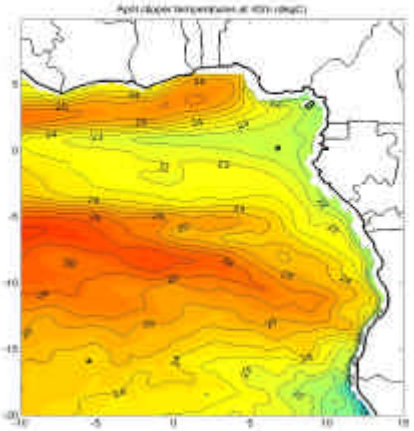

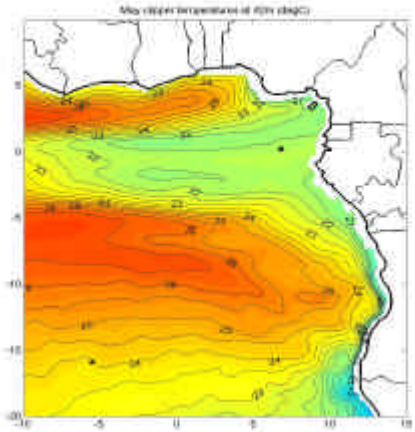

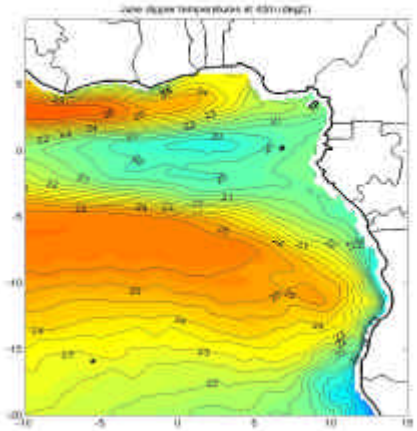

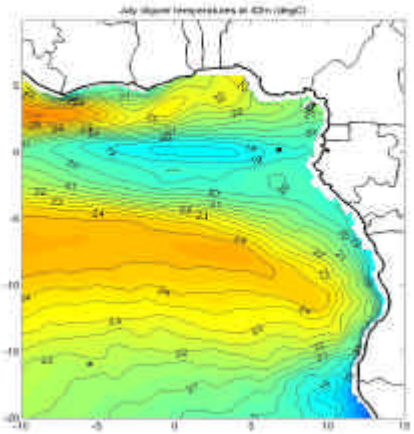

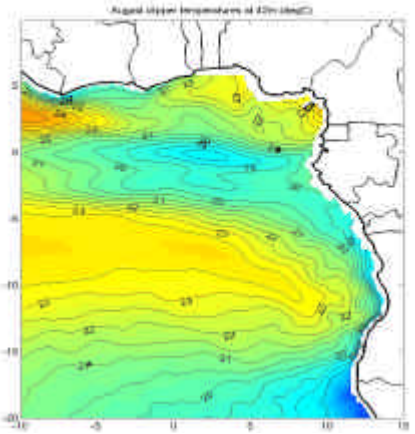

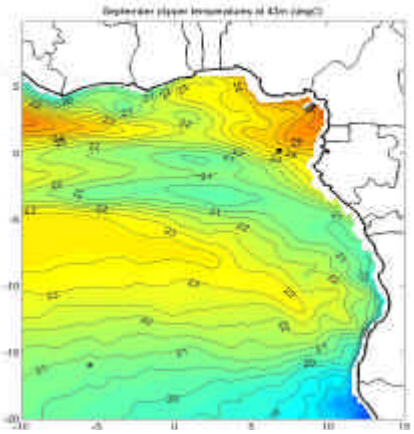

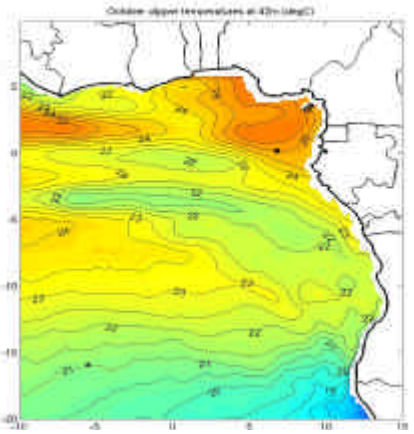

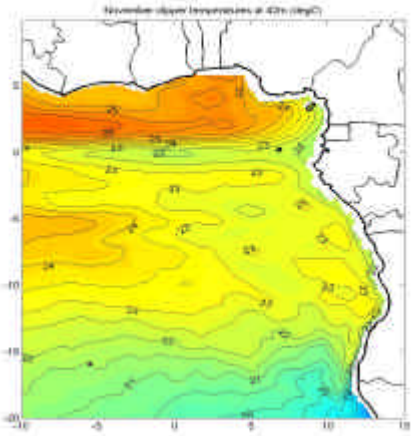

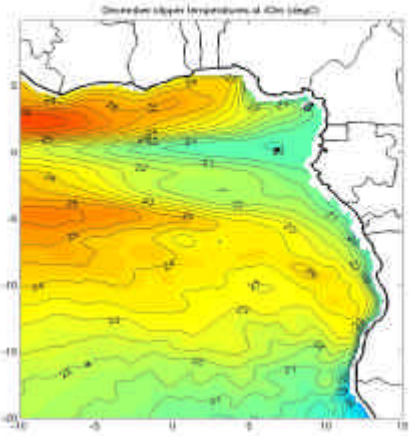
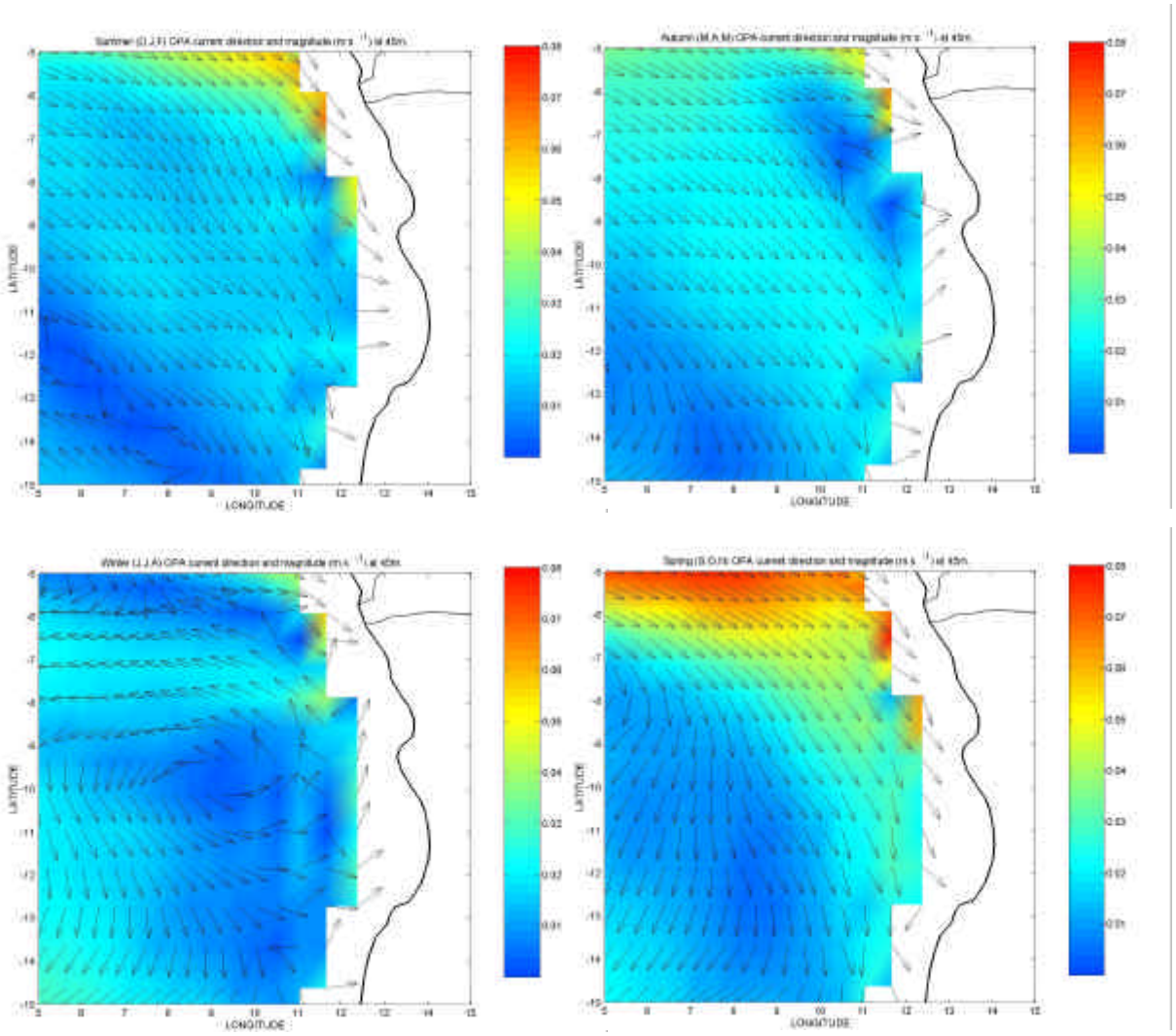
Appendix 6: Seasonal mean resultant horizontal flow pattern and magnitude at 45m as resolved by the CLIPPER model.